Epithelial Reparative Capacity Regulates Extracellular Matrix Dynamics and Innate Immunity

by

Joshua C. Snyder

B.S. in Biochemistry, Grove City College, 2004

Submitted to the Graduate Faculty of

University of Pittsburgh School of Medicine in partial fulfillment

of the requirements for the degree of

Doctor of Philosophy

University of Pittsburgh

2009

UNIVERSITY OF PITTSBURGH

School of Medicine

This dissertation was presented

by

Joshua C. Snyder

It was defended on

April 30, 2009

and approved by

Bruce R. Pitt, Ph.D., Professor and Chair, Environmental and Occupational Health

Aaron Barchowsky, Ph.D., Associate Professor, Environmental and Occupational Health

Bruce A. Freeman, Ph.D., Professor and Chair, Department of Pharmacology

Tim D. Oury, M.D., Ph.D., Associate Professor, Departmental of Pathology

Dissertation Advisor: Barry R. Stripp, Ph.D., Professor, Department of Pulmonary, Allergy, and Critical Care Medicine

Copyright © by Joshua C. Snyder

2009

Epithelial Reparative Capacity Regulates Extracellular Matrix Dynamics and Innate Immunity

Joshua C. Snyder

University of Pittsburgh, 2009

The mammalian lung supports the transport and diffusion of inspired and expired gasses that are critical for aerobic life. With every inspiration the lung is exposed to environmental agents including microbes, virus, and environmental pollutants. In the event that injury occurs the epithelium is repaired by an abundant facultative progenitor pool and a sequestered population of adult tissue stem cells. Chronic lung diseases, such as asthma, chronic obstructive pulmonary disease, and bronchopulmonary dysplasia, are characterized by extensive epithelial remodeling resulting in a reduction to the number of non-ciliated bronchiolar Clara cells. Given the established role for Clara cells as abundant facultative progenitors, these data suggest that epithelial repair has been compromised. In addition to affects on the epithelium, these diseases are also accompanied by extensive subepithelial fibroproliferation, mesenchymal remodeling, and elevated extracellular matrix deposition as well as a profound increase to lung inflammation. It has been postulated, but never tested *in vivo* that mesenchymal remodeling and uncontrolled deposition of extracellular matrix may be a result of impaired airway epithelial reparative capacity. Moreover, the finding that airway epithelial cells are essential for modulation of innate immunity suggests that the enhanced inflammatory response described in chronic lung disease may be a result of attenuated airway epithelial cell function. Therefore, this dissertation tests the hypothesis that airway epithelial reparative capacity moderates extracellular matrix deposition and innate immunity. Through the use of *in vivo* models of injury, inflammation, and attenuated

Clara cell function, this dissertation research work identifies a previously uncharacterized process in which extracellular matrix is dynamically and reversibly regulated during productive epithelial repair and severely disrupted by blocking stem cell mediated repair. In addition, the use of mouse models of decreased Clara cell abundance and secretion demonstrate airway epithelium modulates pulmonary innate immunity through regulation of macrophage behavior and inhibition of pulmonary inflammation. This work defines two phenotypes that are the result of attenuated epithelial repair and supports the paradigm that epithelial reparative capacity may be a principal determinant of lung disease.

TABLE OF CONTENTS

LIST OF TABLES

LIST OF FIGURES

PREFACE

This dissertation would not be possible if not for the gracious support of scientific mentors, peers, and continuous loving support from family and friends. To all of you, I am so thankful for your mentoring, friendship, and love.

I would like to thank my mentor **Barry Stripp** for his outstanding scientific support and excellent mentoring. His patience and direction made my tenure in the lab an outstanding experience and fostered my development as a research scientist. His successful career and family life demonstrated to me that there is life outside of science and that a successful research program does require sacrificing family life. **Paul Reynolds** played an instrumental role in my early graduate career, providing great advice and was an excellent friend, even though he insisted on taking us on cycling excursions up the steepest hills in Pittsburgh. I am greatly appreciative for **Sue Reynolds** and her mentoring. She was a wonderful mentor with the unique ability to see all the caveats to an experiment. Without strong technical support a graduate student would never succeed. Thank you to **Brian Brockway** and **Jeffrey Drake** for their friendship, technical expertise, and help with countless mouse experiments and injections. Without **Chris Burton** and **Lixia Luo** our mouse colony would be a nightmare, thank you for your incredible support. I am especially thankful for the long lasting friendships of fellow graduate students **Roxana**

Teisanu and **Anna Zemke**. Their scientific discussions and moral support were second to none. Thanks again Stripp Lab.

I would also like to thank **Don DeFranco** for his oversight in my transition into the Molecular Pharmacology program and then off campus to Duke University, he was instrumental in making this a smooth transition. Also members of my **Dissertation Committee** provided thoughtful insight and support throughout my dissertation research work.

Without the support of my family I wouldn't be here. Thanks **Mom** and **Dad** for your support, love, and the sacrifices you made just to get me to college. Without my wife **Kristen**, I would have given up long ago. The countless late night experiments and near emotional collapses would not have been overcome without your love, patience, and motivation.

1.0 INTRODUCTION

The conducting airway epithelium is a critical component of the mammalian lung, which provides a primary barrier between host and environment and facilitates transport of inhaled and exhaled gas into and out of the lung. Recent reports have also highlighted the immunoregulatory properties of the airway epithelium. Therefore, the persistent environmental challenges to the conducting airway epithelium pose a significant threat to epithelial function and homeostasis. Therefore, it is critical to maintain the structure and function of the airway epithelium. As such, the conducting airway epithelium maintains tremendous reparative capacity through utilization of a unique progenitor cell hierarchy. In the setting of chronic lung disease (CLD), there is significant remodeling of the epithelium and underlying mesenchyme leading to attenuated epithelial function and aberrant extracellular matrix (ECM) accumulation. It has been postulated that inhibition of epithelial repair through altered progenitor cell behavior may play a critical role in initiation or progression of CLD, however, this paradigm has never been tested directly *in vivo*. Understanding the role that airway epithelial repair may play in the development or exacerbation of lung disease will be critical for the development of cell and molecular therapy. Therefore, this dissertation deals principally with the fundamental paradigm that epithelial reparative capacity moderates ECM dynamics and innate immunity. However, before this paradigm is discussed further, a more thorough review of the relevant literature is warranted.

Chapter 2.0 of this dissertation will provide an in depth and focused review of the conducting airway epithelium to convey the necessary background information to the reader and highlight significant knowledge gaps in the field. The unique structure and function of the epithelium lining the conducting airways, cellular and molecular strategies for repair, and how progenitor cell utilization may be altered in the setting of lung disease will be discussed. At the conclusion of the chapter, a rationale for the experiments supportive of this dissertation will be formally presented (Figure 5). Chapter 3.0 will provide experimental insight into roles for the epithelium in controlling ECM accumulation. Specifically, the hypothesis that epithelial reparative capacity regulates ECM dynamics is tested. As discussed above, epithelial function is also thought to be attenuated in the setting of CLD. Chapter 4.0 will focus on elucidating a mechanism by which the epithelium may moderate innate immunity. A mouse model of CLD, in which epithelial function has been attenuated, is used to test the hypothesis that Clara cells moderate the inflammatory response through regulation of macrophage behavior. In chapter 5.0, the implications of this dissertation will be discussed further, future directions outlined, and ongoing work presented.

1.1 NOTE TO THE READER

Figures and figure legends referred to in the text are included immediately following their description in the text. Supplementary materials from chapter 3.0 and 4.0 are included in Appendix A and B, respectively. Appendix C includes publications that are the result of this dissertation work. Appendix D is a list of abbreviated terms.

2.0 THE CONDUCTING AIRWAY EPITHELIUM: STRUCTURE, FUNCTION, MAINTENANCE, AND CONTRIBUTION TO DISEASE[1]

2.1 INTRODUCTION

Epithelial branching during the process of lung development establishes distinct functional zones, each of which are characterized by a unique cellular composition and repertoire of local progenitor cells. Instrumental to lung homeostasis are the myriad of functions that the airway epithelium provide, including host defense and immunoregulation. Therefore, an essential component of lung homeostasis is maintenance of the differentiated properties of the airway epithelium at steady-state and restoration following injury. Significant new insights into cellular and molecular mechanisms of epithelial maintenance have been made in recent years that provide insights into the pathophysiology of lung disease. This chapter focuses on the complex structure-function relationship in the airway epithelium as it relates to host defense and immunoregulatory roles of the airway epithelium. A detailed review of the cellular mechanisms that are utilized to maintain the airway at steady-state and repair following injury is also included. Deregulation of this process may contribute to airway disease including perturbations to epithelial function and mesenchymal remodeling. At the conclusion of the chapter a brief section outlining the experimental rationale that is designed to test this concept is included and is the basis for this dissertation research project.

2.2 LUNG STRUCTURE

The conducting airway epithelium is a dynamic structure that is essential for delivery of inhaled gases to the distal alveolar epithelium where gas exchange takes place. In order to supply sufficient oxygen rich gas to the alveolus, the conducting airway epithelium is highly branched with an abundant number of small airways lined by bronchiolar epithelium. The branching pattern becomes increasing complex near the distal alveolar epithelium. The terminal bronchioles in larger mammalian species branch further into respiratory bronchioles, which in turn branch into alveolar ducts, and terminate in the alveolus. One terminal bronchiole alone can give rise to 14 respiratory bronchioles, from which 1,500 alveolar ducts can branch, terminating in approximately 4,500 alveolar sacs, with 20,000 alveoli[2]. The complexity is especially evident when considering that that there are on average 38, 883 terminal bronchioles in the upper right lobe of human lung alone[3]. In addition, with each successive branch airway diameter continues to decrease. The diameter of the trachea is approximately 16mm while diameters of terminal and respiratory bronchioles are almost two orders of magnitude smaller, 0.6 and 0.4 mm in diameter, respectively. Equally important functions of the epithelium are regulation of host defense and intrinsic reparative capacity following microbial or xenobiotic initiated tissue damage. To accomplish these dynamic functions the epithelium of the mammalian lung is compartmentally organized along the proximal to distal axis, distinct regions of which are defined by their unique cellular composition[4]. The normal human tracheal and bronchial epithelium is a pseudostratified

epithelium predominantly comprised of basal, ciliated, goblet, and serous cells. More distal within intrapulmonary conducting airways is a simplified columnar epithelium defining the bronchiolar airway epithelium. The bronchiolar epithelium of humans is comprised of ciliated cells, nonciliated secretory Clara cells, relatively few basal cells, and devoid of goblet cells[5-7]. Conducting airways of the human lung terminate in a transitional zone of respiratory epithelium referred to as the respiratory bronchiole. Respiratory bronchioles include conducting portions lined by cuboidal bronchiolar epithelium that branch from the terminal bronchioles, comprised of Clara and ciliated cells in addition to frequent alveoli that bud from the airway wall[2,7].

Despite functional conservation of epithelial compartments between species, their relative size and cellular composition varies. The most dramatic anatomical difference between species is evidenced by the number of intrapulmonary conducting airway branches and the relative abundance of bronchial versus bronchiolar epithelium. Multiple generations of intrapulmonary bronchi observed in humans and non-human primates are limited to one or two generations in mice, in which bronchioles predominate[8]. Moreover, bronchioles in mouse airways transition directly into alveolar ducts implying the transitional respiratory bronchiolar zone typical of larger mammalian species is severely attenuated or altogether absent[9,10]. Corresponding differences are observed in cell types lining airways of the mouse lung. Basal cells are restricted to the tracheal epithelium while ciliated cell abundance diminishes significantly along the proximal to distal axis and Clara cells become particularly abundant within bronchiolar airways[11]. Cell types of the alveolar epithelium show minimal differences between species[12]. A schematic depicting the overall structure of the conducting airway and alveolar epithelium of mouse is presented in Figure 1.

The complex anatomical organization of these cellular components is regulated by a highly coordinated and stereotypic developmental program, as assessed by interrogation of mouse models. Lung development initiates following fate specification within the ventral foregut endoderm and can be defined by NKX2.1 expression[13]. Recent data indicate that branching occurs through a combination of three geometric branch types in a combination with 3 stereotypical series. The timing and order of these branching modes are genetically regulated[14]. Regulation of cell proliferation and fate are tightly linked to this process, as signaling perturbations impacting these processes lead to a variety of defects in lung branching and specification of epithelial lineages[13,15,16]. These signaling events involve reciprocal interactions between epithelial and mesenchymal cell types resulting in coordinated growth and differentiation[17-19]. In particular, WNT/CATNNB1 signaling has been shown to be a critical mediator of proximal to distal patterning of the lung epithelium during embryonic development[20-22]. Even though far less is known of signaling axes that contribute to epithelial behavior in the adult lung, it is clear that the epithelial-mesenchymal signaling axis is retained and its regulation critical to tissue homeostasis[23,24].

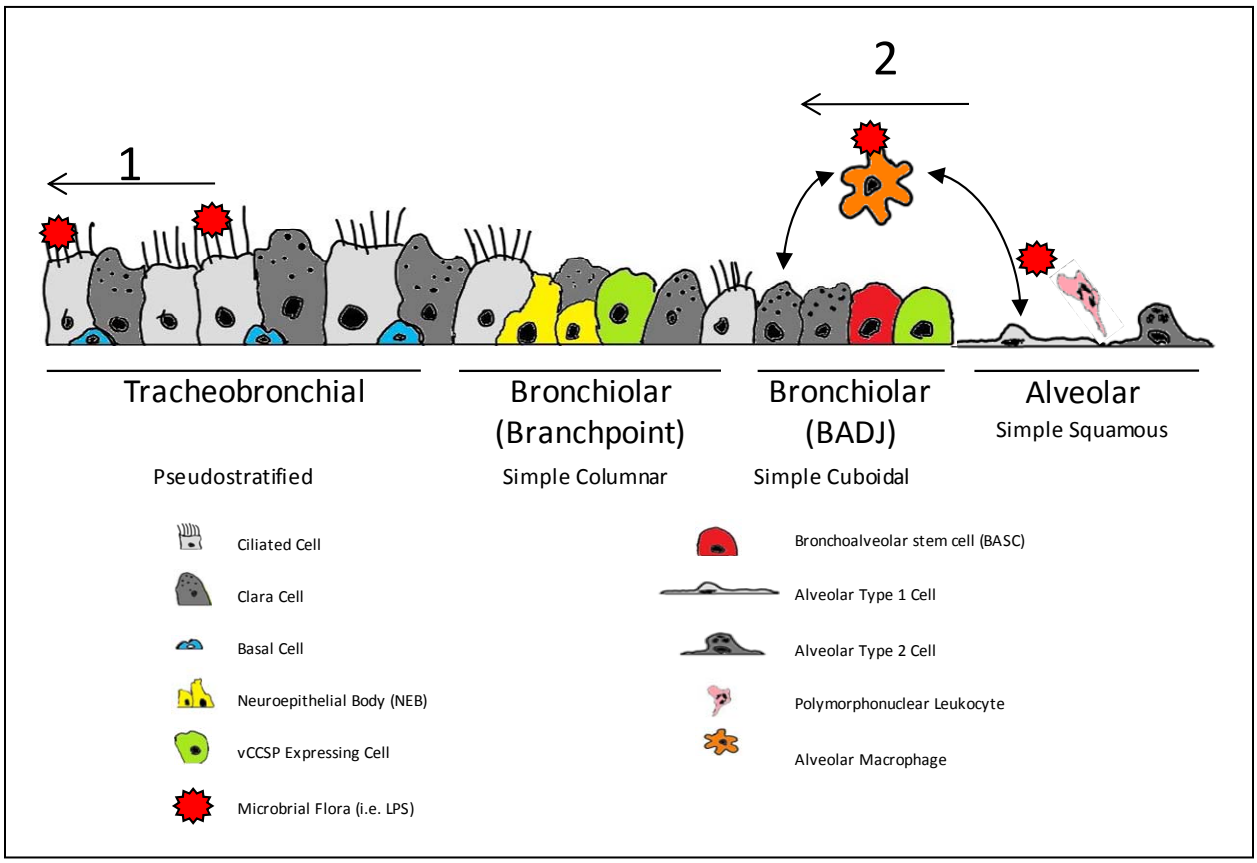

Figure 1. Cellular composition and function of the airway epithelium.

The epithelium lining mammalian airways is compartmentalized along the proximal to distal axis into four distinct zones, which can be further subdivided based upon cellular composition, structure, and function. The schematic represents changes in cellular composition and function according to airway location in the mouse lung (proximal to the left, distal to the right). The pseudostratified tracheobronchial epithelium is characterized by an abundance of ciliated and basal cells and a lower incidence of non-mucus secretory cells. Secretory cells in proximal airways of larger mammalian species tend to be of more varied phenotype and include serous and goblet cells. Basal cells are less abundant within mouse bronchial airways relative to bronchi of larger mammalian species. The epithelium of bronchi is largely composed of columnar ciliated and secretory cells. Secretory cells of both tracheal and bronchial airways in mice share some molecular properties of bronchiolar Clara cells, but differ in their mechanism of replacement and responsiveness to airway inflammation. Bronchiolar airways are the most distal conducting airway and are composed of ciliated cells and Clara cells. Other cell types of the conducting airway

Figure 1 Continued.

include rare pulmonary neuroendocrine cells that when organized into clusters are commonly referred to as neuroepithelial bodies (NEB's) and are often located at or near airway branchpoints. The conducting airway epithelium of the rodent lung terminates abruptly at the bronchoalveolar duct junction where airways open into alveolar ducts and clusters of alveoli composed of squamated Type I (AT1) cells and cuboidal type II cells (AT2). AT1 cells have a greatly attenuated structure and are essential for gas transfer[25] while AT2 cells produce surfactants essential for regulation of lung compliance and innate immunity[26]. Larger mammalian species have a transitional respiratory bronchiole that includes bronchiolar epithelium with frequent alveolar buds that protrude from the bronchiolar wall (not shown). Epithelial compartmentalization plays a vital role in protecting the lung from microbial infection and inhaled pollutants through two major mechanisms: **(1)** Particles and microbes adsorbed to the viscous mucus layer are cleared through concerted ciliary beating within the subtending periciliary layer (PCL), resulting in effective clearance with minimal need for an immunologic response. This process is referred to as mucociliary clearance. **(2)** If mucociliary clearance is overwhelmed or evaded, both innate and adaptive arms of the host immune response are activated. Recent work has demonstrated the importance of epithelial and macrophage cross-talk in innate immunity[27,28].

2.3 EPITHELIAL FUNCTION: MUCOCILIARY CLEARANCE AND IMMUNOREGULATION

2.3.1 Mucociliary Clearance

The complex cellular composition of the airway epithelium provides key defensive properties for the lung (Figure 1). As reviewed extensively by Knowles and Boucher[29], the first line of defense to inhaled particulates, oxidants, and biological flora is the airway surface fluid (ASF). The ASF is comprised of the mucus layer, of which the predominant protein components are MUC5AC and MUC5AB, and a subtending periciliary liquid layer (PCL) that provides an unrestricted media for ciliary beating and effective mucus transport. Inhaled micro-organisms and environmental stimuli are immediately ensnared in the dense mucus of the ASF preventing further entry to the more susceptible distal conducting and alveolar compartments. Through precise regulation of PCL height, ciliated cells coordinately regulate mucociliary clearance. Effective mucociliary clearance is estimated to take six hours, implying that this mechanism alone is not enough to protect from infection[29]. As such, the ASF also includes several anti-microbial proteins that inhibit bacterial proliferation to allow for effective removal through mucociliary clearance without infection thus minimizing the need for a massive inflammatory response[30]. Defects to mucociliary clearance can have devastating effects, as is the case in cystic fibrosis (CF). In CF, mutations to the chloride channel CFTR, most notably a deletion of

phenylalanine 508[31], result in impaired chloride transport and electrolytic and fluid imbalance. This results in decreased viscosity of the PCL, reduced ciliary beating, and decreased mucociliary clearance, ultimately leading to chronic infection, mucus plugging, and lung disease[32].

2.3.2 Immunoregulatory Properties of the Lung Epithelium

An abundance of literature exists investigating the role of the hematopoietic derived resident lung macrophage in regulation of the inflammatory response. In an elegant study, Koay and colleagues demonstrated the critical role that resident lung macrophages play in lung inflammation. The resident lung macrophage population was ablated through intratracheal instillation of clodronate liposomes. This resulted in a blunted response to LPS as measured by neutrophil recruitment to the lung, TNF-α production, and NF-kB activity in the lung[33]. In addition to elucidating the role for macrophages in LPS elicited inflammation, this study also implicated the lung epithelium as a downstream target of the macrophage.

To formally test the immunoregulatory properties of the lung epithelium several methods have been utilized, including sophisticated transgenic manipulation of various components of the NF-kB signaling cascade as well as chemically compromising epithelial function. A critical regulator or NF-kB signaling is the IkB complex which binds to NF-kB thus inhibiting the pathway by preventing NF-kB translocation into the nucleus. Upon activation of TLR4 signaling by LPS, IkB proteins, specifically IkBα are targeted for proteosomal degradation through phosphorylation at Ser32/36 by IkB kinases (IKK1 and IKK2) allowing for NF-kB translocation into the nucleus and transcription of target genes[34]. The first study to look at the role for lung

epithelial cells focused on the alveolar epithelium. In this study, a dominant negative form of IkBα, which is resistant to degradation due to alanine substitutions at Ser32/36 and therefore inhibits Nf-KB signal transduction, was constitutively expressed in alveolar type 2 cells under the regulation of the SPC promoter. These mice displayed a blunted response to LPS induced inflammation in the lung as measured by a reduction in nuclear NF-kB, recruited PMNs, total inflammatory cells, and the production of the CXC chemokine KC.[35] A more recent study suggests that the airway epithelium participates in regulating the inflammatory response. In this study, adenoviruses expressing either a dominant negative IkBα or a RelA (p65) subunit of Nf-KB were instilled intratracheally in mice expressing an NF-kB reporter and exposed to LPS. Mice instilled with virus expressing dominant negative IkBα or RelA inhibited and potentiated lung inflammation, respectively, as measured by NF-kB reporter activity in the airway epithelium and chemokine/cytokine production[36]. Evidence that the principal airway epithelial component of the inflammatory response, came from a study in which constitutively active IkBkinase 2 (IKK2) or dominant negative IkBα were placed under doxycycline regulated expression in Clara cells. This study demonstrated that constitutive NF-kB signaling in Clara cells promotes lung inflammation. In contrast, inhibition of NF-kB signaling in Clara cells can revert the action of constitutive IKK2 activity and markedly inhibit LPS induced inflammation.[37] Additional work has highlighted the importance of Clara cells by selectively injuring this population through administration of naphthalene (for a mechanism of action please refer to section 2.5.2). This study indicated that transient ablation of Clara cells inhibit the inflammatory response to LPS[27]. Additional work has suggested that the Clara cell and macrophage signaling axis is critical for the response to LPS as measured by production of epithelial and macrophage specific chemokines and cytokines. This process is initiated by secretion of paracrine signaling

molecules from macrophages, such as TNF-α, that target the airway epithelium as an intermediate signaling cell type required for production of neutrophilic chemotactic factors[28]. Collectively, these results indicate that the distal airway and respiratory epithelial cells play a prominent role in providing important immunoregulatory properties essential for the regulation of innate immunity (Figure 1). Despite these studies very little is known regarding possible signaling molecules secreted by Clara cells that may regulate macrophage cross-talk.

2.3.3 Clara cell secretory protein (CCSP)

Among the many functions of Clara cells, the most prominent is secretion. The principal secreted protein product of the Clara cell[38,39] and founding member of the secretoglobin class of proteins, Clara cell secretory protein (CCSP, Scgb1a1), is the predominant protein product of ASF whose expression precipitously declines in chronic lung disease[40-44]. These data suggest that epithelial secretion has been compromised as a result of the epithelial remodeling and Clara cell injury in the setting of CLD. CCSP is a 16 kDa homodimer with a small internal hydrophobic binding pocket that binds to progesterone[45], metabolites of PCB[46], calcium[47,48], and phospholipids[49]. Previous studies suggested that CCSP may directly regulate phopholipase A2 activity, however, it is now known that this is through an indirect mechanism in which CCSP sequesters Calcium through chelation at Asp48.[48] To study the effects of CCSP deficiency on lung function, mice homozygous null for CCSP (CCSP-/-) were generated that differ in their ability to modulate fibronectin deposition[46,50,51]. Exposure of CCSP-/- mice to pulmonary irritants, pollutants, and microbes has revealed that Clara cell secretions can moderate immunoregulatory aspects of the airway epithelium[52-59]. Few studies have demonstrated a robust

steady-state phenotype in CCSP-/- mice, despite their altered gene expression profile which include increased expression of other secretoglobins (Scgb3a1 and Scgb3a2).[56,60]

However, recent work has highlighted the potential for Clara cell modulation of macrophage behavior, as naïve CCSP-/- mice display alterations to the macrophage proteome compared to wild-type (WT). Specifically, CCSP deficiency causes an undefined post-translational modification to AnnexinA1 (ANXA1) resulting in a shift to a more acidic isoform as identified by two dimensional difference gel electrophoresis (2D-DIGE[61]) and peptide identification using MALDI-TOF mass spectroscopy[62]. This raises the interesting possibility that Clara cells may regulate macrophage behavior through a CCSP dependent mechanism. It remains to be determined how CCSP deficiency and attenuated Clara cell function impacts the functionality or behavior of lung macrophages and innate immunity. Therefore this dissertation work will seek to assess the direct link between altered Clara cell secretory function and macrophage behavior.

Contrary to initial assumptions, recent work has revealed that the airway epithelium is more than an inert barrier to inhaled microbiological flora. Rather, through precise differentiation of cell types organized within distinct functional zones, relative to anatomical location, the epithelium plays an active role in host defense. Collectively, these data indicate that airway epithelial specification, effective repair, and maintenance are critical for lung homeostasis. Defects to these processes or significant epithelial remodeling may contribute to CLD through altered epithelial function and perturbations to the host defense properties of the lung. The remainder of the chapter reviews the cellular and molecular mechanisms involved in epithelial maintenance that are essential for establishing the differentiated properties of the epithelium. An emphasis will be placed on defining the putative stem cell hierarchies

endogenous to the conducting airway epithelium, their molecular regulators, and evaluate their contribution to lung disease. Before these issues can be discussed in depth, a brief introduction into the classification of a stem cell hierarchy is warranted.

2.4 DEFINING A LUNG STEM CELL HIERARCHY

Identification of the hierarchical organization of progenitor cells into what is commonly referred to as a stem cell hierarchy has classically been described in tissues that display a high rate of cellular turnover such as the small intestine and skin. Specifically, the intestinal epithelium, as a result of persistent epithelial damage, is in a constant state of regeneration resulting in cellular turnover of approximately 5 days[63]. Tissue stem cells of this hierarchy have been defined using functional assays that interrogate proliferative frequency, self-renewal, and differentiation potential.[64] Small numbers of intestinal stem cells are thought to reside at or near the base of the intestinal crypt and give rise to a more abundant population of highly proliferative transit-amplifying cells located more proximally within the crypt[65,66]. Transit-amplifying cells of the intestinal epithelium represent an obligate progenitor cell pool lacking differentiated characteristics and are committed to a high rate of proliferation necessary for generation of differentiating progeny[67]. A model depicting a classical stem cell hierarchy is presented in Figure 2. This strategy for rapid tissue replacement is shared by the skin, in which an obligate transit-amplifying progenitor cell that is both abundant and broadly distributed within the epidermis continuously generates differentiating progeny through a stochastic mode of cell fate determination[68,69]. In the skin, resting tissue stem cells are maintained in a quiescent state and are only activated to proliferate in response to depletion of the transit-amplifying pool, through a process thought to be highly regulated by calcineruin, BMP, and NFATc1[70,71]. The relative

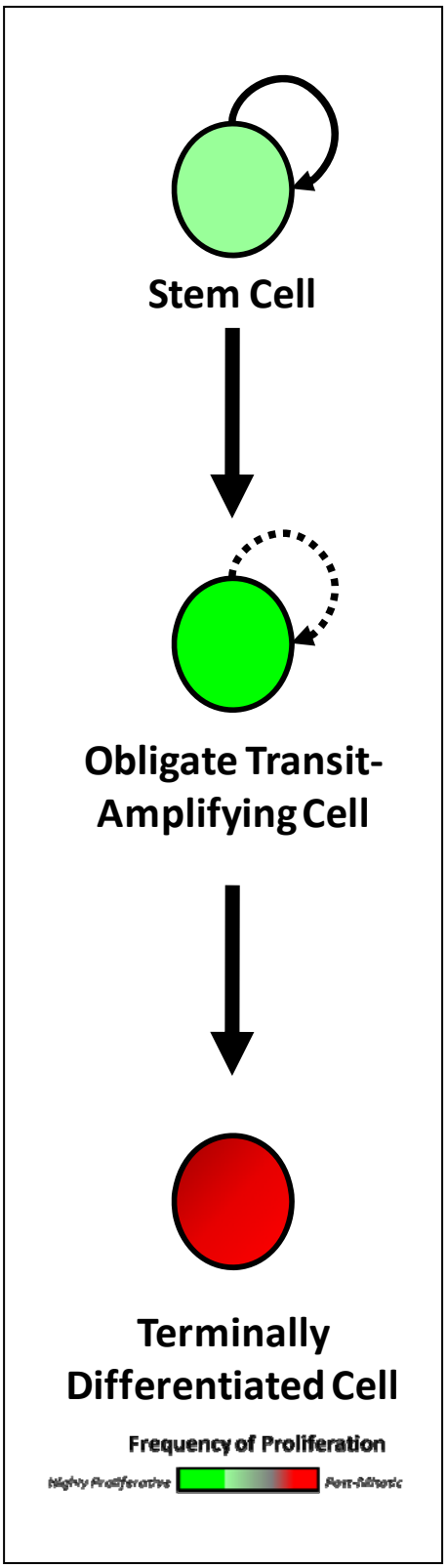

Figure 2. Classical stem cell hierarchy (intestine and skin).

Figure 2 Continued.

In rapidly renewing tissues such as the intestine, a classical stem cell hierarchy maintains epithelial heterogeneity and function. As discussed in depth in the text, stem cells self-renew, (curved solid arrow), give rise to an obligate transit-amplifying cell population, and infrequently proliferate. The obligate transit-amplifying cell does not fulfill functions of differentiated cells but instead divides frequently giving rise to terminally differentiated post-mitotic cells. Obligate transit-amplifying cells have limited self-renewal capacity (broken curved arrow) and as such are short lived in classical stem cell hierarchies like the gut. (proliferative frequency is depicted in color).

quiescence of tissue stem cells in comparison to their more abundant transit-amplifying progeny has become a controversial topic in recent studies investigating intestinal stem cells. However, the property of DNA label retention remains a commonly used assay for the identification and localization of resident tissue stem cells[64].

The epithelium lining pulmonary airways turns over slowly during the normal process of tissue maintenance. Methods used to calculate the rate of epithelial turnover rely on indirect approaches that are based upon measurements of cell proliferation and lineage tagging. Measurements of cell proliferation have principally relied upon stable incorporation of labeled DNA precursors such as bromodeoxyuridine (BrdU) or [H^3]-thymidine into the DNA of cells traversing S-phase. Using this approach, estimates of the steady state instantaneous proliferative fraction were determined to be 1.3% in tracheal epithelium[72] and 0.06% in bronchiolar epithelium[73]. Data generated from continuous labeling of the steady-state bronchiolar epithelium further demonstrated that the frequency of proliferation within this compartment was 1% per day[74]. Assuming a direct relationship between the rate of epithelial cell loss and replacement, these data suggest that epithelial cells have an average life span of 100 days in bronchioles. Direct measurement of ciliated cell half life, as a measure of epithelial turnover, made by Rawlins and Hogan indicated that this subpopulation of epithelial cells has an estimated half-life of either 6 or 17 months in trachea and bronchioles, respectively[75]. Estimates made using either approach indicate that the epithelium of the trachea turns over more rapidly than that of bronchioles. While both methods are technically flawed, due to the inability to directly assess Clara cell turnover, these studies demonstrate that the frequency with which the airway epithelium turns over is similar to that described for the endocrine pancreas and other foregut derived tissues[76] but differs significantly from the rapid rate of epithelial turnover observed in

tissues derived from hindgut endoderm, such as the small intestine[64]. These data suggest that there are fundamental differences in the regulation of progenitor cells between slowly and rapidly renewing tissues[77,78].

Recent work has called into question the existence of stem cells in slowly renewing tissues[79,80]. As indicated above, the lung epithelium is replaced far more slowly than either the gut or the epidermis, a property that is reflected in the functional characteristics of airway progenitor cells in resting versus proliferative states. Therefore, it is not surprising that progenitor cell hierarchies of the lung and other slowly renewing tissues do not fit the classical stem cell hierarchies described in tissues of rapid turnover[77]. In fact, Hu and colleagues, through use of in vivo injury models, have recently described the existence of a stem cell capable of renewing the endocrine pancreas, a tissue that until recently was thought to be maintained solely through self-duplication of differentiated β cells[81]. This and previous work in lung to be discussed in more detail below, illustrate a deviation from the classical stem cell hierarchy marked by lack of an obligate transit-amplifying progenitor cell activity in the steady state. Rather, slowly renewing tissues such as lung are maintained at steady state by an abundant facultative transit-amplifying progenitor that fulfills characteristics of a differentiated cell type in the quiescent state, yet retains proliferative capacity and the ability to generate daughter cells capable of generating other specialized lineages. Therefore, the endogenous stem cell at steady-state likely remains quiescent. A proposed model depicting the stem cell hierarchy in the conducting airway epithelium and its utilization at steady-state and following injury is presented in Figure 3. Studies utilizing in vivo injury models have revealed stem cells do exist in the adult lung and can be functionally distinguished from facultative progenitors based upon their

resistance to environmental stimuli and spatial localization in the conducting airway (Figure 4). These studies are highlighted in detail below.

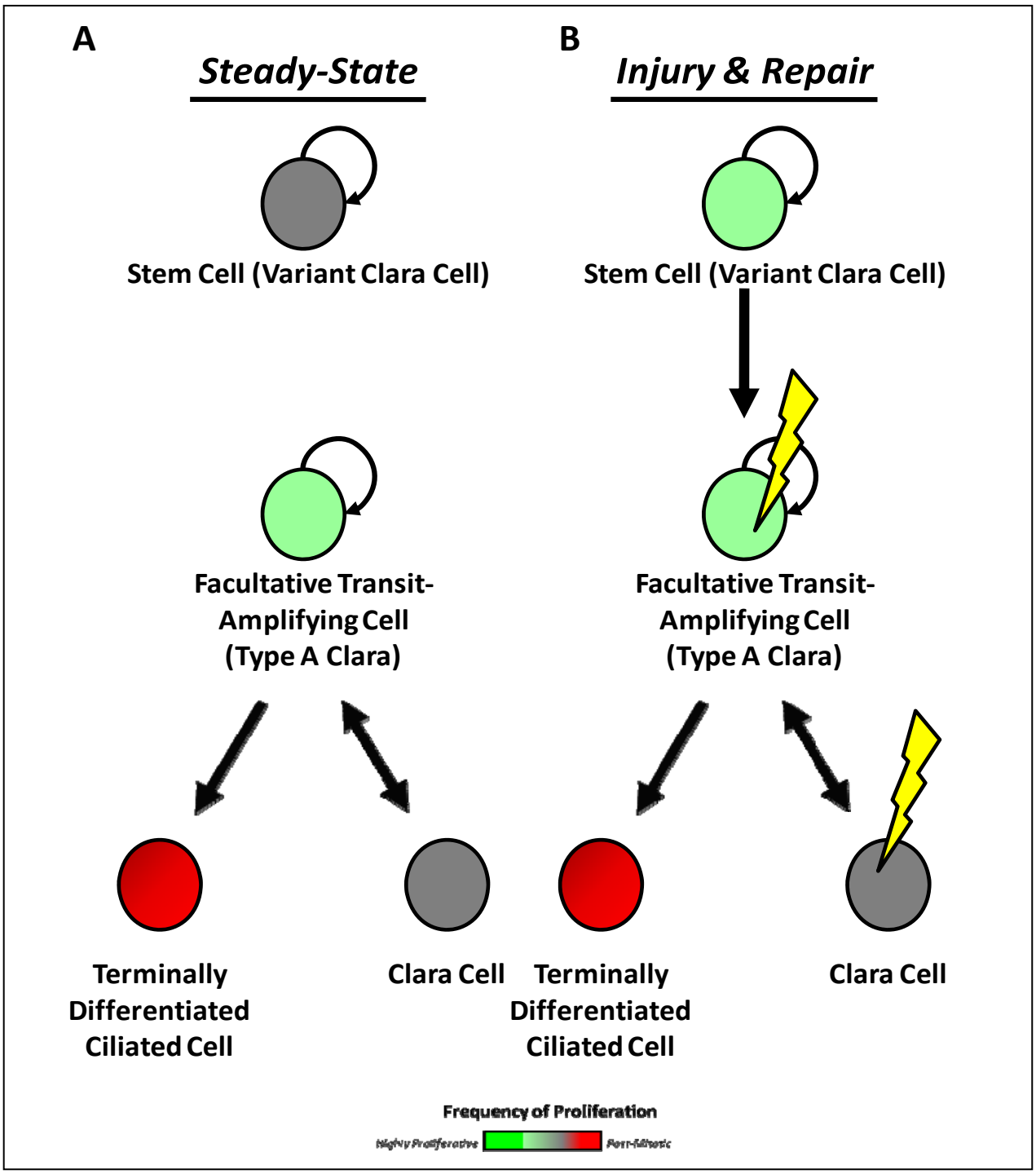

Figure 3. The stem cell hierarchy of the bronchiolar epithelium.

Slowly renewing epithelial tissues like the lung are not maintained by a classical stem cell hierarchy at steady-state. The proliferative index of the airway epithelium is low relative to rapidly renewing tissues like the

Figure 3 Continued.

intestine. (A) It has been postulated that an abundant facultative transit-amplifying cell maintains the epithelium. Clara cells fulfill a variety of differentiated cell functions including secretion of immunoregulatory molecules. However, these cells are not post-mitotic. Rather they have the ability to de-differentiate to a Type A Clara cell (facultative transit amplifying cell), proliferate, and differentiate to post-mitotic ciliated cells and differentiated Clara cells. Unpublished observations (Giangreco A., Submitted) indicate that facultative transit amplifying cells self-renew (black curved arrow) and maintain cellular diversity of the epithelium at steady-state. Therefore airway epithelial stem cells remain quiescent and do not contribute to steady-state epithelial maintenance. (B) However, using injury models (yellow lightning bolt) that selectively target the abundant facultative transit-amplifying cells and Clara cells, it has been shown that a stem cell population is sequestered to distinct microenvironments within the conducting airway epithelium. This cell type proliferates rapidly following injury and quickly restores the cellular diversity of the conducting airway epithelium including the facultative transit amplifying cell. (proliferative frequency is depicted in color).

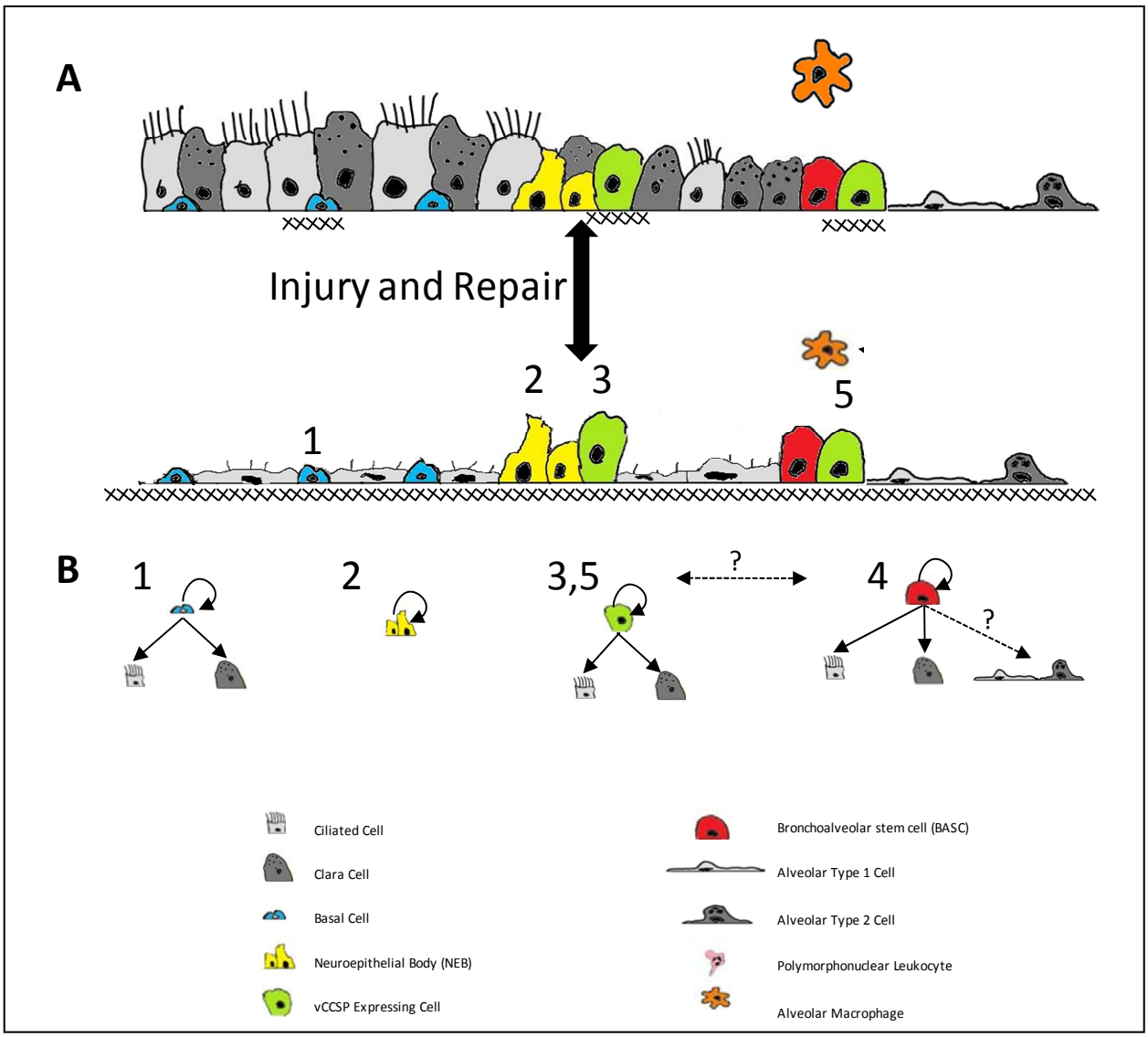

Figure 4. Progenitor cells of the conducting airway epithelium.

Using *in vivo* and *in vitro* injury models the airway epithelium has demonstrated remarkable reparative capacity. **(A)** In the tracheobronchial epithelium, polydocanol or sulfur dioxide injury in mice has revealed the existence of a subpopulation of injury resistant label retaining basal cells capable of restoring each cell type of the proximal airway epithelium. Retroviral lineage tracing has also been used to hierarchically organize human bronchial epithelial cells according to their clonogenic and differentiation potentials. Progenitor cells of the bronchiolar epithelium include an abundant pool of Clara cells and naphthalene-resistant cells. Both Clara cells and naphthalene resistant cells express CCSP yet only Clara cells are ablated following naphthalene exposure.

Figure 4 Continued.

Naphthalene resistant CCSP expressing cells, termed variant CCSP expressing cells (vCE), localize to neuroepithelial bodies (NEB's) within proximal bronchioles, the bronchoalveolar duct junction (BADJ) of terminal bronchioles, and are capable of replenishing the cellular diversity of the epithelium following injury. Recent data have described a cell with similar properties to vCE cells that can be defined based upon their co-expression of CCSP and proSP-C. This cell type has been referred to as a bronchoalveolar stem cell (BASC) based upon the ability of fractionated cells to express markers of airway and alveolar lineages in vitro. The precise relationship between BASCs and vCE is not known. Also depicted is dynamic regulation and turnover of ECM during injury and repair. In other organs such as skin, this is a well known phenomenon that occurs during wound repair, however, it remains to be described in the context of airway epithelial repair. **(B)** Representation of cell fate for progenitor cell types represented in "A".

2.5 PROGENITOR CELLS IN AIRWAY REPAIR

2.5.1 Tracheobronchial Epithelium

Studies investigating progenitor cells of the tracheobronchial epithelium have benefited from a combination of *in vivo*, *in vitro*, and cellular transplantation models to reveal contributions made by distinct cell types of the normal epithelium towards maintenance and renewal. In vivo models have used a variety of agents to injure the epithelium including detergents such as polydocanol,[72] toxic gases such as ozone[82], nitrogen dioxide[82,83] or sulfur dioxide[72] parenterally administered toxicants such as naphthalene[84], and mechanical wounding of the epithelium[85]. Using these models both basal and nonciliated secretory cells have been shown to exhibit progenitor potential. In this context, the term progenitor cell refers to any proliferative cell defined by stable incorporation of [H^3]-thymidine or BrdU into its nuclear DNA. Cell fractionation and retroviral lineage tracing coupled with functional analysis in reconstituted tracheal grafts has allowed detailed analysis of the differentiation potential and clonogenic capacity of these progenitor cells in both mouse and human epithelia. These approaches have revealed subpopulations of tracheobronchial basal cells that can be distinguished according to their label retention, differentiation potential, clonogenic capacity, and the ability to efflux Hoechst 33342 dye (termed side population cells)[72,86-88]. Recently, related experiments using more sophisticated

in vivo lineage tagging approaches have confirmed results from xenograft experiments and indicate that a subpopulation of cytokeratin 14 expressing cells exhibit both multipotent differentiation potential and significant clonogenic capacity[89,90]. Collectively these data reveal a number of progenitor cell types that contribute to maintenance and repair of the tracheobronchial epithelium, some of which exhibit significant clonogenic potential in vitro or in tracheal grafts and is suggestive of the existence of local tissue stem cells in adult proximal airways.

The observation of a less abundant population of infrequently cycling basal cells within intercartilagenous regions of the tracheal epithelium and the ducts of submucosal glands provided the first direct evidence suggesting the existence of stem cells within tracheobronchial airways. These cells were found to express high levels of cytokeratin 5 and when isolated were greatly enriched for in vitro clone-forming cells. Among the clone forming cells approximately 5% had the capacity to generate large clones analogous to highly clonogenic cells observed *in vivo* and in transplantation experiments[91]. These findings reinforce the concept that basal cells are a heterogeneous population that includes abundant transit-amplifying populations in addition to a rare subset of cells with properties of resident tissue stem cells which include label retention, localization to a defined microenvironment, and clonogenic potential (Figure 4).

2.5.2 Bronchiolar Epithelium

Cell type selective toxicants have been used extensively to reveal progenitor cell types contributing to epithelial repair. Seminal work by Evans and colleagues used oxidant gases to selectively injure ciliated cells and show that airway epithelium is repaired through a non-ciliated progenitor[82]. They went on to demonstrate that proliferating Clara cells lose ultrastructural

features typical of the quiescent state, giving rise to a cell type that was termed the type A Clara cell. Based upon this analysis, type A Clara cells were distinguished from their mature quiescent counterparts based upon lack of secretory granules and smooth endoplasmic reticulum, and their ability to incorporate labeled DNA precursors. Type A cells contribute to repair by actively proliferating and differentiating into mature Clara cells and terminally differentiated ciliated cells. These studies identified Clara cells as an abundant facultative transit-amplifying progenitor cell with the capacity for bipotential differentiation and suggested that the normally slow rate of epithelial renewal in the steady-state could be dramatically increased in the setting of airway injury[83] (Figure 3A,B). Clara cells are analogous to transit-amplifying cells of the gut and epidermis, yet have the important distinction of quiescence and other specialized functions in the steady-state including immunoregulation and xenobiotic metabolism, thus they are referred to as facultative transit amplifying cells rather than obligate transit amplifying cells.

Experimental demonstration of an airway epithelial pool of putative tissue stem cells was made through use of injury models, in which the abundant facultative progenitor cell, the Clara cell, was specifically ablated. Clara cells represent one of the principal sites in the lung at which endogenous and xenobiotic lipophilic compounds are metabolized through phase I oxidation reactions such as those catalyzed by cytochrome P450 (CyP450) monooxygenases. This function of Clara cells renders them particularly susceptible to injury by xenobiotic chemicals that serve as substrates for members of this class of enzymes, and represents the basis for selective ablation of Clara cells in mice following exposure to naphthalene[92-94]. Specifically, cytochrome p450 2F2 is expressed in Clara cells of the conducting airway epithelium and bioactivates naphthalene to a stereoselective and highly reactive 1R-2S-Napthalene oxide[95]. The utilization of high doses of naphthalene overwhelms phase II metabolism, severely depletes

glutathione stores, and leads to cellular toxicity due to accumulation of highly reactive epoxides and quinones capable of forming protein aducts[96]. Use of this injury model in mice allowed identification of two putative stem cell niches in bronchioles based upon the resistance to naphthalene induced injury and distribution of regenerating epithelial foci containing nascent Clara cells (Figure 4). The first was located predominantly at airway branchpoints found in close proximity to neuroepithelial bodies (NEB)[84]. NEB associated regenerative foci harbored two proliferative populations of nonciliated cells, one expressing Clara cell secretory protein (CCSP) and one expressing the pulmonary neuroendocrine cell (PNEC) specific marker, calcitonin gene related peptide (CGRP)[73,97,98]. A second microenvironment contributing to replacement of depleted Clara cells was located in the terminal bronchiolar epithelium adjacent to the bronchoalveolar duct junction (BADJ)[84]. Chemically resistant proliferative cells located at the BADJ express the secretory cell marker CCSP and unlike regenerative foci in more proximal airways, lack a restricted association with PNEC's[99].

The critical role played by NEB and BADJ associated CCSP expressing cells in repair of Clara cell depleted airways was demonstrated using a transgenic mouse model allowing conditional ablation of naphthalene sensitive and resistant CCSP expressing cells. In this model, airway repair was completely abrogated through directed expression of the suicide gene herpes simplex virus thymidine kinase (HSV-tk) in all CCSP expressing cells. These data suggested that CGRP (+) PNECs are not the progenitors of the airway epithelium[74]. These studies clearly identified up to two distinct populations of CCSP expressing cells that are sequestered within the bronchiole of normal adult mice. Of these populations, rare NEB and BADJ associated CCSP expressing cells share the property of infrequent proliferation relative to their more differentiated Clara cell counterparts[74,99]. Similarities between rare naphthalene resistant CCSP expressing

cells and tissue stem cells of other organs form the basis for their designation as a putative bronchiolar stem cell that is sometimes referred to as either the variant Clara cell (vClara) or variant CCSP expressing cell (vCE)[74]. Further distinctions were made between bronchiolar stem and Clara cells based upon the observation of rare CCSP expressing cells that co-express the alveolar type 2 cell marker surfactant protein C (SP-C), that these cells were localized to the BADJ, and that they were resistant to naphthalene. Cells with this molecular phenotype were observed in preparations of distal airway/alveolar epithelial cells and could be enriched from this crude cell preparation based upon their unique expression of stem cell antigen-1 (SCA-1) and CD34. The observation that in vitro culture of these cells resulted in the expression of aquaporin 5, a gene commonly associated with AT1 epithelial cells, led to the conclusion that they harbored the capacity for both bronchiolar and alveolar differentiation and formed the basis for their designation as bronchoalveolarstem cells (BASCs)[100]. However, no in vivo data directly demonstrate that a BADJ associated CCSP expressing population has the capacity for bronchiolar and alveolar differentiation. As such, the similarity between variant Clara cells and BASCs has not been established (Figure 4B). Moreover, recent studies investigating the cell surface phenotype of epithelial cells from mouse conducting airways indicate that although cell surface SCA-1 allows for discrimination of conducting airway and alveolar epithelial cells, it does not distinguish the local stem cell population residing within distal bronchioles from the more abundant population of Clara cells[101]. Collectively, these data indicate that the airway epithelium harbors a unique stem cell hierarchy that maintains the unique cellular heterogeneity required for normal physiological function. How this progenitor cell hierarchy is deregulated in the setting of CLD has yet to be determined. However, several hypotheses have been suggested and are presented in the following section.

2.6 ROLES FOR PROGENITOR CELLS IN CHRONIC LUNG DISEASE

2.6.1 Chronic Lung Disease Pathology

Chronic lung diseases (CLD), such as obliterative bronchiolitis (OB), chronic obstructive pulmonary disease (COPD), and asthma are characterized by remarkable epithelial and mesenchymal remodeling that includes but is not limited to: chronic injury to the airway epithelium, decreased abundance of Clara cells, goblet cell hyperplasia, mucus cell metaplasia, subepithelial basement membrane thickening, fibrotic nodules causing stenosis of small airways, airway smooth muscle hypertrophy, and uncontrolled lymphocytic, neutrophilic, and monocytic inflammation[102-105]. Accordingly, understanding the etiology and progression of CLD has been complicated due to the complex network of cellular cross-talk present in the lung. Defective airway epithelial repair has been proposed as an early event in the initiation of CLD and chronic defects in reparative capacity and cellular composition may further contribute to disease progression and susceptibility to exacerbation[106]. This implies that normal functions for facultative progenitor and stem cells are compromised. Evidence suggesting that this may be the case comes from analysis of biomarkers of epithelial remodeling that have been used to follow severity and progression of lung disease. Levels of CCSP in airway lining fluid or serum are uniformly reduced in the setting of chronic lung disease as discussed above, suggesting that

epithelial remodeling involves altered differentiation or cell death of this critical bronchiolar progenitor, as CCSP is a marker for Clara cells lining the conducting airway epithelium[6,107].

2.6.2 Chronic Injury and Defective Epithelial Repair

Increasing evidence from studies in humans and animal models suggest that chronic injury and inflammation inhibits normal epithelial repair and differentiation leading to remodeling of the entire epithelial mesenchymal trophic unit (EMTU)[105]. Chronic exposure to xenobiotic and biological flora has been postulated to play a causative role in the development and exacerbation of chronic lung disease. As an example, cigarette smoke causes extensive airway epithelial injury, a robust inflammatory response in the lung, and is the principal epigenetic factor contributing to the development of chronic obstructive pulmonary disease[108]. Cigarette smoke can have a variety of detrimental effects on the lung including damage to the epithelial, mesenchymal, and endothelial compartments[109]. This includes damage to Clara cells as indicated by decreased abundance of CCSP protein in asthmatic BAL and lung tissue sections[110]. *In vitro* studies have demonstrated that cigarette smoke can severely blunt epithelial wound repair by decreasing the rate of cell proliferation, migration, and altering extracellular matrix remodeling[111,112]. Paradoxically, in another study, *in vitro* models indicated that low levels of cigarette smoke condensate can significantly increase proliferative potential of epithelial cells[113]. Together, these observations have been extended to *in vivo* model in which chronic cigarette smoke exposure in mice was shown to attenuate epithelial repair following naphthalene induced Clara cell injury[114]. Epithelial cell injury and persistent inflammation that are both associated with cigarette smoking have also been demonstrated to blunt tissue repair in

models of epidermal wound healing[115]. These studies indicate that proper epithelial repair can be severely altered by environmental challenge.

2.6.3 Extracellular Matrix Deposition and Remodeling

As discussed above (section 2.2.), the diameter of the conducting airways greatly attenuates along the proximal to distal axis. Therefore, proper epithelial and mesenchymal structure is necessary to prevent occlusion of the airways and inhibition of gas transfer. In fact, occlusion of the small airways is often a result of invasion of the airway lumen by fibrotic foci generated from aberrant ECM accumulation and fibro-proliferation, over-production of mucus, smooth muscle hypertrophy, and excessive cellular exudates [116,117]. Occlusion ultimately leads to compromised lung function through declining airflow into and out of the alveolus. Therefore understanding mechanisms leading to uncontrolled epithelial and mesenchymal remodeling of the airway is essential for developing strategies for therapeutic intervention in chronic lung diseases.

Mechanisms contributing to tissue remodeling involve changes in the abundance and activity of key matrix remodeling enzymes leading to excessive depletion of elastin[118] and other structural matrix components critical for maintenance of tissue architecture. However, tissue remodeling also includes fibroproliferative responses that lead to inappropriate deposition of matrix molecules. Recent studies have indicated that the proteoglycan hyaluronon (HA), a normal component of basement membrane, deposited during epithelial injury and essential for restoration of lung homeostasis[119]. In fact, recent work has shown that CD44 and TLR4/TL:R2 are critical for clearance and signaling of HA fragments, respectively[120,121]. Mice deficient for

CD44 are more susceptible to bleomycin induced lung injury as marked by increased mortality, inflammation, and deposition of HA in the lung[120]. On the other hand deletion of TLR4 and TLR2 negatively impacts mortality rates following bleomycin induced lung injury, as HA can also promote epithelial survival[121]. These studies demonstrate that ECM deposition following lung injury plays an instrumental role in repair. However, if removal or degradation of this ECM protein is inhibited allowing for accumulation of this matrix protein, restoration of lung homeostasis is severely impaired. Despite these studies, little is known regarding the cellular cross-talk between injured and repairing epithelium and the underlying mesenchyme. It has been postulated that the epithelial mesenchymal trophic unit (EMTU) is essential for proper epithelial repair and that in the context of defective repair this may lead to aberrant and chronic mesenchymal remodeling that includes extensive fibroproliferation, ECM deposition, and development of fibrosis. Further studies are warranted to determine the impact on ECM deposition and turnover during airway epithelial specific injury and repair, and how this process may be affected by inhibiting stem cell mediated repair.

2.7 MOLECULAR REGULATION OF THE STEM CELL HIERARCHY

Defining the molecular regulators of the stem cell hierarchy is critical as defects to progenitor cell utilization may result in loss of epithelial cell function and mesenchymal remodeling. Currently, investigation into mechanisms regulating the airway stem cell hierarchy have focused predominantly on genetic manipulation of candidate signaling pathways and molecules with established roles as regulators of lung development or carcinogenesis. These include canonical WNT signaling through stabilization of β-catenin (CATNNB1) in addition to signaling through MAP kinase, KRAS, PTEN, GATA-6, and BMI1. These studies have typically relied upon knock-out, ectopic expression strategies, or the use of conditional gene manipulation approaches, that lead to altered expression of key regulatory molecules. Ectopic activation of CATNNB1, KRAS signaling, or developmental loss of either GATA-6, PTEN, PI3 kinase and p38α MAP kinase, have all been found to result in increases in the abundance of CCSP/Pro-SPC dual immuno-positive cells that are believed to represent bronchiolar stem cells[23,100,122-127]. Changes in the pool size of bronchiolar progenitor cells have been investigated in many of these models through analysis of the cell surface phenotype described by Kim and co-workers, including SCA-$1^{positive}$/$CD34^{positive}$ cells within the $CD45^{negative}$/$CD31^{negative}$ viable fraction of dissociated lung cells[100]. However, even though changes in these signaling pathways result in the expansion of putative stem cells based upon the use of these markers, the absence of a comprehensive molecular phenotype for bronchiolar stem cells that distinguishes them from other airway

progenitor cell types suggests that the impact of altered signaling on stem cells *per se* can not easily be determined. In this context, functional changes in epithelial repair capacity involving use of injury models that are known to result in activation of putative stem cells has the potential to provide a more direct means to interrogate changes in progenitor function. For instance, activation of CATNNB1 signaling within the bronchiolar epithelium of the late embryonic mouse lung results in an increase in the abundance of naphthalene resistant bronchiolar cells, expansion of a Sca-1^{positive}/CD34^{negative} fraction of airway epithelial cells that co-expressed CCSP and Pro-SPC, and reduced autofluorescent character of fractionated epithelium, a property representative stem cells[101]. However, the lack of identified signaling pathways that regulate airway epithelial repair continues to prevent more sophisticated analysis of the molecular regulation of stem cell mediated repair and therefore warrants a more global and unbiased description of the molecular signature of airway epithelial repair.

2.8 RATIONALE

There are only a handful of studies describing the basic mechanisms of airway epithelial repair. The signaling pathways between the epithelium and underlying mesenchyme following injury remain equally enigmatic. The few studies interrogating these mechanisms have focused on *ex vivo* and *in vitro* model systems calling into question their relevance to the complexity of the *in vivo* environment. This warrants an unbiased approach to identify novel *in vivo* molecular regulators of airway epithelial repair. The basic behavior of progenitor cells, their molecular regulators, and how each is impacted by disease would provide novel insights into disease pathogenesis and reveal new therapeutic targets that may allow modification of disease outcome. Furthermore, understanding the effects of abrogating epithelial repair on modulation of the EMTU and epithelial function will be equally important, especially as it relates to the initiation and progression of CLD. Therefore, this dissertation work seeks to test the hypothesis that **Epithelial reparative capacity moderates ECM dynamics and innate immunity (Figure 5).**

The existence of endogenous lung epithelial stem cells remains a controversial issue. To facilitate a more thorough understanding of progenitor cell behavior and the putative stem cell hierarchy will require development of novel endpoints to answer the fundamental questions outlined above. Moreover identification of molecular regulators of this hierarchy and how alterations to the hierarchy may perturb epithelial and mesenchymal function will be equally important. The studies presented in this dissertation work will bring the scientific community

one step closer to the development of cellular and molecular strategies for therapeutic treatment of lung disease.

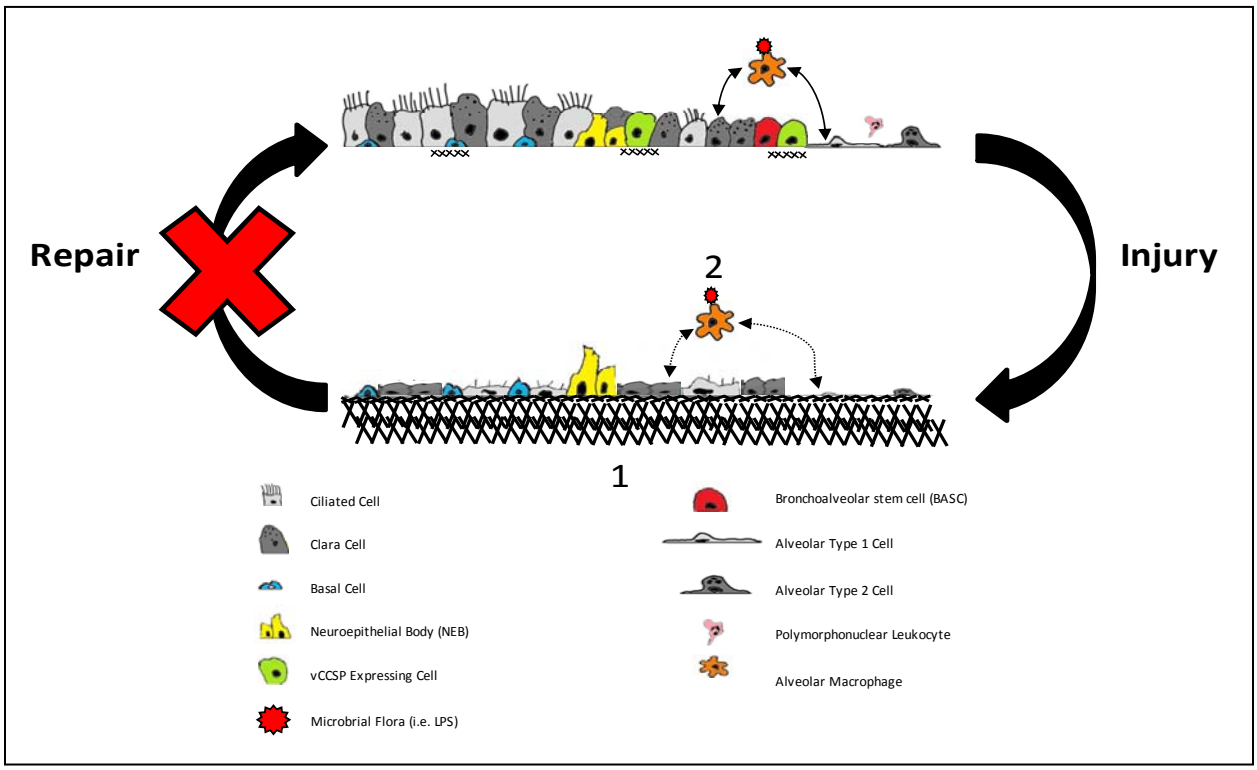

Figure 5. Dissertation research rationale.

(1) A significant paradigm that has emerged suggests that airway epithelial repair is essential for maintenance of ECM dynamics in the lung. This implies that the aberrant and excessive accumulation of ECM in chronic lung disease may be a result of attenuated epithelial reparative capacity. Though this is an appealing model, there is no *in vivo* data suggesting that ECM accumulates during conducting airway epithelial injury and repair, nor is there evidence to suggest that blocking repair results in uncontrolled ECM deposition. In chapter 2 this paradigm is tested using *in vivo* models of productive and abortive airway epithelial repair. (2) As described in the text and presented in Figure 1, the airway epithelium plays an important role in host defense. Recent work has demonstrated that significant cross-talk occurs between Clara cells and resident lung macrophages which directly regulates the inflammatory response. Therefore elucidating the factors secreted by Clara cells will provide significant insight into mechanisms regulating host defense. In addition, the significant remodeling of the airway epithelium observed in CLD suggests that epithelial function has been altered (broken arrows). However, the signaling pathways that have been perturbed have yet to be identified. In chapter 4, using *in vivo* models of epithelial injury, decreased Clara cell

Figure 5 Continued.

function (note the lack of secretory granules in Clara cells), and inflammation, the hypothesis that Clara cells moderate the inflammatory response through regulation of macrophage behavior is tested.

3.0 THE REPARATIVE CAPACITY OF AIRWAY EPITHELIUM IMPACTS DEPOSITION AND REMODELING OF EXTRACELLULAR MATRIX[128].

3.1 EXPERIMENTAL RATIONALE AND HIGHLIGHTED RESULTS

Defective epithelial repair in the setting of chronic lung disease has been suggested to contribute to uncontrolled extracellular matrix deposition and development of fibrosis. This hypothesis was tested through gene expression profiling of total lung RNA isolated from mouse models of selective epithelial cell injury that are associated with either productive or abortive repair. Analysis of gene expression in repairing lungs of naphthalene exposed mice revealed prominent clusters of up-regulated genes with putative roles in regulation of the extracellular matrix and cellular proliferation. Further analysis of tenascin C, a representative matrix protein, in total lung RNA revealed a transient 4.5 fold increase in mRNA abundance 1 day following injury and a return to steady-state levels by recovery day 3. Tenascin C was deposited in the peribronchiolar mesenchyme immediately following injury and was remodeled to basement membrane subtending the bronchiolar epithelium during epithelial repair. Epithelial restitution was accompanied by a decrease in tenascin C mRNA and protein expression to steady-state levels. In contrast, abortive repair using a transgenic model allowing ablation of all reparative cells led to a progressive increase in tenascin C mRNA within lung tissue and accumulation of its gene product within the sub-epithelial mesenchyme of both conducting airway and alveolar

epithelium. These data demonstrate that the extracellular matrix is dynamically remodeled in response to selective epithelial cell injury and that this process is activated without resolution in the setting of defective airway epithelial repair.

3.2 INTRODUCTION

The epithelial-mesenchymal trophic unit (EMTU) is a complex arrangement of epithelial cells, fibroblasts, smooth muscle, and extracellular matrix[106]. Dynamic interactions between these components are critical for the process of lung development and continue into adulthood for regulation of normal tissue homeostasis and repair[13,129]. Chronic lung injury leads to permanent alterations to both cellular and extracellular components of the EMTU that lead to permanent declines in lung function. This is clearly seen in chronic lung diseases such as asthma and chronic obstructive pulmonary disease. Pathological changes to lung tissue that are associated with these diseases include fibroproliferation, accumulation and remodeling of extracellular matrix components, and altered epithelial cell function which together lead to airway obstruction[102,104,105]. However, the complexity of these interactions in the intact lung and the inability to effectively model these interactions in vitro, have led to difficulties in identifying critical factors that initiate the process of pathological tissue remodeling. Roles for epithelial cell dysfunction in the initiation and/or progression of this process have been proposed, although not tested *in vivo*[106,130].

The airway epithelium provides both a physical and biological barrier that functions to protect the host against invading microorganisms and inhaled pollutants[27,36,37,131,132]. The epithelium of bronchiolar airways turns over with very slow kinetics and is maintained in the

steady-state by the infrequent proliferation of an abundant facultative progenitor cell that is commonly referred to as the Clara cell[77,78,83,99]. Injury resulting in the depletion of Clara cells, such as that resulting from exposure to the aromatic hydrocarbon naphthalene, is repaired through the activation of local tissue stem cells residing at airway branch point associated neuroepithelial bodies (NEBs) and the bronchoalveolar duct junction (BADJ)[73,74,84,99,100]. Further studies have revealed that stem cells localized at the BADJ, termed bronchoalveolar stem cells (BASC)s, can be identified *in vivo* by co-expression of CCSP and sufactant protein C (SPC), isolated according to cell surface phenotype, and may have the *in vitro* capacity to generate cells of both bronchiolar and alveolar lineages[100]. Further research is necessary to understand the microenvironmental cues that regulate stem cell mediated epithelial repair.

Roles for matrix remodeling in regulation of airway repair are suggested from studies investigating mouse models carrying null alleles for selected matrix metalloproteinases. Matrix metalloproteinases (MMP)s are a family of membrane associated or secreted proteases which upon activation have the ability to degrade components of the ECM, epithelial cell junctions, and liberate tethered growth and chemotactic factors in response to wounding[133]. In recent work, matrix metalloproteinases have been shown to play key roles in regulating epithelial repair in the lung[134,135]. Chen and co-workers demonstrated that TIMP1 functions to inhibit airway epithelial repair, raising the possibility that increased levels of TIMP1 that are observed in diseases such as obliterative bronchiolitis may both attenuate epithelial reparative capacity and promote fibrosis[135]. These studies reinforce the concept that epithelial defects within the EMTU may initiate uncontrolled fibroproliferation and extracellular matrix (ECM) deposition[106]. To date, a description of ECM dynamics in the setting of stem cell mediated airway epithelial repair has not

been conducted. Therefore this study will investigate the molecular signature of epithelial repair to determine if ECM is a component of the injury and repair response.

In vitro studies have shown that inhibition of epithelial repair can augment pro-fibrotic signaling pathways, thereby supporting the model that epithelial repair can regulate ECM dynamics[136]. However, this has never been formally tested *in vivo.* In addition to providing a molecular signature of epithelial repair, this study will test the hypothesis that epithelial reparative capacity is a key regulator of extracellular matrix remodeling. Previously validated *in vivo* models of Clara cell ablation are utilized to demonstrate that ECM deposition, as measured by Tenascin C (TNC) mRNA and protein abundance, are dynamically and reversibly regulated during repair of epithelial lesions in airways. In contrast the loss of epithelial reparative capacity results in continued deposition of extracellular matrix without resolution. This study provides the first *in vivo* evidence that ECM deposition is a dynamic component of the EMTU during productive airway epithelial repair and suggests that defects to epithelial reparative capacity directly leads to matrix deposition through alterations within the EMTU.

3.3 MATERIALS AND METHODS

3.3.1 Animal Housing

Mice used in this study were housed in an AAALAC certified institutional vivarium under specific pathogen free conditions, 12 hour light/dark cycle, provided food and water *ad libitum*, and sentinels screened quarterly for pathogens. All mouse experimental procedures were approved by Duke and University of Pittsburgh IACUC.

3.3.2 Models of Airway Injury:

3.3.2.1 Ganciclovir Administration

Adult FVB/N CCtk mice were exposed to ganciclovir (GCV) as previously described[98,137]. Cytovene IV (GCV sodium, Hoffman-LaRoche, Inc., Nutley, NJ) was dissolved in pyrogen free saline and administered chronically through a 14 day miniosmotic pump (ALZET Osmotic Pumps, #2109D, ALZA Corp., Palo Alto, CA) resulting in a dosage of 4.5 mg/kg ganciclovir daily. Body weights were measured to evaluate realtime the extent of injury.

3.3.2.2 Naphthalene Administration

Male adult FVB/N (The Jackson Laboratory, Bar Harbor, ME) mice were injected intraperitoneal with Naphthalene (Sigma, St. Louis, MO) dissolved in sterile Mazola corn oil as previously described[73]. In brief, mice were injected with naphthalene (dosage indicated in text) in the

morning (8:00-10:00am) to normalize to diurnal fluctuations in glutathione. Body weights were measured to evaluate realtime the extent of injury.

3.3.3 Tissue Processing

At the time of sacrifice, mice were anesthetized through an intraperitoneal injection of ketamine and xylazine. Following entry into a surgical plane, mice were dissected and thoracic cavity opened. Plasma was collected from the right atrium using a 1ml tuberculin syringe followed by separation at 10,000 g for 10 minutes in a BD Microcontainer plasma separator tube (BD Microtainer, Becton, Dickinson and Company, Franklin Lakes, NJ). Mice were exsanguinated through scission of the inferior vena cava and trachea cannulated with an I.V. Catheter (BD Insyte, Becton Dickinson and Company, Franklin Lakes, NJ). Bronchoalveolar lavage (BAL) fluid was collected in 1 ml of PBS. The Left lung and accessory lobe were resected and homogenized in 2 ml 4M GIC and RIPA buffer with 1mM PMSF for total RNA and protein isolation, respectively. The remaining right lung lobes were inflation fixed at constant pressure for 20 minutes in 10% (v/v) buffered formaldehyde (Ricca Chemical Company, Arlington, TX). The right cranial lobe was cryopreserved in optimal cutting temperature (OCT) medium, sectioned in 5um increments with a cryostat (Microm HM550), and adhered to positively charged microscope slides (Ever Scientific, Unifrost Plus Microscopic Slides, EMSC200W+).

3.3.4 RNA Isolation and Microarray Analysis

RNA was isolated from left lung according to protocol by Chomczynski and Sacchi[138]. RNA quality was determined using a Nanodrop-1000 spectrophotometer (Nanodrop Technologies, Wilmington, DE) and Agilent 2100 Bioanalyzer (Agilent, Foster City, CA). All Microarray analysis was performed at the University of Pittsburgh Cancer Center Clinical Microarray core using Codelink 20K Mouse Bioarrays (Applied Microarrays, Tempe, AZ) according to manufacturers' suggested protocol. Bioinformatic analysis was conducted as previously described[139]. Differentially expressed genes were determined using the Scoregenes software package (Jerusalem, Israel). Relative change in gene expression was determined in a pair wise comparison of treatment to control. A significant change in gene expression passed the following criteria: t-test p-value <0.01, threshold number of misclassifications (TNOM) = 0, and regulation ≥ 2 fold relative to control. Genes fulfilling these criteria were hierarchically clustered using Scoregenes and visualized as a heat-map in Treeview (Eisen Laboratory, LBL, Berkely, CA).

3.3.5 Realtime PCR

Determination of relative mRNA abundance in total lung RNA was determined using quantitative realtime PCR according to established protocol. In brief, RNA was reverse-transcribed using a High-Capacity cDNA Synthesis Kit (Applied Biosystems, Foster City, CA) and an Applied Biosystems Veriti Thermocycler (Applied Biosystems, Foster City, CA). cDNA, RealMaster Mix (Qiagen, Valencia, CA), and gene specific Taqman FAM labeled probes and

primers (Applied Biosystems, Foster City, CA) were combined into a 96-well optical plate using the EpMotion 5070 automated pipeting system (Eppendorf, Hamburg, Germany) to increase precision of realtime data. Realtime PCR was conducted on a Realplex^4 EpgradientS (Eppendorf, Hamburg, Germany) according to protocol. The $\Delta\Delta^{CT}$ for realtime PCR was calculated to determine relative mRNA abundance[140]. An unpaired 1-tailed student's t-test was used to determine statistical significance ($p < 0.05$; where indicated by asterisk).

3.3.6 Enzyme Linked Immunosorbant Assay

CCSP protein in BAL and plasma samples was assayed with a CCSP sandwich ELISA. In brief, IgG purified (Millipore) goat anti rat-CCSP antiserum (capture antibody) was diluted in ELISA coating buffer, and incubated in a 96 well polystyrene high binding plate overnight (Costar 3590). After sample and rCCSP standard incubation, the plate was probed with rabbit anti rat-CCSP antiserum (primary detection antibody) and goat anti rabbit-HRP (Biorad). Absorbance was measured at 450nm using a microplate reader (EL808 Ultra Microplate Reader, Bio-tek instruments, INC).

3.3.7 Immunofluorescence and Microscopy

4-color immunofluorescence imaging was conducted using the following primary/secondary antibodies and nuclear stains. *Primary antibodies:* goat anti rabbit-CCSP (In House), rabbit anti human-tenascin-C (Chemicon), $Mouse_{IgG2a}$ anti-α-smooth muscle actin (Sigma), *Secondary*

antibodies: donkey anti-goat-660 (Invitrogen), donkey anti-rabbit-488 (Invitrogen), goat anti-mouse$_{IgG2a}$-594 (Invitrogen), *Nuclear stain:* DAPI (Sigma). Tissue sections were post-fixed in 100% ethanol for 10 minutes and rehydrated with sequential 3 minute washes in 95, 85, and 70% ethanol. The sections were incubated with Trypsin (Cellgro) for 5 minutes at 37°C and blocked in 5%BSA/PBS for 30 minutes. Primary antibody was diluted in 5%BSA/PBS and applied to each section overnight at 4°C in a humidified chamber followed by secondary antibody incubation in 5%BSA/PBS for 1 hour. Cross-reactivity of secondary antibodies was eliminated by blocking with normal goat serum. The slides were cover-slipped with DAPI(Sigma) and Fluouromont G mounting media (Southern biotech). Microscopic analysis was conducted using a Zeiss Observer.Z1 inverted fluorescent microscope (Carl Zeiss Inc.) and images processed in AxioVision Release 4.6.3 (Carl Zeiss Inc.) software.

3.4 RESULTS

3.4.1 Airway epithelial injury and repair regulates pro-mitotic signaling pathways and ECM dynamics.

Naphthalene induced acute Clara cell injury is repaired through activation of endogenous bronchiolar stem cells[74,99]. During repair both the epithelium, the initial target site of injury, and the underlying peri-bronchiolar mesenchyme proliferate[74]. To better define the cellular and molecular dynamics of the reparative process following naphthalene exposure, genome wide mRNA expression profiling was performed. Wildtype FVB/N adult male mice were exposed to 275mg/kg naphthalene and RNA isolated from total lung homogenate from unexposed control and 1, 2, 3, or 6 days after injury and used to screen oligonucleotide microarrays (N = 4/exposure group). Bioinformatic analysis identified a total of 4,751 transcripts with a significant > 2 fold change in gene expression. Genes were hierarchically clustered according to expression and displayed in Figure 6A as a heat-map. Using these selection criteria the gene expression signature of the repairing airway was determined to comprise of 3,552 up-regulated and 1,199 down regulated gene transcripts (Figure 6A, † and ‡, respectively).

A previous study established that the majority of down-regulated genes directly reflected loss of Clara cells and provided new tools to investigate the dynamics of Clara cell loss and regeneration[139]. This study focused solely on up-regulated gene transcripts, specifically those involved in regulation of cell proliferation and matrix remodeling. The relative mRNA

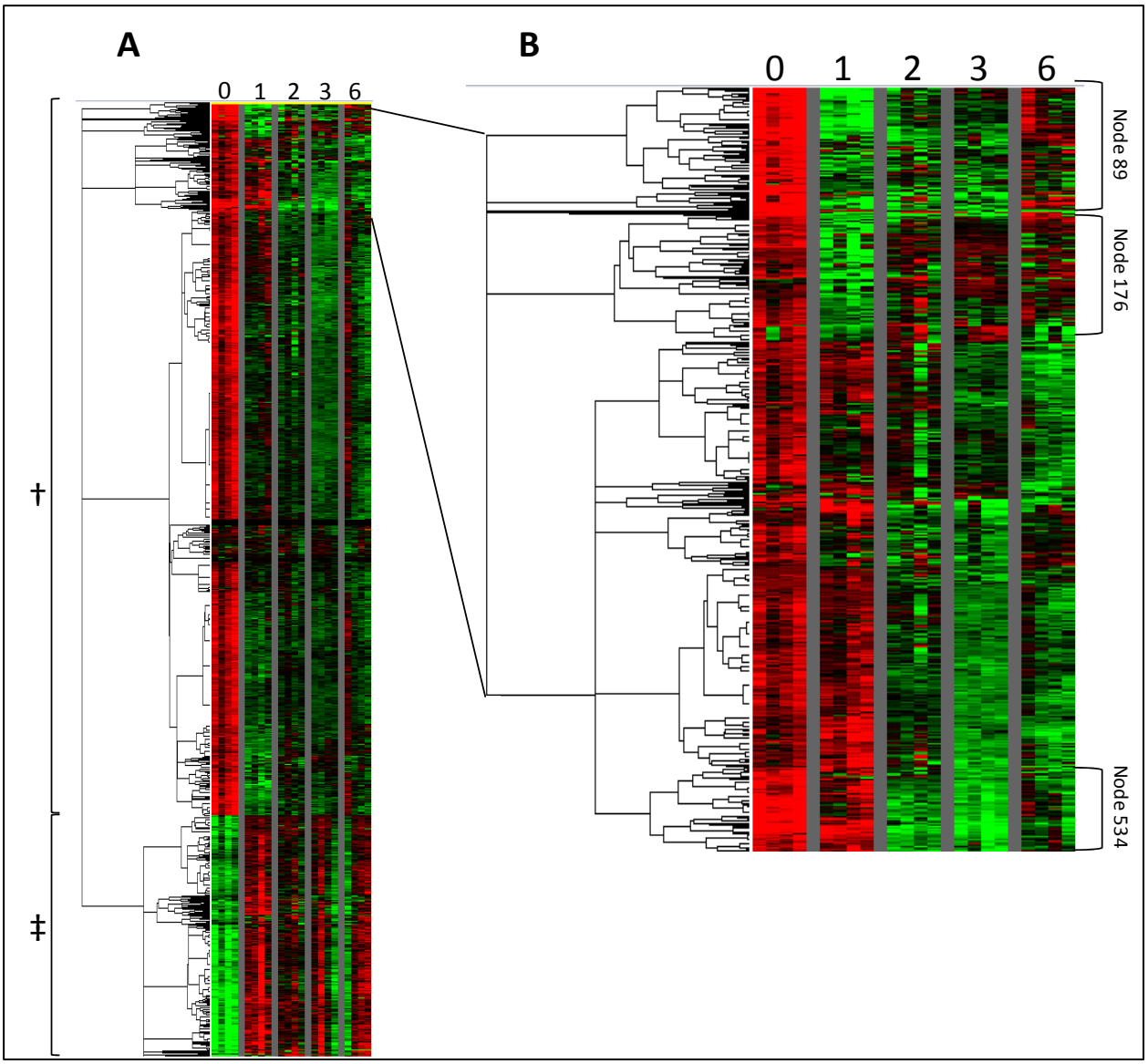

Figure 6. The gene expression signature of productive repair.

RNA from control (0) and1, 2, 3, or 6 days after naphthalene induced injury was isolated from whole lung homogenate and used for microarray analysis (N = 4/exposure group). Statistically significant gene expression changes relative to control were clustered and presented as a heat map. Red and green indicate down and up-regulated gene expression relative to control, respectively. Heat map representation of (A) all significant gene clusters and (B) magnification of the most informative gene clusters. Annotations for Nodes 89, 176, and 534 are included in Appendix A.1 Tables 1-3, respectively. († and ‡ denote clusters that are up-regulated and down-regulated relative to control, respectively).

abundance of representative genes from nodes 89, 176, and 534 (Figure 6B, Annotations are included in Appendix A.1 Supplementary Tables 1-3) were analyzed by realtime PCR to validate the bio-informatic process as well as verify gene expression changes to candidate signaling pathways (Figure 7 A-F, G, and H respectively). Genes selected for validation included AKP2, a potential marker for tissue stem cells (Figure 7A), pro-mitotic signaling molecules (Figure 7B,C, G), ECM modifiers (Figure 7D, E), and ECM (Figure 7F, H). Each of these genes demonstrated significant changes in gene expression over the time course of naphthalene induced airway injury and repair that were predicted by microarray analysis.

The expression pattern of selected genes identified by microarray screening throughout the processes of airway injury, repair, and resolution was investigated in more detail. Changes in the mRNA abundance of amphiregulin (AREG), tumor necrosis factor receptor superfamily member TNFSFR12A, and tenascin C (TNC), were interrogated by realtime PCR analysis of total lung RNA isolated from unexposed controls, 1, 2.5, 4, 8, and 12 hours or 1, 2, 3, 5, 10, 30 days after naphthalene (250mg/kg) injury (Figure 8). Naphthalene induced airway injury resulted in a rapid and dramatic increase in the abundance of AREG mRNA which was elevated by 3.1 fold 1.0 hour after exposure and reached a maximum increase of 12.8 fold 8.0 hours after exposure (Figure 8A). Messenger RNA abundance for AREG remained significantly elevated during the reparative phase following naphthalene exposure that included recovery day 5, and returned to near steady-state levels by day 10 and 30 (Figure 8A). Expression of TNFSFR12A mRNA showed a similar profile of expression to that of AREG, differences being a delay in gene induction and more rapid return to baseline levels (Figure 8B). Peak induction of TNFSFR12A occurred at the same 8 hour repair time point as observed for AREG, achieving >6-fold the level observed in steady-state lung. Expression of TNC mRNA was significantly increased by 2.5-fold

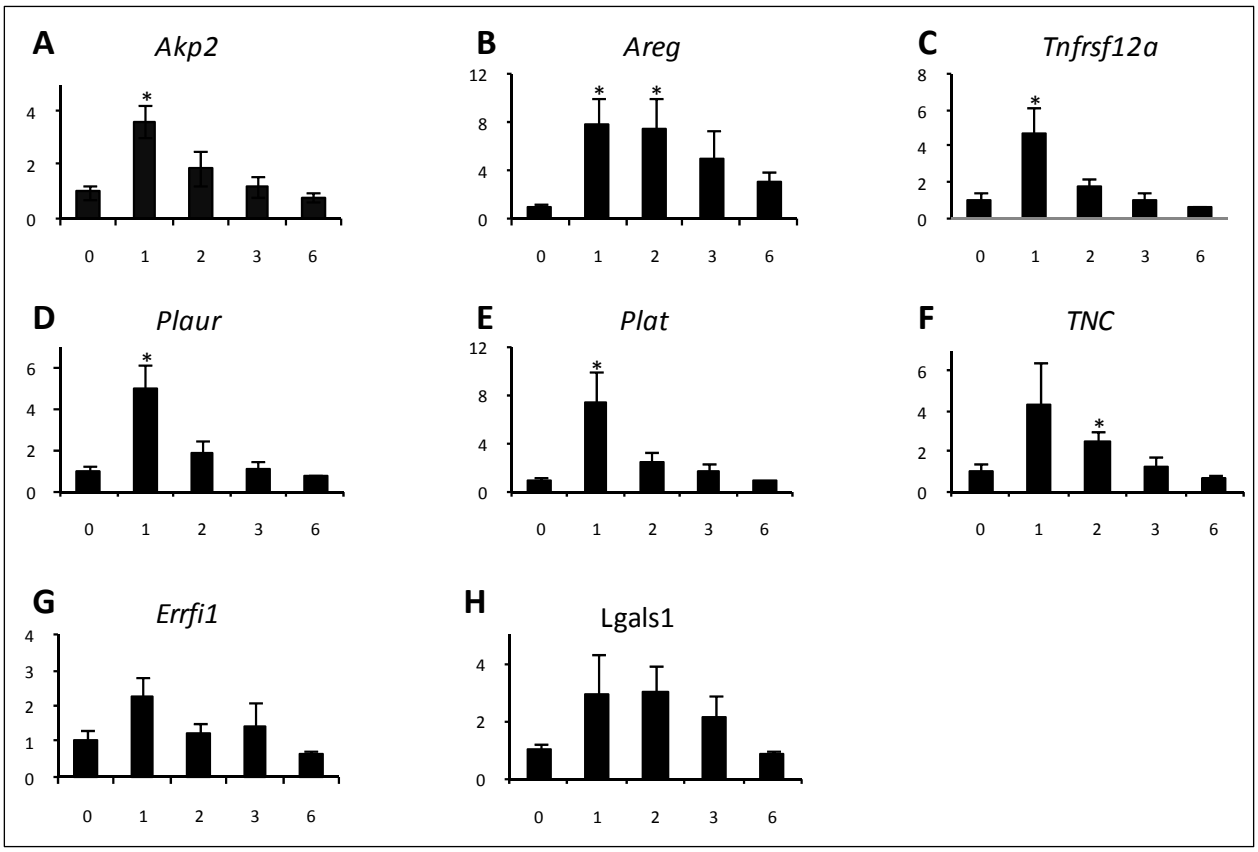

Figure 7. Realtime PCR validation of microarray analysis.

Messenger RNA abundance in total lung RNA samples from control (0) and 1, 2, 3, or 6 days after naphthalene injury was determined by realtime PCR analysis using Taqman probes and primers. Clusters were validated by quantifying mRNA abundance of representative genes from (A-F) Node 89, (G) Node 176, (H) Node 534. Data are presented as mean ±SEM.

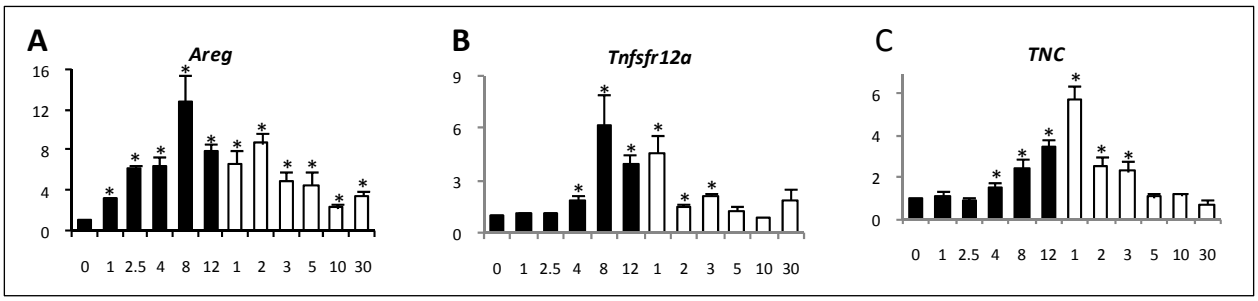

Figure 8. Pro-mitotic signaling pathways and ECM are dynamically regulated during acute Clara cell injury, productive repair, and resolution.

Total lung RNA was isolated from control (0) and 1, 2.5, 4, 8, or 12 hours (Black bars) and 1, 2, 3, 5, 10, or 30 days (White bars). Realtime PCR analysis was conducted to measure mRNA abundance of gene transcripts representative of (A,B) pro-mitotic signaling pathways and (C) ECM. Data are presented as mean ±SEM.

at 8.0 hours following injury, achieved peak levels of 5.8 fold steady-state levels at recovery day 1, and returned to near steady-state levels by 5 days (Figure 8C). These data indicate that robust and transient up-regulation of transcripts encoding pro-mitotic signaling molecules and ECM occurs following naphthalene induced Clara cell ablation and the ensuing phase of tissue repair.

3.4.2 ECM is reversibly and dynamically regulated during airway epithelial repair.

The kinetics of TNC protein accumulation during airway injury and repair was investigated. TNC was localized by immunofluorescence and the relationship to epithelial renewal and alterations in peribronchiolar mesenchyme evaluated through colocalization with CCSP (Figure 9A, D, E) and α-smooth muscle actin (α-SMA; Figure 9 C-E), respectively. Localization of TNC immunoreactivity within the steady-state epithelium revealed a subset of weakly positive mesenchymal cells that were positive for the myofibroblast/smooth muscle cell marker α-SMA (Figure 9B-D). No TNC immunoreactive protein was detected within other cell types of the airway or alveolar compartments. Magnification of panel 9D revealed the intense colocalization of TNC and α-SMA (Figure 9E). Acute Clara cell injury, as assessed by CCSP immunolocalization was prominent by day 1 (Figure 9F, I, J). The distribution and abundance of TNC immunoreactivity was dramatically altered during the early phase of repair after naphthalene exposure. Analysis of TNC immunoreactivity at 1 day post-exposure, the time point showing peak TNC mRNA accumulation, revealed intense up-regulation in the subepithelial mesenchyme (Figure 9G, I, and J). Colocalization with α-SMA revealed that deposition of TNC occurred within the underlying mesenchyme showing a broader range of expression than that defined by SMA immunoreactivity (Figure 9I, J).

To further define the dynamics of matrix remodeling that accompanied airway injury and repair, TNC, CCSP, and SMA were localized by immunofluorescent staining of lung tissue at 3,

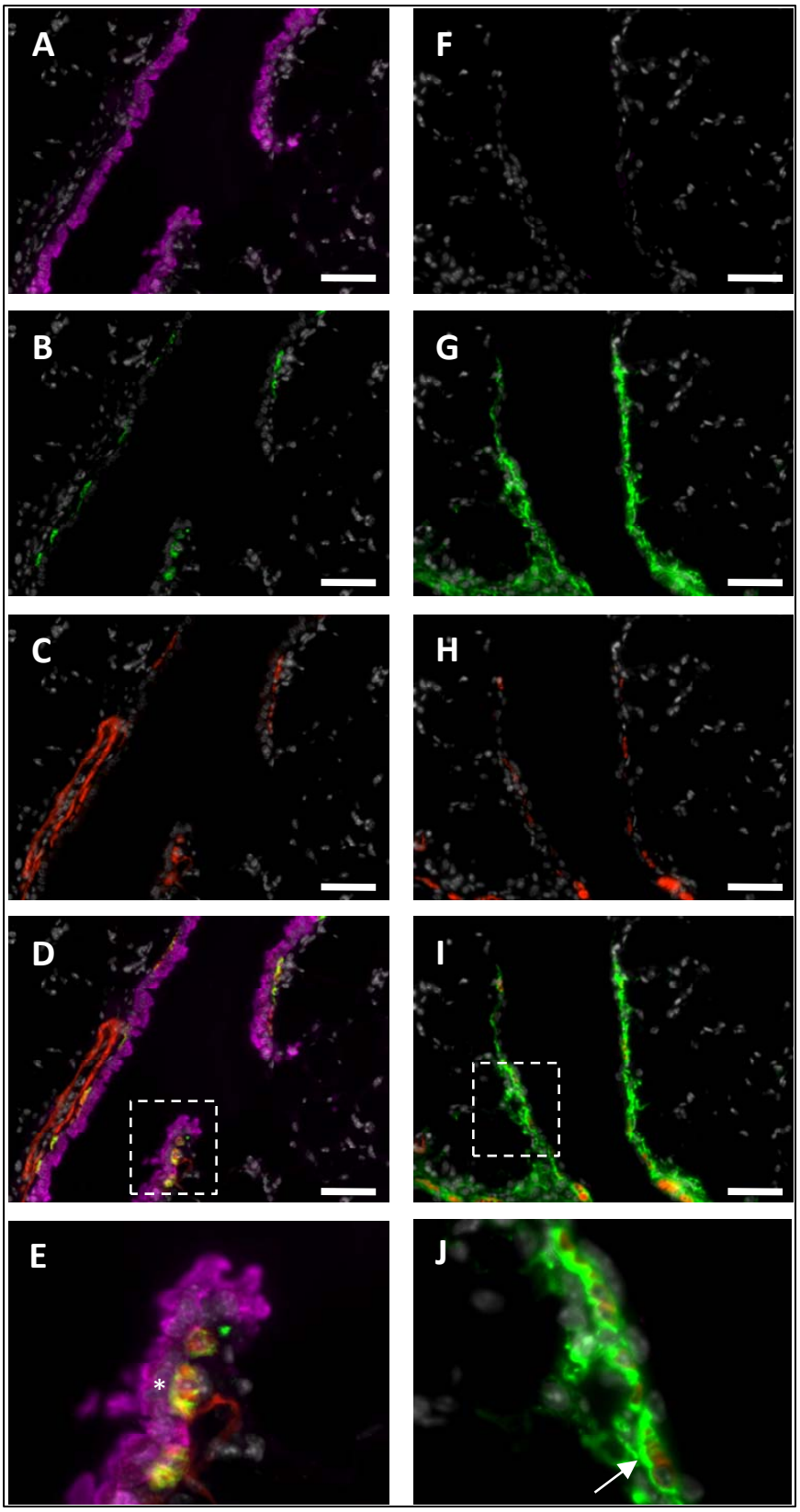

Figure 9. Extracellular matrix is deposited during productive airway epithelial repair.

Figure 9 Continued.

CCSP, TNC, and α-SMA were immuno-localized on formalin fixed and cryo-preserved lung tissue isolated at (A-E) control (0) and (F-J) 1 day post naphthalene. Representative pseudo-colored photomicrographs are shown of DAPI (Grey) merged with (A,F) CCSP (Magenta), (B, G) TNC (Green), or (C, H) α-SMA (Red). (D, I) 4-color merged images of control and 1 day post injury. (E, J) Magnification of areas denoted by a dashed rectangle (D,I). (Asterisk denotes co-localization, arrow indicates TNC subtending α-SMA positive cells) Representative images of the distal airway epithelium at 400x (scale bar = 50 μm).

5, and 30 days after injury (Figure 10 A-E, F-J, K-O, respectively). Domains of epithelial regeneration were defined by small clusters of CCSP(+) cells observed in terminal bronchioles at recovery day 3 (Figure 10 A, D, E). These repairing regions showed evidence of expansion at recovery day 5 (Figure 10F, I, J), with further expansion noted by recovery day 30 (Figure 10K, N, O). This pattern of repair closely mirrored the kinetics of cell proliferation and renewal observed in previous studies[99,139]. During this period of epithelial renewal TNC immunoreactive protein showed an overall decrease in abundance by day 3, displaying evidence for reorganization to the basement membrane immediately subtending the repairing airway epithelium (Figure 10E). A continuing decline in TNC immunoreactive protein was observed by day 5, with residual immunoreactivity observed in the sub-epithelial basement membrane (Figure 10J). The abundance and distribution of TNC immunoreactivity returned to near steady-state levels by recovery day 30 (Figure 10K-O). This pattern of TNC immunolocalization was also observed in the subepithelial region of more proximal airways (Appendix A.3 Figure 24). This dynamic pattern of altered TNC immunoreactivity demonstrates that nascent extracellular matrix is deposited following injury, reorganized to basement membrane subtending regenerating and injured airway epithelium, and returns to steady-state levels upon completion of successful airway epithelial repair. These data indicate that ECM is reversibly and dynamically regulated during productive airway epithelial repair.

3.4.3 Deficiency in epithelial repair leads to persistent matrix deposition.

Chronic lung injury has been associated with uncontrolled fibro-proliferation and deposition of ECM components including TNC[141]. Even though defects in epithelial repair have been

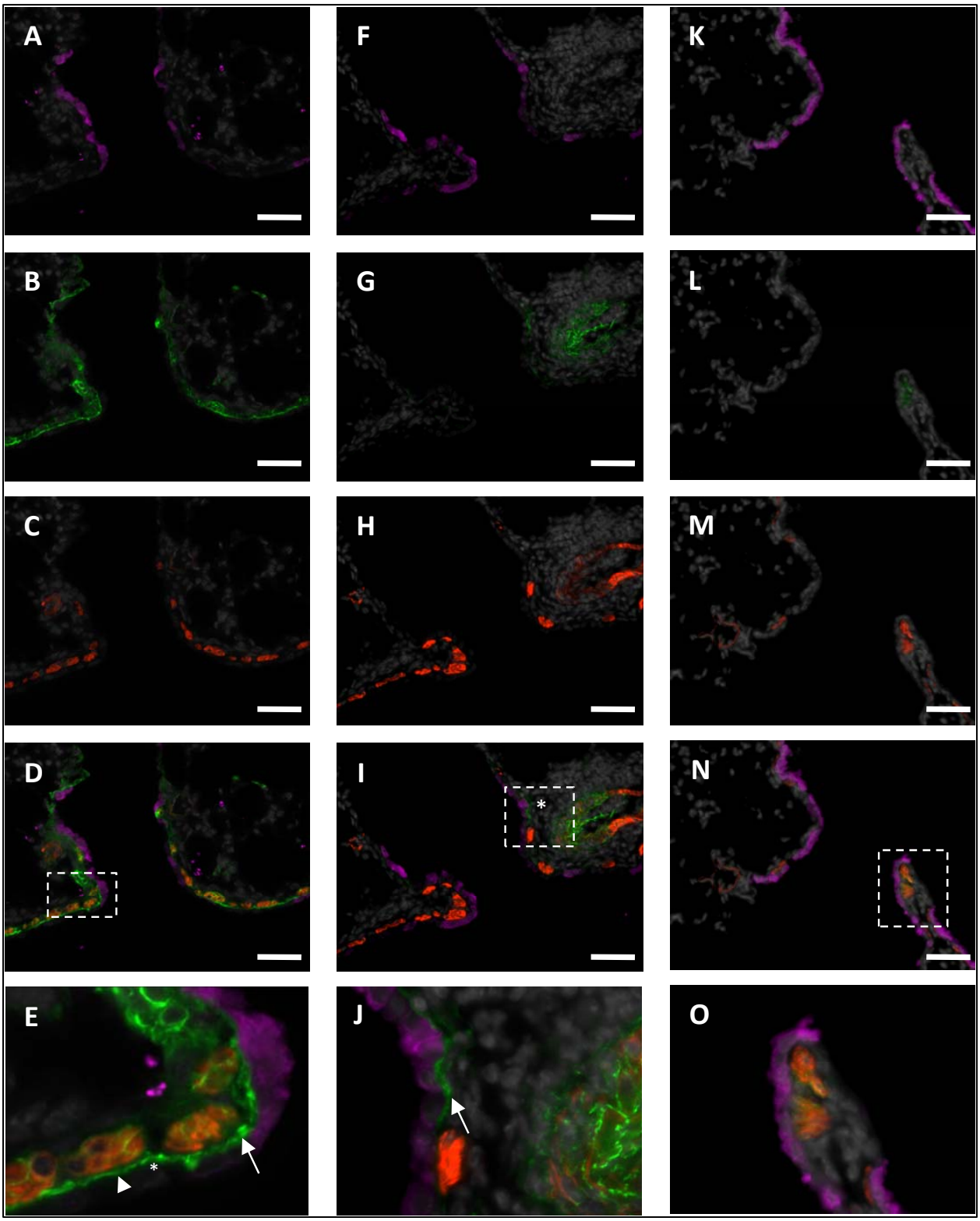

Figure 10. Epithelial repair is associated with matrix remodeling leading to restoration of steady-state levels and distribution.

Figure 10 Continued.

CCSP, TNC, and α-SMA were immuno-localized on formalin fixed and cryo-preserved lung tissue isolated at (A-E) 3, (F-J) 5, and (K-O) 30 days post naphthalene injury. Pseudo-colored images of DAPI (Grey) merged with (A,F,K) CCSP (Magenta), (B, G, L) TNC (Green), or (C, H,M) α-SMA (Red) of representative distal airway epithelium. (D, I, N) 4-color merged images of 3, 5, and 30 days post injury. (E, J, O) Magnification of areas denoted with by a dashed rectangle in (D,I, N). (Asterisk denotes TNC positive basement membrane independent of subtending α-SMA cells, arrowhead indicates TNC subtending injured epithelium associated with underlying α-SMA cells, arrow indicates TNC localized to basement membrane subtending regenerating units). Representative images of the distal airway epithelium at 400x (scale bar = 50 μm).

proposed as a contributing factor in fibroproliferation and matrix deposition this has not been demonstrated directly. To determine whether the transient increases in matrix deposition observed during productive repair of injured airways would be altered in a model of unproductive repair, in which repair was abrogated due to loss of tissue stem/progenitor cells. To achieve this, transgenic mice (CCtk) expressing *Herpes simplex virus* thymidine kinase (HSV-tk) in CCSP expressing cells were exposed to ganciclovir (GCV) to injure the airway epithelium and abrogate repair[74]. This model results in irreversible injury of all CCSP(+) epithelial cells and has been shown to result in alveolar dysfunction as well as fibroproliferation [137]. RNA was isolated from unexposed control (CCtk(-)) and CCtk (+) mice 3, 6, or 9 days after chronic GCV exposure in order to compare the gene expression signatures of injury/productive repair with injury/unproductive repair. Bioinformatic analysis identified 1,729 gene transcripts that were regulated by greater than two-fold between GCV injured CCtk mice relative to untreated control mice. These genes were hierarchically clustered and are presented as a heat-map in Figure 11A. The abortive airway epithelial repair gene signature is comprised of 1,656 genes whose mRNA's were increased by 2-fold or greater and 73 mRNA species showing greater than 50% decreases in their abundance (Figure 11A). Down-regulated gene transcripts were previously used to identify new and existing markers for mature Clara cells[139]. In an effort to further compare the productive and unproductive gene signatures, genes showing a robust pattern of mRNA induction were identified and displayed in node 278, which comprised 278 genes (Figure 11B and Appendix A.2, Table 4). The mRNA abundance for selected genes was determined using realtime PCR and recapitulated results obtained by microarray analysis (Figure 11 C-J). A difference between productive and abortive repair was observed for AKP2 and ERRFI1

(Compare Figure 7 with Figure 11), neither of which showed changes in mRNA abundance with abortive repair (Figure 11).

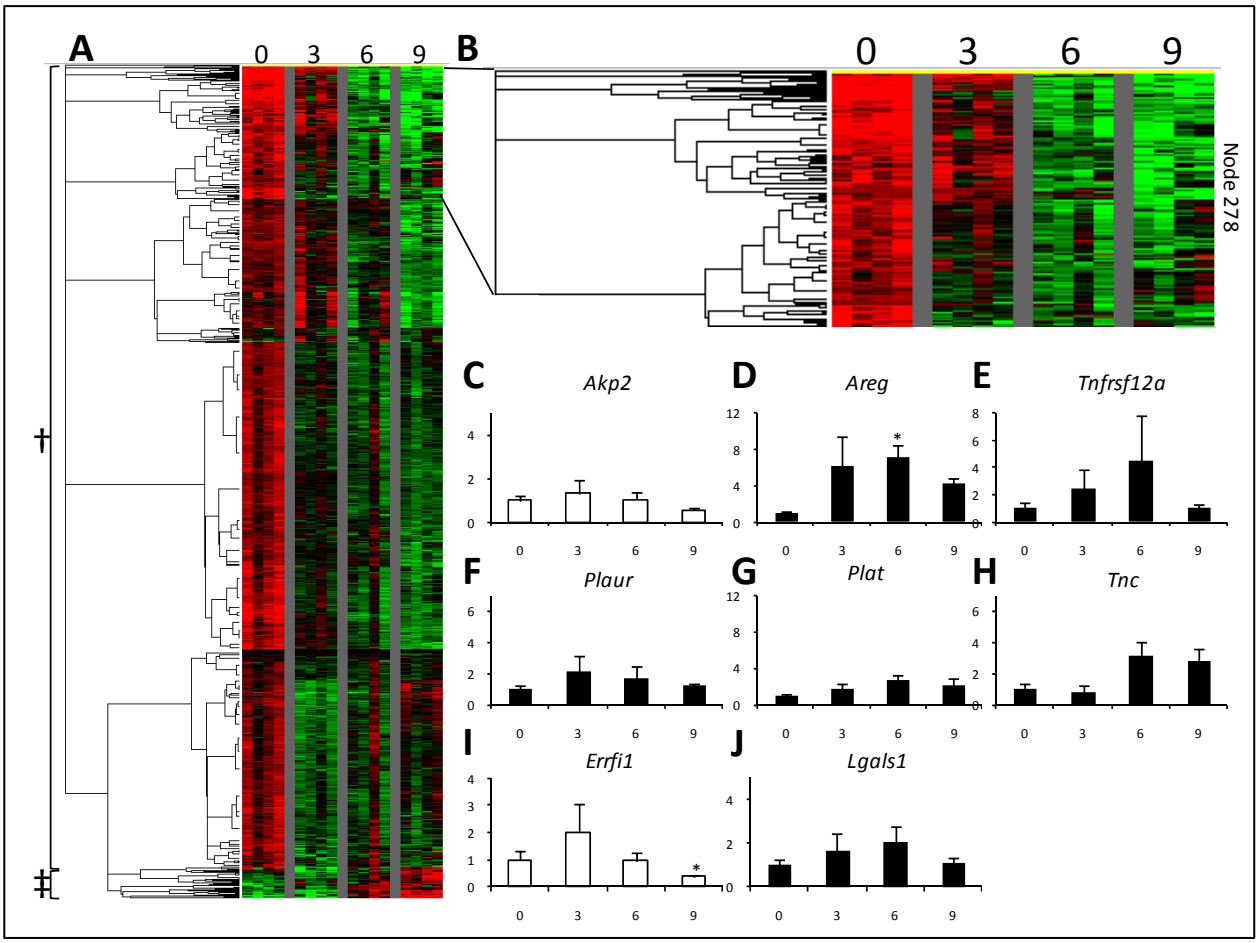

Figure 11. The gene expression signature of unproductive repair.

RNA from control (0, unexposed CCtk (-)) or CCtk (+) mice exposed to GCV chronically for 3, 6 or 9 days was isolated from total lung homogenate and mRNA abundance determined using microarray analysis (N =4/exposure group). Statistically significant gene expression changes relative to control were clustered and presented as a heat map. Red and green indicate down and up-regulated gene expression relative to control, respectively. Heat map representation of (A) all significant gene clusters and (B) magnification of the most informative gene clusters (Node 278). Annotations can be found in Appendix A.2, Table 4. († and ‡ denote clusters that are up-regulated and down-regulated relative to control, respectively). (C-J) mRNA abundance of genes representative of Node 278 were determined in total lung RNA samples from control (0) and 3, 6, or 9 days of chronic GCV exsposure by realtime PCR analysis using taqman probes and primers. White bar graphs indicate genes that were not regulated during chronic GCV exposure and therefore not present in Node278, but were

Figure 11 Continued.

included for comparison to productive repair. Y-axis scaling was adjusted to Figure 7 graphs to allow for comparison of fold-change in productive vs unproductive repair. Data are presented as mean ±SEM.

11 C, I; White Bars). These data support the notion that stem cell amplification and inhibition of EGFR signaling has been abrogated with loss of epithelial reparative capacity[142,143]. The abundance of AREG mRNA was chronically elevated in the abortive repair model compared to the transient increase observed in mice displaying productive repair (Figure 11D). In contrast, the mRNA for TNFRSF12A was transiently up-regulated in both injury models (Figure 11E). Genes whose products participate in remodeling of the extracellular matrix were chronically up-regulated in mice showing abortive repair, though less abundant (Figure 11F, G), as were those for extracellular matrix molecules TNC and LGALS1. These data indicate that there are significant differences in the abortive repair gene signature compared to productive repair that have potential to impact tissue remodeling.

To further explore the dynamics of extracellular matrix remodeling observed during abortive airway epithelial repair, the abundance and distribution of TNC expression was determined as a function of Clara cell abundance in control and GCV exposed CCtk mice. CCSP abundance was measured in total lung RNA, BALF, and serum to assess injury of Clara cells using molecular endpoints (Figure 12A-C). Ganciclovir exposure resulted in a reduction in CCSP mRNA abundance to 7.82% and 0.84% of control levels at days 6 and 10, respectively (Figure 12A). This was paralleled by decreases in CCSP content within airway lining fluid, which was reduced to 0.52% of control and undetectable levels at exposure days 6 and 10 (Figure 12B), respectively, as well as reduction in serum (Figure 12C). Evaluation of TNC mRNA abundance by realtime PCR revealed a 3.44 and 9.70 fold up-regulation at exposure days 6 and 10, respectively (Figure 12D). These results suggest that ECM, as assessed by TNC mRNA abundance, is continually deposited during defective epithelial repair. To verify that this was true at the level of protein accumulation TNC immunoreactive protein was measured by

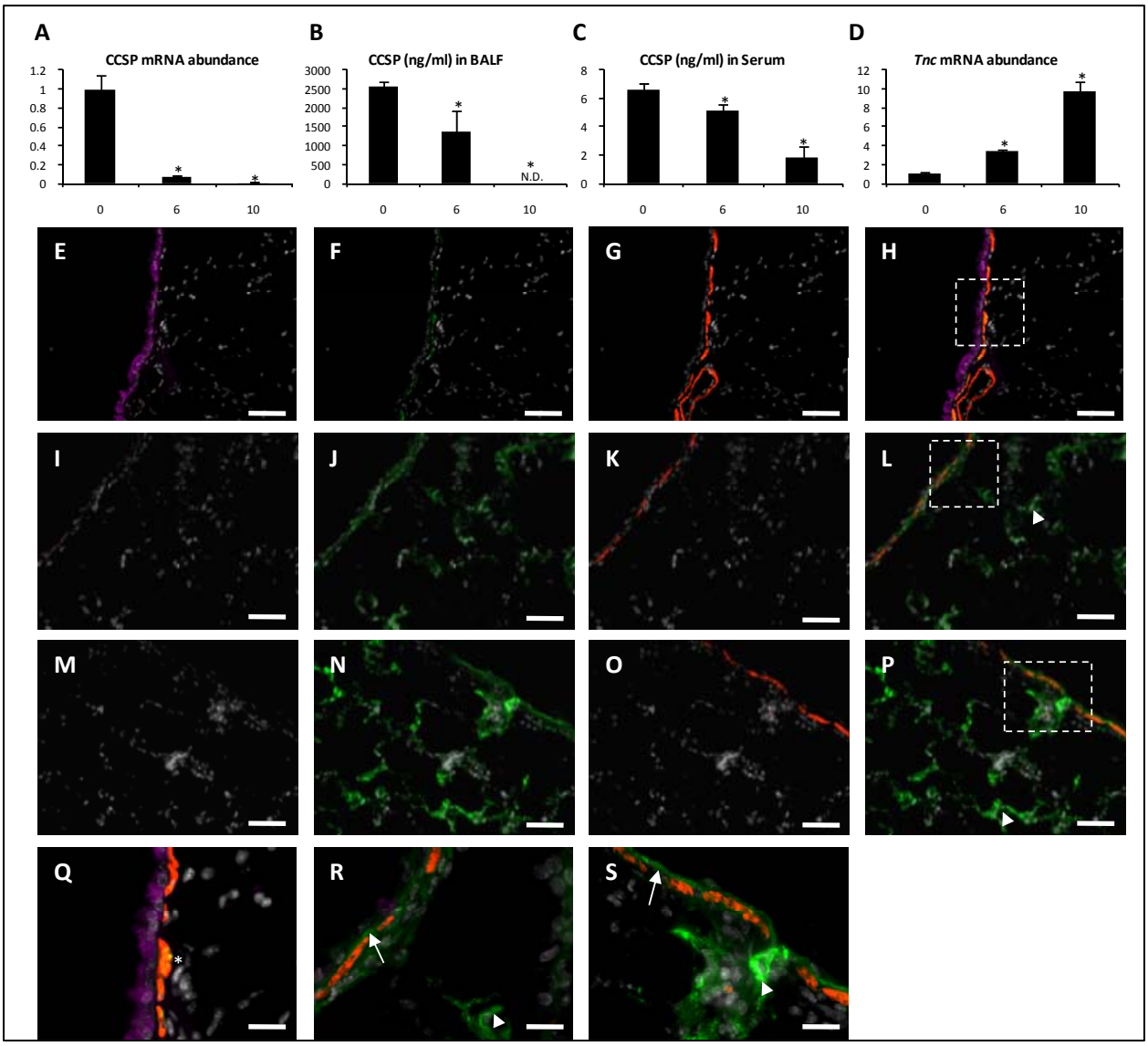

Figure 12. Multi-compartmental deposition of ECM in lungs of mice with non-repairing conducting airway epithelium.

Control (0, unexposed CCtk (-)) or CCtk (+) mice were administered GCV chronically for 6 or 10 days. (A) CCSP mRNA abundance in total lung RNA as measured by realtime PCR. (B,C) CCSP protein in BALF and serum, respectively, was measured using an ELISA. (D) TNC mRNA abundance in total lung RNA as measured by realtime PCR. CCSP, TNC, and α-SMA were immuno-localized on formalin fixed and cryo-preserved lung tissue isolated at (E-H) Control (0, unexposed CCtk (-)), (I-L) 6, and (M-P) 10 days following chronic GCV administration. Pseudo-colored images of DAPI (Grey) merged with (E, I, M) CCSP (Magenta), (F, J, N) TNC

Figure 12 Continued.

(Green), or (G, K, O) α-SMA (Red) of representative distal airway epithelium. (H, L, P) 4-color merged images of control, 3 and 10 days GCV treatment, respectively. (Q-S) Magnification of areas denoted with dashed rectangle in (H, L, K), respectively. (Asterisk indicates colocalization of TNC and α-SMA, arrow indicates TNC in basement membrane subtending injured airway epithelium, arrowhead indicates TNC deposited in the alveolar compartment). Representative images of the distal airway epithelium at 400x (scale bar = 50 μm).

immunofluorescent colocalization with CCSP and α-SMA. Analysis of control tissue revealed abundant CCSP (+) epithelial cells (Figure 12E, H, Q), the stereotypic distribution of TNC (Figure 12F, H, Q), and SMA (Figure 12G, H, Q). CCSP immunoreactive cells were greatly diminished 6 days after ganciclovir exposure (Figure 12 I, L, R) and was accompanied by increased TNC-immunoreactive protein subtending the airway and alveolar epithelium (Figure 12J, L, R). The abundance and distribution of α-SMA-immunoreactivity remained unchanged 6 days after chronic injury (Figure 12K, L, R). A further decrease in the abundance of CCSP-immunoreactive cells was observed following 10 days of ganciclovir exposure (Figure 12M, P, S). This was associated with further accumulation of TNC immunoreactive protein at the basement membrane subtending airway epithelium as well as peribronchiolar and alveolar mesenchyme (Figure 12N, P, S). No changes in α-SMA-immunoreactivity were observed (Figure 12O, P, S). These results indicate that defective airway epithelial reparative capacity results in chronic ECM deposition in airway and alveolar compartments. These data collectively provide the first experimental evidence that defects in epithelial reparative capacity are sufficient to drive excessive ECM deposition *in vivo*.

3.5 DISCUSSION

Defects in epithelial maintenance have been postulated to contribute to uncontrolled ECM deposition in fibroproliferative chronic lung diseases [136,144]. However, direct supportive evidence is lacking. This problem was addressed through the use of mouse models in which selective airway injury is associated with either productive or unproductive repair. Genome wide expression profiling identified clusters of regulated genes that included those encoding pro-mitotic signaling molecules and components of the extracellular matrix. Using tenascin C (TNC) as a prototypical matrix protein, this study demonstrates that ECM abundance is transiently up-regulated during acute injury and productive repair, and that this process continues without resolution in the setting of airway injury with unproductive repair. These data are the first to provide direct experimental evidence that ECM is dynamically regulated in the repair response to selective epithelial cell injury and that epithelial repair defects are sufficient to drive excessive matrix deposition typically observed in chronic fibroproliferative lung diseases.

Increased deposition of TNC has recently been shown to be a marker of chronic fibro-proliferative lung disease, such as obliterative bronchiolitis (OB)[141]. Furthermore gene expression analysis of tissue samples from non-smoking COPD patients revealed major alterations to gene transcripts involved in ECM deposition[145]. The observation that TNC can be deposited in response to epithelial cell injury but is only resolved following repair suggests that restoration of epithelial homeostasis is a critical factor in resolving otherwise persistent matrix

accumulation. ECM deposition is controlled by the combined regulation of protein synthesis and degradation. Studies in human lung indicate that TNC is expressed in cells of the subepithelial mesenchyme during development and in disease[146,147]. I*n vitro* studies also indicate that fibroblasts are a source of TNC expression[148]. It is likely that the increased expression of TNC in these studies occurs in the subepithelial mesenchyme as a result of fibroblast activation secondary to epithelial cell injury.

These data demonstrate that transcriptional activation of TNC occurs rapidly after injury and is immediately attenuated following initiation of productive repair. This is paralleled by a dramatic increase in TNC immunoreactive protein within the sub-epithelial mesenchyme. As productive repair ensues, TNC pools were initially reduced, resulting in either residual or reorganization of TNC protein at the basement membrane. Basement membrane associated TNC was later depleted at the time of epithelial renewal. These data imply that matrix deposition following epithelial injury and productive repair occurs in three stages: 1) transient synthesis of nascent TNC during the injury phase, 2) mesenchymal degradation, and 3) epithelial associated degradation during repair. In contrast these data demonstrate that TNC mRNA abundance and production are chronically elevated in both airway and alveolar compartments in the setting of unproductive repair. Previous studies have shown that chronic defects in airway repair result in disruption of alveolar homeostasis, which may provide the basis for the accumulation of TNC in this compartment[137].

Repair of acute epithelial lesions in airways is a highly regulated process involving a complex interaction between multiple cell types as well as the underlying ECM[106,149]. Lesions induced by exposure to naphthalene are highly selective for conducting airways due to its bioactivation within Clara cells, the abundant pool of facultative progenitors. The ensuing repair

process involves proliferation of naphthalene resistant cells that have been considered to be the local population of tissue stem cells[99]. Regulation of stem cell activity is likely mediated by concerted intrinsic and extrinsic cues derived from the surrounding cellular and a-cellular environment, referred to as a stem cell niche [150]. Currently the role of the ECM in regulation of niche dynamics and stem cell function has yet to be elucidated in the lung. This study shows that during productive epithelial repair, the ECM molecule TNC is dynamically regulated, including reorganization to basement membrane subtending regenerating and injured epithelium. Several studies have focused on the role of TNC in regulation of the stem cell niche, and suggest that TNC may regulate both proliferation and developmental progression of neural stem cells in the developing central nervous system [151,152]. These data are consistent with those from other studies demonstrating a critical role for TNC in regulating hematopoiesis [153]. Recent studies have implicated that TNC is upregulated following injury and is required for both proliferation and migration of scratch wounded cultured astrocytes [154]. Structural modeling and in vitro models have indicated that TNC-EGF domains can bind to EGFR and promote migration independently of effects on cell proliferation [155,156]. Together these data suggest that the deposition of TNC and reorganization to basement membrane subtending injured and regenerating epithelium may play a critical role in niche dynamics through regulation of proliferation and differentiation or migration of epithelial progenitors and nascent epithelium, respectively. Moreover, the chronic up-regulation of TNC in the setting of unproductive epithelial repair may also impact fibroblast behavior causing increased proliferation and cellular motility, thus exacerbating ECM production and remodeling. Future studies will test these observations in the setting of airway epithelial repair using mice deficient for TNC.

Since RNA was extracted from total lung homogenates, a caveat to this study is the under estimation of changes in gene expression that occurs during the process of airway injury and repair. Despite this caveat, other novel findings of the present study included the identification of several pro-mitotic signaling pathways regulated during airway epithelial repair. These included amphiregulin (AREG), a ligand for the epidermal growth factor receptor (EGFR), and TNFRSF12A, receptor for TWEAK, both of which have been shown to regulate hepatic progenitor cells[157-159]. Future studies will investigate the contribution made by these signaling pathways in regulation of airway repair and remodeling.

The airway epithelium provides a primary barrier between the host and the environment and plays an essential role in immuno-modulation in the lung. As such, immediate and effective repair after injury is required for maintaining lung homeostasis. Chronic fibroproliferative lung diseases are characterized by a remarkable deposition of ECM protein. In this study, the first experimental evidence to suggest that airway epithelial reparative capacity regulates ECM dynamics is presented. Furthermore, this study demonstrates that dynamic regulation of ECM is a component of productive airway epithelial repair and may play an essential role in regulation of this process.

4.0 CLARA CELLS ATTENUATE THE INFLAMMATORY RESPONSE THROUGH REGULATION OF MACROPHAGE BEHAVIOR[160]

4.1 EXPERIMENTAL RATIONALE AND HIGHLIGHTED RESULTS

Chronic lung diseases are marked by excessive inflammation and epithelial remodeling. Reduced Clara cell secretory function and corresponding decreases in the abundance of the major Clara cell secreted protein, CCSP, are characteristically seen in these disease states. To define the impact of Clara cell and CCSP depletion on regulation of the lung inflammatory response, chemical and genetic mouse models of Clara cell and CCSP deficiency (CCSP-/-) coupled with *P. aeruginosa* lipopolysaccharide (LPS) elicited inflammation were used. Exposure of Clara cell depleted or CCSP-/- mice to LPS resulted in augmented inflammation as assessed by polymorphonuclear leukocyte recruitment to the airspace. Gene expression analysis and pathway modeling of the CCSP-/- inflammatory response implicated increased TNF-α signaling. Consistent with this model was the demonstration of significantly elevated TNF-α in airway fluid of LPS stimulated CCSP-/- mice compared to similarly exposed wildtype (WT) mice. Increased LPS elicited TNF-α production was also observed in cultured lung macrophages from CCSP-/- mice compared to wild type mice. Moreover, macrophages from Clara cell depleted and CCSP-/- mice displayed increased TLR4 surface expression. These results provide evidence that Clara cells can attenuate inflammation through regulation of macrophage behavior

and suggest that epithelial remodeling leading to reduced Clara cell secretory function is an important factor that increases the intensity of lung inflammation in chronic lung disease.

4.2 INTRODUCTION

Chronic lung diseases (CLD), such as chronic obstructive pulmonary disease (COPD) and asthma are a global health problem with COPD expected to be the third leading cause of mortality by 2020 and asthma currently affecting 300 million people worldwide[161,162]. Pathological remodeling of the lung in CLD includes changes in the abundance and differentiated properties of the airway epithelium, subepithelial fibrosis, increased basement membrane thickness, and smooth muscle hypertrophy. These pathological alterations are accompanied by excessive inflammation contributing significantly to declining lung function, morbidity, and ultimately mortality [105,163]. The abundance of low molecular weight non-mucinous secretory proteins in airway lining fluid and serum have been directly correlated with severity of CLD [164]. Levels of Clara cell secretory protein (CCSP, *Scgb1a1*) are dramatically reduced in either serum or airway lining fluid of patients with COPD, asthma, bronchopulmonary dysplasia, silicosis, and post-transplant rejection [41-44,165-168]. More recent evidence suggests that the levels of CCSP in serum can also be used as a diagnostic screen for acute lung injury (ALI*), acute respiratory distress syndrome (ARDS), and acute pollutant exposure[169-171]. The loss of CCSP in airways from CLD patients may be due to either decreased abundance of Clara cells or a reduction in the *de novo* synthesis of CCSP. For instance, a guanine to alanine substitution at position 38 of CCSP has been identified. This position is within the minimal promoter region of CCSP and is associated with decreased synthesis of CCSP

in asthma and sarcoidosis[172-175]. Even though these studies associate epithelial remodeling and reduced secretory function with progression of CLD it is not clear if secretory cell dysfunction directly contributes to the disease process.

CCSP is the principal secreted product of the nonciliated bronchiolar Clara cell and the founding member of the secretoglobin family of secretory proteins [60,176]. X-ray crystallography studies have revealed that mature CCSP forms a homodimeric structure of monomers arranged in an anti-parallel orientation that are held in alignment by two di-sulfide bridges. This structure has a small internal hydrophobic binding pocket that is able to bind phospholipids, including phosphatidylcholine and phosphatidylinositol[177]. CCSP has also been proposed to bind to other small lipophilic compounds including: exogenous ligands such as methylsulfony PCB[46] and endogenous ligands such and progesterone[178,45]. *In vitro* studies have also revealed that CCSP is able to inhibit phospholipase A2 activity, possibly through sequestration of calcium.[47] Two different lines of CCSP-/- mice have been developed that differ in their steady-state phenotypes, but each show evidence for alterations in their susceptibility to environmental agents and injury-related induction of tissue inflammation [46,50,52,54]. CCSP-/- mice mount an increased inflammatory response to live *P. aeruginosa* administered intra-tracheally as measured by increased total inflammatory cell exudates in bronchoalveolar lavage (BAL) as well as secretion of pro-inflammatory cytokines, implicating a role for CCSP regulation of innate immunity[57]. However, these studies failed to define molecular mechanisms by which CCSP regulates lung inflammatory responses. The recent demonstration that CCSP deficiency leads to altered post-translational modification of Annexin A1 (ANXA1) within ciliated cells and macrophages

suggests that epithelial and inflammatory cell function may be influenced by Clara cell secretions through a paracrine signaling mechanism [62].

The present study was designed to test the hypothesis that Clara cells moderate the lung response to inflammatory stimuli. Clara cell depletion and CCSP deficiency enhance the LPS elicited inflammatory response in vivo. Furthermore, macrophages from CCSP-/- mice show increased LPS-stimulated TNF-α production and cell surface TLR4 relative to macrophages from wild type mice. These data suggest that Clara cells can attenuate the inflammatory response through regulation of macrophage behavior and that reduced Clara cell secretory function seen in patients with CLD may enhance lung inflammation.

4.3 MATERIALS AND METHODS

4.3.1 Animal husbandry

Inbred CCSP-/- 129J, CCSP-/- C57Bl6/J congenic, and WT FVB/N mice were maintained as in house breeding colonies under specific pathogen free conditions in an AAALAC accredited vivarium. WT strain 129Sv/Ev and C57Bl/6J mice were purchased directly from the supplier (Taconic, Germantown, NY and The Jackson Laboratory, Bar Harbor, ME) and housed for a minimum of two weeks prior to experimentation. Mice were maintained on a 12 hour light/dark cycle and provided food and water *ad libitum*. Sentinel screening was conducted on a quarterly basis to determine pathogen status. For *in vivo* exposures male 129Sv/ev mice aged 6-10 weeks were used. All *in vitro* experiments were conducted with male and female C57Bl/6 WT and CCSP(-/-) mice aged 6-12 weeks. Animal procedures and cell isolations were approved by Duke and the University of Pittsburgh's IACUC.

4.3.2 Naphthalene and LPS dual exposure

WT adult male C57Bl/6 mice and FVB/N were exposed to 250mg/kg and 275mg/kg naphthalene, respectively. Naphthalene was dissolved in Mazola corn oil and injected into the peritoneal cavity as described previously [84]. Groups that received a dual exposure were aerosol

challenged with a 10ng deposited dose of LPS 24 hours after naphthalene injection. Mice were recovered for 2 or 7 days post naphthalene treatment.

4.3.3 LPS exposure

WT and CCSP-/- 129Sv/ev mice (6-10wks of age, male) were co-exposed to *P. aeruginosa* 10 lipopolysaccharide (Sigma, L8643, St Louis, MO) as previously described, resulting in an estimated deposited dose of 10ng [55]. 5mg of lipopolysaccharide from *P. aeruginosa* 10 (Sigma, L8643, St Louis, MO) were reconstituted in 4ml of sterile and pyrogen free 0.9%NaCl (Hospira, Lake Forest, IL). Immediately prior to exposures, aliquots of 1.25 mg/ml LPS were diluted to 62.5µg/ml in sterile 0.9% NaCl. 5ml of the 62.5ug/ml LPS solution were loaded into a jet nebulizer (DeVilbiss, Somerset, PA) and nebulized with breathing quality air (Valley Natural Gases, Wheeling, WV) at 15psi for 20 minutes. Animals were sacrificed by administering general anesthesia to achieve a surgical plane followed by exsanguination.

4.3.4 Analysis of polymorphonuclear leukocyte (PMN) recruitment, apoptosis, and necrosis

Inflammatory cells were sampled by total lung lavage. Briefly, animals were cannulated with a 20_{GA} BD Insyte™ Autoguard™ I.V. Catheter. Each animal was lavaged a total of 8 times with 1 ml of sterile PBS. Cells were collected by centrifugation at 4°C and resuspended in 1.0 ml PBS. Total cell counts were determined in technical triplicates using a Z1 Coulter Particle Counter (BeckmanCoulter, Fullerton, CA). Particles >7um were counted in order to exclude red blood

cells and cellular debris. Polymorphonuclear leukocyte (PMN) apoptosis was measured using a BD FACS CANTO Flow Cytometer™ (BD Biosciences). PMNs were identified by staining with Ms-Ly6G/Ly-6C (Gr-1) directly conjugated APC-Cy7 (BD Pharmingen, Cat# 557661) for 15 minutes [179]. Cells were also stained for AnnexinV-FITC and PI as a measure of apoptosis and necrosis, respectively (Biovision, Mountain View, CA). Appropriate unstained and single stained controls were analyzed in order to set compensation voltages. Apoptotic and necrotic PMN were defined as Gr-1^{pos}/annexinV ^{pos}/PI^{neg} and Gr-1^{pos}/annexinV ^{pos}/PI^{pos} populations, respectively. Unstained total BAL cells were used for microscopic classification of cell types using a differential staining kit according to manufacturer's recommendation (Protocol®, Fisher Scientific).

4.3.5 Gene expression analysis

RNA was isolated from left lung according to protocol [138]. CodeLink UniSet Mouse 20K I Bioarrays (GE Healthcare Bio-Sciences Corp., Piscataway, NJ) were used for gene-expression profiling of isolated total RNA. Determination of RNA integrity, generation of biotin labeled cRNA, hybridization to the array, array scanning, and data collection was conducted at the University of Pittsburgh Cancer Institute Clinical Genomics Facility.

4.3.6 Bioinformatic analysis

Data analysis was conducted in three steps as previously described [180,181]. This included: **1)** Generation of complete data tables including full annotations, **2)** Normalization of raw data and

statistical analysis to determine significant changes in gene expression, **3)** Identification of clusters of similarly expressed genes, and **4)** Pathway modeling. Raw data were annotated using the freeware program *Source* (Stanford University, Stanford, CA). Data were next imported into the *ScoreGenes* software package (Jerusalem, Israel) for data normalization, statistical analysis, and clustering [182]. Raw data were log2 transformed and normalized to the average across all groups. Significant gene expression changes were assessed by fulfilling two criteria: a significant student's t-test p-value and a threshold number of misclassifications (TNOM) equal to 0 according to previously established data mining methods [183]. LPS responsive and CCSP independent genes were revealed by identifying all genes in WT and CCSP-/- data sets that were differentially expressed compared to control (TNOM = 0, t-test p-value <0.1) and not dependent upon genotype (TNOM > 0 in a WT vs CCSP-/- comparison). LPS responsive and CCSP dependent genes were determined by first identifying all LPS responsive genes. These genes were further evaluated for genotype dependent expression differences by pair-wise comparisons of WT and KO data sets (TNOM = 0, and t-test p-value <0.1). Independent clustering of the LPS responsive/CCSP independent and LPS responsive/CCSP dependent genes was conducted in the *ScoreGenes* package using the "pcluster" command. Data was visualized using *Treeview* software as previously described [184]. Finally, *PathwayArchitect*^{TM} (Stratagene, La Jolla, CA) was used as a means to create biological pathways. This software package allowed for transformation of gene lists into biological pathways based on known functional characteristics of the selected genes. The ontological definitions are based upon the composite of human curated databases and analysis of published abstracts through language processing algorithms. Microarray analysis was conducted according to MIAME.

4.3.7 Protein characterization of bronchoalveolar lavage

WT and CCSP-/- mice were lavaged twice with 1ml of sterile PBS and centrifuged at 300g for 5 minutes to remove cells and debris. Protein enriched supernatants were assayed for cytokine and chemokine protein abundance using a Luminex system (Luminex Corp, Austin, Texas) with either Mouse-18-plex or Mouse-6-plex chemokine/cytokine detection kits (Biorad, Hercules, CA). CCSP was measured in BAL with a CCSP ELISA that was designed in-house using CCSP anti-serum from goat and rabbit.

4.3.8 Mouse tracheal epithelial cultures

Primary airway epithelial cultures were established and maintained at the air liquid interface (ALI) using the method of You and colleagues [185]. Cultures prepared from WT and CCSP-/- mice were exposed to LPS on day 10 of air-liquid culture, as maximal expression of the secretory cell marker CCSP occurs at this time. Epithelial cells were exposed on the basolateral surface to 1μg/ml *P. aeruginosa* lipopolysaccharides (Sigma, St. Louis, MO) in normal growth medium. A basolateral stimulus was conducted, as an apical stimulus can have detrimental effects to epithelial integrity [186]. Apical surface fluid was harvested 0, 6, or 24 hours after LPS exposure by washing the apical surface of cultures with 500μl sterile PBS and assayed for cytokine/chemokine protein expression using a mouse-6-plex assay as outlined above. RNA was extracted from epithelial cells using an SV Total RNA Isolation System (Promega, Madison, WI) according to manufacturer's instructions. ALI experiments were repeated with three independent epithelial cell isolations.

4.3.9 Ex vivo LPS exposure of WT and CCSP-/- macrophages

Lung macrophages were isolated from naïve WT and CCSP-/- C57Bl/6 (non-sex/age matched) mice as previously described by Schurr and colleagues[187] and exposed to *P. aeruginosa* LPS (Sigma). 3 WT and 3 CCSP-/- animals were lavaged 8 times with 1ml of PBS. Cells were recovered by centrifugation at 300 x g for 10 minutes and resuspended in media composed of DMEM (Cambrex), 10% FBS (ThermoFisher, Waltham, MA), penicillin-streptomycin (50IU/ml), and 2mM L-Glutamine (Chemicon). Cells were incubated for 2 hours to allow for adherence to the tissue culture plate. Media was replaced with LPS spiked media at concentrations indicated in figure legends. Cells were incubated with LPS containing media for 6 hours and the supernatant collected for further analysis. TNF-α protein concentration was determined using a mouse TNF-α cytoset sandwich ELISA according to manufacturer's recommendations (Biosource, Invitrogen, Carlsbad, CA). The *ex vivo* macrophage experiments were repeated with two independent macrophage isolations.

4.3.10 Macrophage Gene Expression Analysis

Alveolar macrophages were isolated from naïve WT and CCSP-/- mice for analysis of TLR4 and CD14 mRNA abundance. WT and CCSP-/- mice were lavaged and cells recovered by centrifugation. 3 mice were pooled per group for a total of 3 groups per genotype (N = 3). RNA was extracted using an SV total RNA Isolation System (Promega, Madison, WI). cDNA synthesis was performed as described above. Realtime PCR was conducted to assay for TLR4 and CD14 mRNA abundance as described below.

4.3.11 TLR4 surface distribution on lung macrophages

Lung macrophages were isolated from WT and CCSP-/- lung and TLR4 distribution analyzed as previously described [188]. Briefly, whole lung lavage and centrifugation was performed to obtain lung macrophages. Flow cytometry analysis was performed using a Becton Dickinson FACS Calibur (BD BioSciences, San Jose, CA) and analyzed with CELLQuest software (BD BioSciences, San Jose, CA). A laser scanning confocal microscope (LSM 510 UV mounted on an Axio Observer microscope, Carl Zeiss, Inc.) was used to obtain the fluorescence and transmitted images. Zeiss LSM510 v4.2 and LSM Image Examiner v3.2 software were used for image acquisition and analysis, respectively.

4.3.12 Realtime PCR

Taqman realtime PCR was conducted on an Applied Biosystems 7000 RealTime PCR System (Applied Biosystems, Foster City, CA). RNA was analyzed for quantity and quality using a Nanodrop 1000 spectrophotometer (Nanodrop Technologies, Wilmington, DE). Equal amounts of RNA were used to generate cDNA using the First strand cDNA synthesis kit according to manufacturer's recommendations (Invitrogen, Carlsbad, CA). Taqman realtime PCR was conducted using validated Taqman probe and primer combinations (Applied Biosystems, Applied Biosystems, Foster City, CA). Relative mRNA abundance was determined by the $\Delta\Delta^{CT}$ method for realtime PCR [140].

4.3.13 Statistical analysis

Statistical analysis was conducted in Minitab 15® for Windows®. Pair-wise comparisons were tested for significance using the student's t-test or a Mann Whitney U test. The general linear model (GLM) and Tukey's *post hoc* analysis was used to test multiple pair-wise comparisons.

4.4 RESULTS

4.4.1 Clara Cell Depletion Exacerbates the LPS Induced Inflammatory Response

To address the contribution of the airway epithelium to the inflammatory response a dual exposure mouse model in which Clara cells were specifically ablated by naphthalene exposure prior to LPS challenge was utilized. A critical component of this experiment was to first identify the time at which naphthalene induced injury resulted in maximal Clara cell ablation and diminished secretory function. WT FVB/N mice were exposed to naphthalene and recovered for 1, 2.5, 4, 8, or 12 hours and 1, 3, 5, 10, or 30 days. Protein abundance of CCSP was measured in the cell free fraction of bronchoalveolar lavage (BAL) as an indicator of both Clara cell ablation and secretory capacity. CCSP protein in BAL increased 1.0 hour after injury indicative of Clara cell de-granulation/hyper-secretion, returned to normal levels by 2.5 hours, and reached a minima from 8 hours to 5 days suggesting Clara cell ablation and diminished secretory capacity had occurred by 24 hours (Figure 13A). This finding parallels other endpoints of Clara cell depletion including depletion of CCSP mRNA within total lung RNA and the loss of CCSP immunoreactive cells within lung tissue by immuno-cytochemistry [189].

To test the physiological impact of Clara cell ablation on the inflammatory response, mice were exposed to naphthalene, LPS, or naphthalene and LPS. The 24 hour recovery time point after naphthalene exposure was selected for further LPS challenge as it represented the interval showing maximal depletion of Clara cells and their major secretory product, CCSP

(Figure 13A). Naphthalene treatment alone resulted in only a subtle increase in lavageable PMNs (Figure 13B, Black). In contrast, 30% of lavageable cells were classified as PMNs one day following treatment with LPS alone (Figure 13B, Grey). Naphthalene and LPS exposure (Dual Exposure, white) resulted in a synergistic increase in PMN recruitment, as evidenced by a PMN contribution of 73% of BAL cells (Figure 13B). As the Clara cell and macrophage signaling axis has been shown to be an important regulator of the LPS induced inflammatory response, the affects of Clara cell ablation on macrophage behavior was investigated [28]. Increased abundance of TLR4 on the surface of lung macrophages has previously been correlated with an exacerbated LPS elicited inflammatory response[188]. Therefore, macrophages from control and naphthalene exposed mice were isolated from BAL and stained for the macrophage marker F4/80 and TLR4. TLR4 surface expression was evaluated on F4/80 positive macrophages through flow cytometry. Increased TLR4 surface expression and clustering has recently been documented to be a critical determinant of the LPS elicited inflammatory response[188,190]. Macrophages isolated from naphthalene exposed mice demonstrated a robust increase in TLR4 surface expression relative to steady state controls (Figure 13C,D). Even though these data do not rule out indirect effects of injury on modulation of the LPS response, they suggest that Clara cells function in an anti-inflammatory capacity within airways by modulating macrophage behavior.

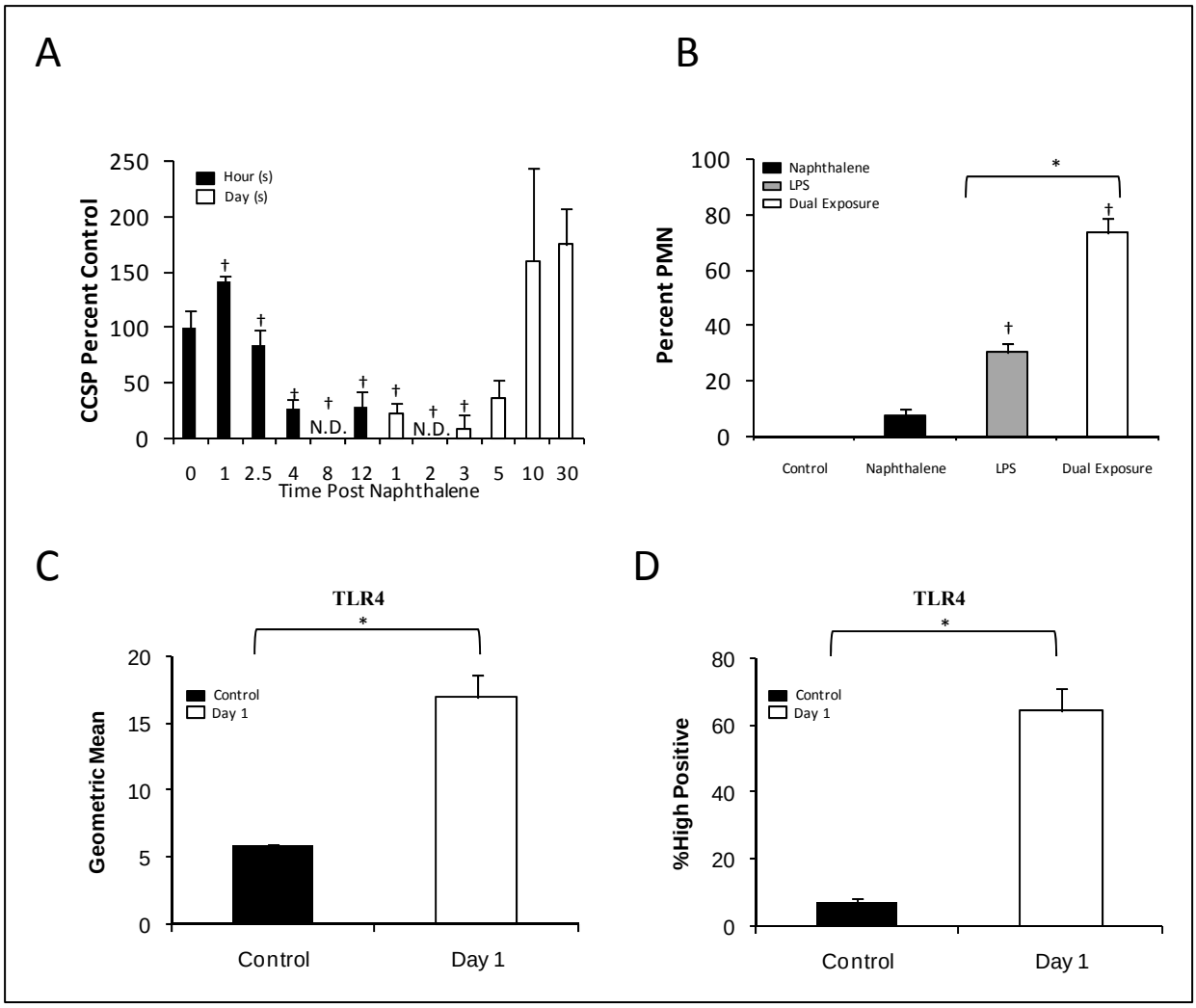

Figure 13. The airway epithelium attenuates the inflammatory response.

WT adult mice were exposed to naphthalene, LPS, or naphthalene and LPS. The abundance of (A) CCSP protein in BALF from 0, 1, 2.5, 4, 8, 12 hours (black, N = 4/group) and 1, 2, 3, 5, 10, 30 days (white, N = 5/group) was measured by an ELISA. (B) Recruited PMNs were analyzed in BAL from control (N = 3), naphthalene (black, N = 3), LPS (grey, N = 3), and naphthalene + LPS exposed (white, Dual Exposure, N = 4) mice. (C and D) TLR4 protein expression was measured on lung macrophages at steady-state (Control, black) and one day after naphthalene (Day 1, white) through cytometric analysis and presented as the geometric mean of TLR4 positive macrophages and percentage of TLR4 high positive macrophages (C and D, respectively). Data presented as mean

Figure 13 Continued.

+/- SEM. (* and †: p-value <0.05 for pairwise comparison of exposure group or comparison to control, respectively; student's t-test (panels A, C, and D) and GLM/Tukey's *post hoc* analysis was used in panel B).

4.4.2 Increased LPS induced recruitment of PMNs to lungs of CCSP deficient mice

Based upon these data, a mechanism whereby Clara cells may modulate the inflammatory response was investigated. Clara cells may attenuate the inflammatory response through a variety of mechanisms including secretion of paracrine factors. Previous studies have shown that CCSP-/- mice display increased lung inflammation relative to WT mice following exposure to inhaled oxidant pollutants [52,54]. Additionally a signaling axis exists between Clara cells and macrophages as revealed by changes to ANXA1 post-translational modifications in macrophages of CCSP-/- mice [62]. Therefore, to test the hypothesis that Clara cells moderate the inflammatory response through a CCSP dependent mechanism, WT and CCSP-/- mice were co-exposed to 10 ng deposited dose of LPS and recovered for 3 or 24 hours. Analysis of cell types recovered from BAL revealed the expected shift in inflammatory cell profile from >99.5% macrophages in BAL of unexposed mice to predominantly recruited PMNs in BAL from both WT and CCSP-/- mice either 3 or 24 hours post LPS exposure (Figure 14A). Even though a similar overall response was observed, differences were apparent in the magnitude of PMN recruitment. PMNs represented 44.9 and 74.4 % of WT and CCSP-/- isolated BAL cells 3 hours post LPS exposure indicating a statistically significant 65.7% increase in PMNs in airways of CCSP deficient mice (Figure 14A). Furthermore, PMNs represented 70.9 and 81.3% of WT and CCSP-/- BAL 24 hours post LPS exposure demonstrating a more subtle but 14.6% increase in PMN contribution to CCSP-/- BAL. Corresponding decreases were observed in the fractional contribution of

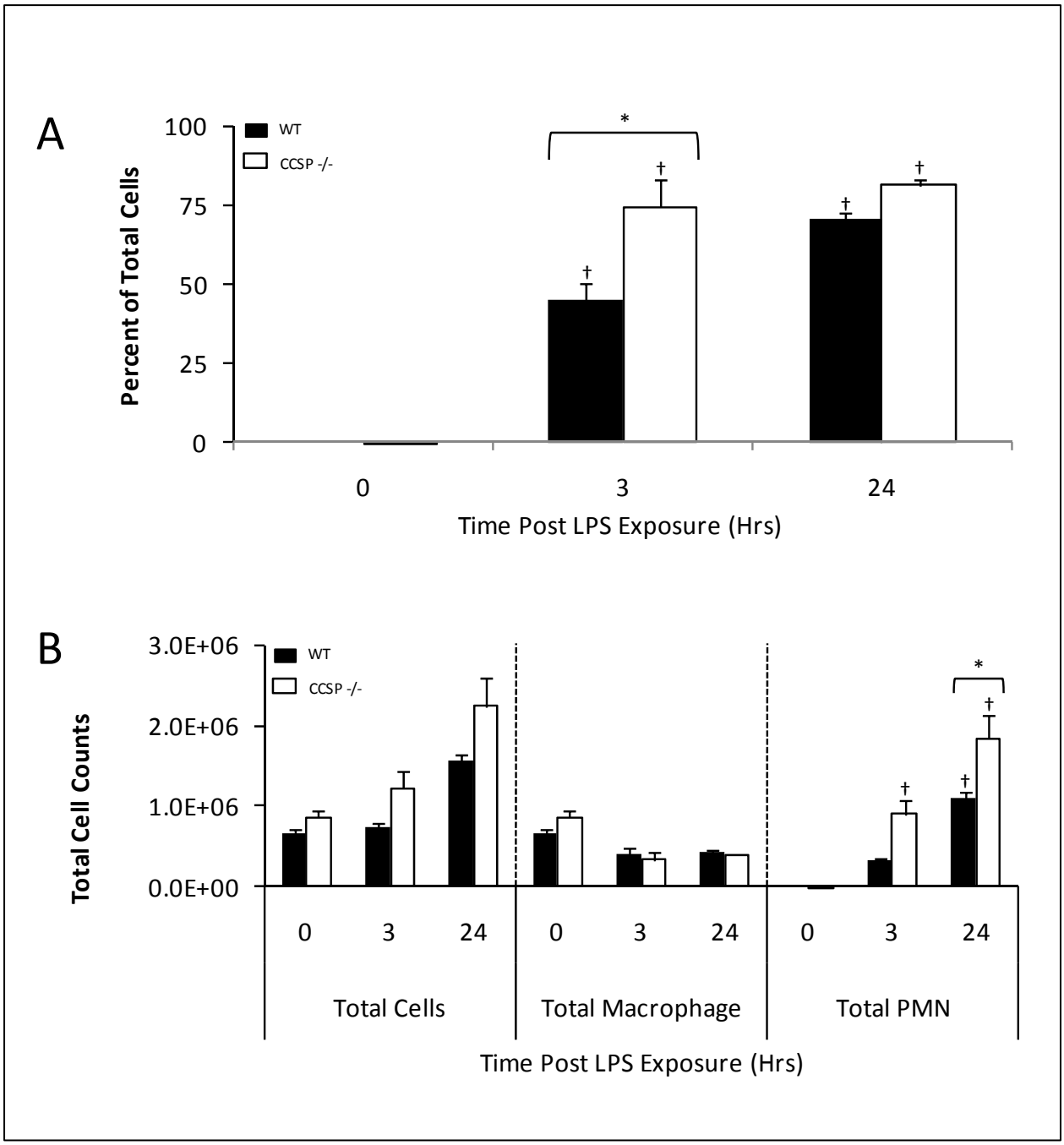

Figure 14. CCSP deficiency augments the LPS induced inflammatory response.

WT and CCSP-/- mice were simultaneously challenged with LPS and recovered for 3 or 24 hours. Control (N = 4) mice were unexposed to LPS (0). Cellular infiltrates were analyzed using a differential cellular stain to determine (A) PMN recruitment. (B) Total cells were determined in WT and CCSP-/- BAL using a Coulter Particle

Figure 14 Continued.

Counter (Left). To reveal cell type specific changes to the total cellular infiltrate total macrophages (center) and PMNs (right) were calculated by multiplication of total cells by the percentage of macrophage or PMN in BAL as determined in differential cell analysis. Data presented as mean +/- SEM. (* and †: Tukey's *post hoc* p-value <0.05 in pair-wise comparisons of WT and CCSP-/- or comparison to control, respectively; WT: Black, CCSP-/-: White).

macrophages to BAL cells recovered from airways of WT and CCSP-/- mice following LPS exposure (data not shown).

Changes in total cell numbers were also measured to better define CCSP dependent differences in inflammatory cell recruitment. Total BAL cell counts were increased by 68% and 43% in BAL of CCSP-/- mice compared to WT mice at 3 and 24 hours post LPS exposure, respectively (Figure 14B, left). No changes were observed in total macrophages recovered in BAL from WT and CCSP-/- mice, despite the decreased fractional abundance in BAL. (Figure 14B, middle). Increased cellular recruitment following LPS exposure could be accounted for by recruitment of PMNs. Consistent with differential cell-type analysis in BAL, PMNs were recruited to significantly higher levels in BAL of LPS exposed CCSP-/- mice compared to similarly exposed WT mice. PMNs in BAL of LPS exposed CCSP-/- mice showed 2.79 fold and 1.66 fold increase over WT control mice at the 3 hour and 24 hour post-exposure time points, respectively (Figure 14B, right).

Instantaneous measurements of PMN abundance represent the sum of recruitment and apoptotic clearance. To determine whether CCSP deficiency was associated with changes in either of these parameters, the abundance of apoptotic and necrotic PMN's was determined within BAL of WT and CCSP-/- mice by FACS analysis 24 hours post LPS exposure. Isolated BAL cells were stained with Gr-1[179] and the fraction of apoptotic cells determined by relative staining for annexin V-FITC and PI. As was the case with cytological identification of cell types, FACS analysis revealed >50% contribution of PMN's to the total cell fraction of BAL from LPS-exposed WT and CCSP-/- mice (Figure 15A, B). The abundance of cells showing cell

surface staining for annexin V and either exclusion or staining with PI indicated no statistically significant differences in apoptotic and necrotic PMNs, respectively, in BAL of CCSP-/- mice compared to WT (Figure 15C-G). These data suggest that CCSP deficiency modifies the initial response to pro-inflammatory stimuli leading to increased PMN recruitment, but has no impact on PMN turnover.

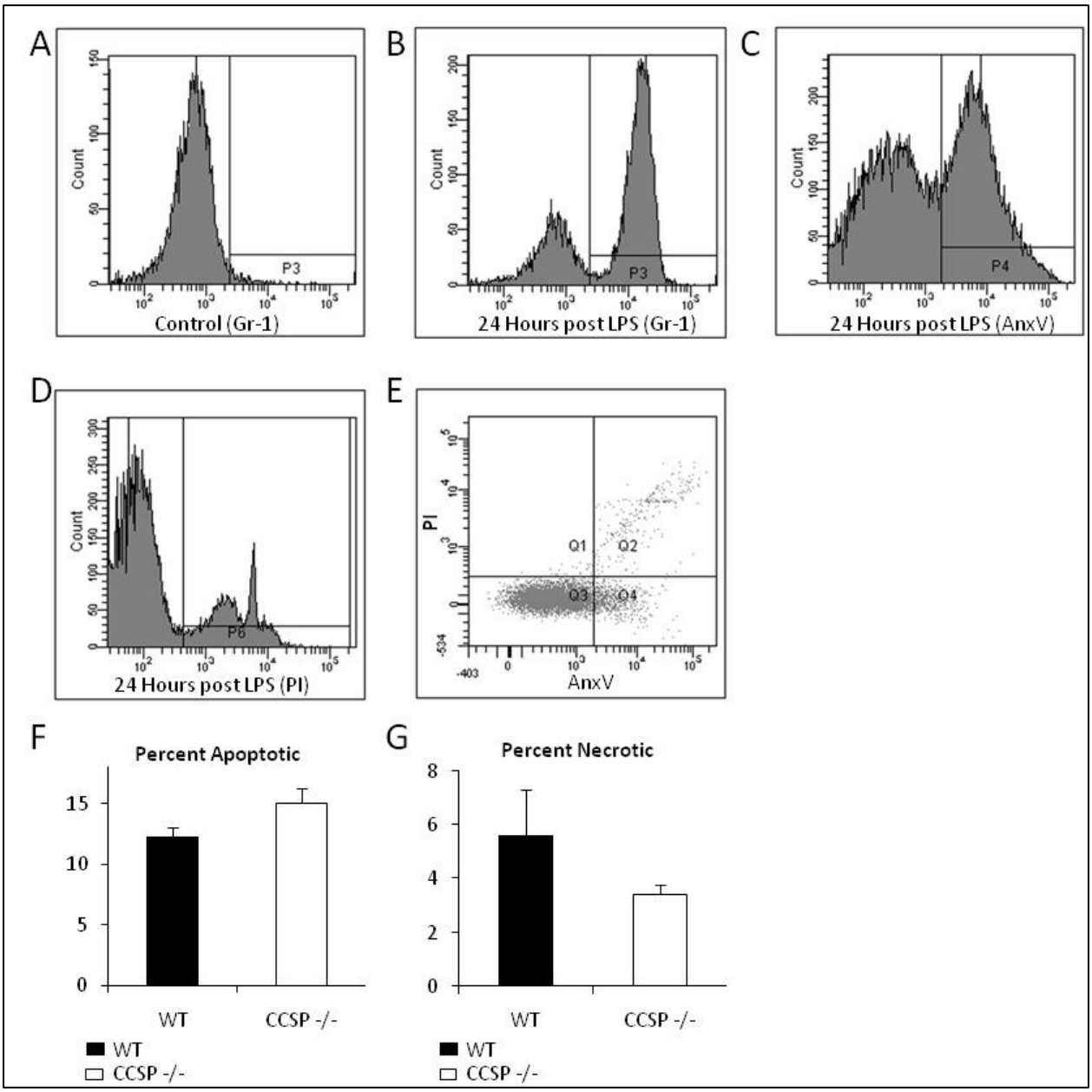

Figure 15. Resolution of the inflammatory response is not impacted by CCSP deficiency.

BAL Cells from WT and CCSP-/- lung were isolated 24 hours post LPS exposure (N = 4) for determination of PMN apoptosis and necrosis. Appropriate one color controls were used to set compensation voltages (data not shown). (A) Unexposed controls were used to determine the Gr-1 (-) fraction of inflammatory cells. (B-D)

Figure 15 Continued.

Isolated cells were stained with Gr1-APC-Cy7, AnxV-FITC, and PI to determine PMN specific apoptosis and necrosis. (E) Scatterplot of PI vs AnxV-FITC Gr-1 (+) cells to determine necrotic and apoptotic PMNS. Quadrants 2 [AnxV(+)/PI(+)] and 4 [AnxV(+)/PI(-)] represent necrotic and apoptotic PMNs respectively. Quantitative analysis of the percentage of (F) apoptotic and (G) necrotic PMN (No significance was reached using a 2-sample student's t-test). Data presented as mean +/- SEM. (WT: Black, CCSP-/-: White).

4.4.3 Microarray analysis reveals CCSP dependent and CCSP independent affects to the LPS response

To better understand mechanisms by which CCSP impacts LPS induced lung inflammation a genome wide expression screen of WT and CCSP-/- lung RNA from mice at 0, 1.5, 6, and 12 hours post exposure to an estimated deposited dose of 10ng LPS. A total of 1815 genes were identified that demonstrated a similar LPS response in WT and CCSP-/- lung. This gene list was designated as CCSP independent and LPS responsive, relevant portions of which are represented as a clustered heat-map in Figure 16A. The representative gene list, fold change relative to WT or CCSP-/- controls, and annotations are presented in Appendix B.1 Supplementary Table 5. A second gene set of 267 transcripts was comprised of genes that were differentially LPS responsive in a WT and CCSP-/- pair-wise comparison. This gene list was designated as CCSP dependent and LPS responsive, relevant portions of which are represented as a clustered heat-map in Figure 16B. The representative gene list, fold change relative to WT, and annotations are presented in Appendix B.1 Table 6. To validate the gene expression signatures displayed in Figure 16, mRNA abundance for genes from each cluster was determined by quantitative real time PCR (data not shown; validated genes indicated in Appendix B.1 Tables 5 and 6).

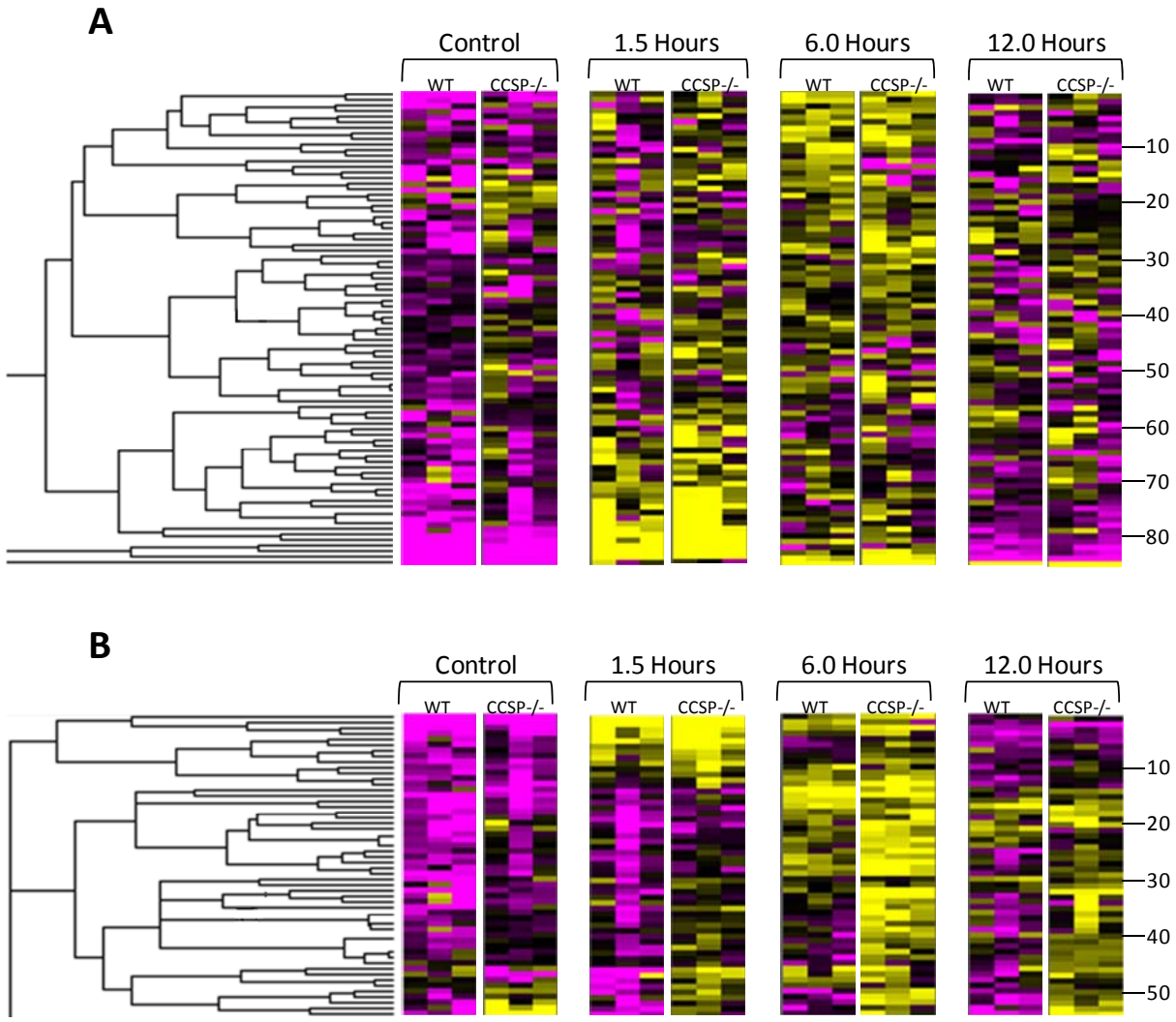

Figure 16. Hierarchical clustering of genome wide expression analysis to identify CCSP dependent and independent components of the LPS induced inflammatory response.

WT and CCSP-/- mice were coexposed to LPS aerosol for 20 minutes and recovered for 1.5, 3, 6, 9, and 12 hours (N 4/group, Control mice were not exposed to LPS). RNA from 0, 1.5, 6, and 12 was screened for total message expression using Codelink 20K Bioarrays (N = 3/group). Hierarchical clustering of gene expression is represented in heat maps where columns are experiments and rows are genes (yellow and magenta indicate decreased and increased expression, respectively, with respect to the average across all time points). The heat map represents a subset of the clusters from (A) CCSP independent/LPS responsive and (B) CCSP dependent /LPS

Figure 16 Continued.

responsive gene signatures. The rows (genes) are annotated in ascending numerical order. For complete annotations including accession number, gene name, and ontology refer to Apendix B.1. (Tables 5 and 6).

4.4.4 Pathway analysis identifies TNF-α and IL-6 as key cytokines involved in the CCSP deficient inflammatory response.

PathwayArchitect™ was used to organize the gene set *in silico* based upon transcriptional regulators and gene product interactions [191-193]. Genes within the LPS responsive CCSP dependent gene cluster were organized into an interactive pathway to provide further insights into regulatory mechanisms accounting for CCSP dependent regulation of the inflammatory response. In addition to these genes, LPS, CCSP, and two known regulated downstream target genes, SCGB3A2 and ANXA1, were included within the gene set to identify evidence of involvement in this pathway. Generation of the *in silico* pathways are described in the materials and methods. The *in silico* generated pathway recapitulated the previously established model of LPS elicited inflammation, including LPS recognition by CD14 and TLR4. Included within this pathway are key nodes of regulation implicated in the CCSP dependent modulation of LPS elicited inflammation. Two key signaling molecules implicated in the CCSP dependent component of the inflammatory response were TNF-α and IL-6 as demonstrated by the high connectivity between genes whose mRNA's were significantly altered in a CCSP-dependent, LPS-dependent fashion (Figure 17A, Red Asterisk). Importantly, neither TNF-α nor TLR4 mRNA abundance were found to be CCSP dependent as indicated by similar responses to LPS treatment between WT and CCSP-/- mice and their absence from the corresponding gene list used for pathway analysis. Rather, Pathway Architect's computational algorithm added TNF-α and TLR4 to the pathway as they were both predicted to be key upstream regulators of genes

represented within the CCSP dependent and LPS dependent gene list. This observation suggests that increased signaling by TNF-α and IL-6 may contribute to the enhanced LPS elicited inflammatory response observed in CCSP-/- mice relative to co-exposed WT mice.

To determine whether the *in silico* prediction of increased IL-6 and TNF-α signaling could be validated *in vivo*, protein abundance in WT or CCSP-/- BAL fluid was determined by cytokine/chemokine multiplex analysis at 0, 1.5, 3, 6, 9, and 12 hours following LPS stimulation. Statistically significant 3.2 and 5.8 fold increases in TNF-α protein abundance were observed in BAL fluid isolated from CCSP-/- mice compared to similarly exposed WT mice at either 1.5 or 3 hours post LPS exposure (Figure 17B). This was accompanied by a trend towards increased IL-6 protein in CCSP-/- BAL fluid 3 hours post LPS exposure compared to WT (Figure 17C), a finding consistent with an over-abundance of TNF-α[194]. These data support the prediction generated from microarray data that there exists CCSP dependent changes in LPS elicited TNF-α and IL-6 protein production *in vivo*.

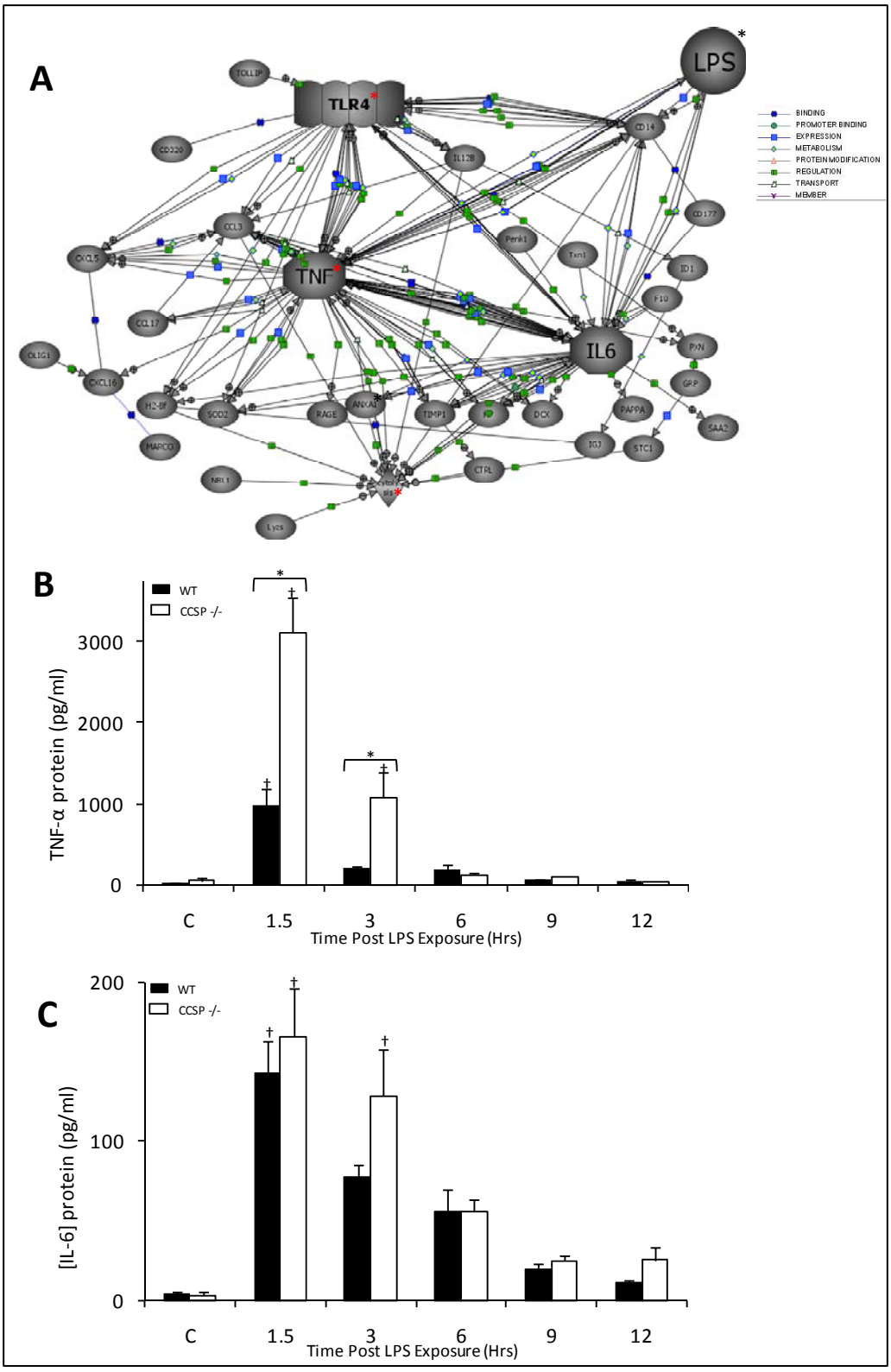

Figure 17. Pathway analysis of the CCSP dependent and LPS responsive gene signature identifies regulatory networks that can be biologically validated.

Figure 17 Continued.

Genes that were identified to be LPS responsive and CCSP dependent (Figure 16B) were utilized to construct an interaction network as discussed in materials and methods. Gene products (ellipses) are linked functionally by connecting lines in accordance with functional annotation (refer to legend). Note the high connectivity of TNF-α and IL-6 in the proposed pathway. (Red and black asterisk denote molecules/processes that were added to the pathway in either an unsupervised (added by the pathway analysis software) or supervised (manually by the user) fashion as discussed in the text. (B and C) WT and CCSP-/- mice were simultaneously aerosol exposed to *P. aeruginosa* and sacrificed 1.5, 3, 6, 9, and 12 hours post exposure (N = 4 per group). Control mice were unexposed to LPS (0). BAL was collected and characterized using a multiplex immunoassay. (B) TNF-α (pg/ml) and (C) IL-6 protein levels are depicted. Data presented as mean +/- SEM. (* and †: Tukey's *post hoc* p-value <0.05 in comparison of WT and CCSP-/- or comparison to control, respectively; WT: Black, CCSP-/-: White).

4.4.5 Airway epithelium and lung macrophages are intrinsically hyper-responsive to LPS stimulation

Previous studies have revealed alterations to airway epithelial cells and macrophages as a result of CCSP deficiency [56,62]. Since each of these cellular compartments play central roles in mediating the lung response to inhaled LPS, their intrinsic responsiveness to LPS was investigated in WT and CCSP-/- in vitro models. Differentiated airway epithelial cell cultures were prepared from WT and CCSP-/- mice. Expression of cell type-specific marker genes was used to verify differentiation status of cultured epithelia and similarity of cultures prepared from WT and CCSP-/- mice. Steady-state analysis of gene expression indicated that in vitro cultures of WT and CCSP-/- epithelium were similarly differentiated prior to and throughout the exposure as indicated by equivalent expression of the ciliated and secretory cell lineage markers FoxJ1 and Cyp2f2, respectively (Figure 18A,B). The expected difference in CCSP gene expression was observed between WT and CCSP-/- cultures, with the latter showing no detectable CCSP mRNA (Figure 18C). Interestingly, CCSP mRNA abundance significantly decreased following 24 hours of LPS exposure (Figure 18C). This observation correlates with a study by Harrod and Jaramillo demonstrating that CCSP promoter activity is attenuated by *P. aeruginosa* exposure both *in vitro* and *in vivo* [195].

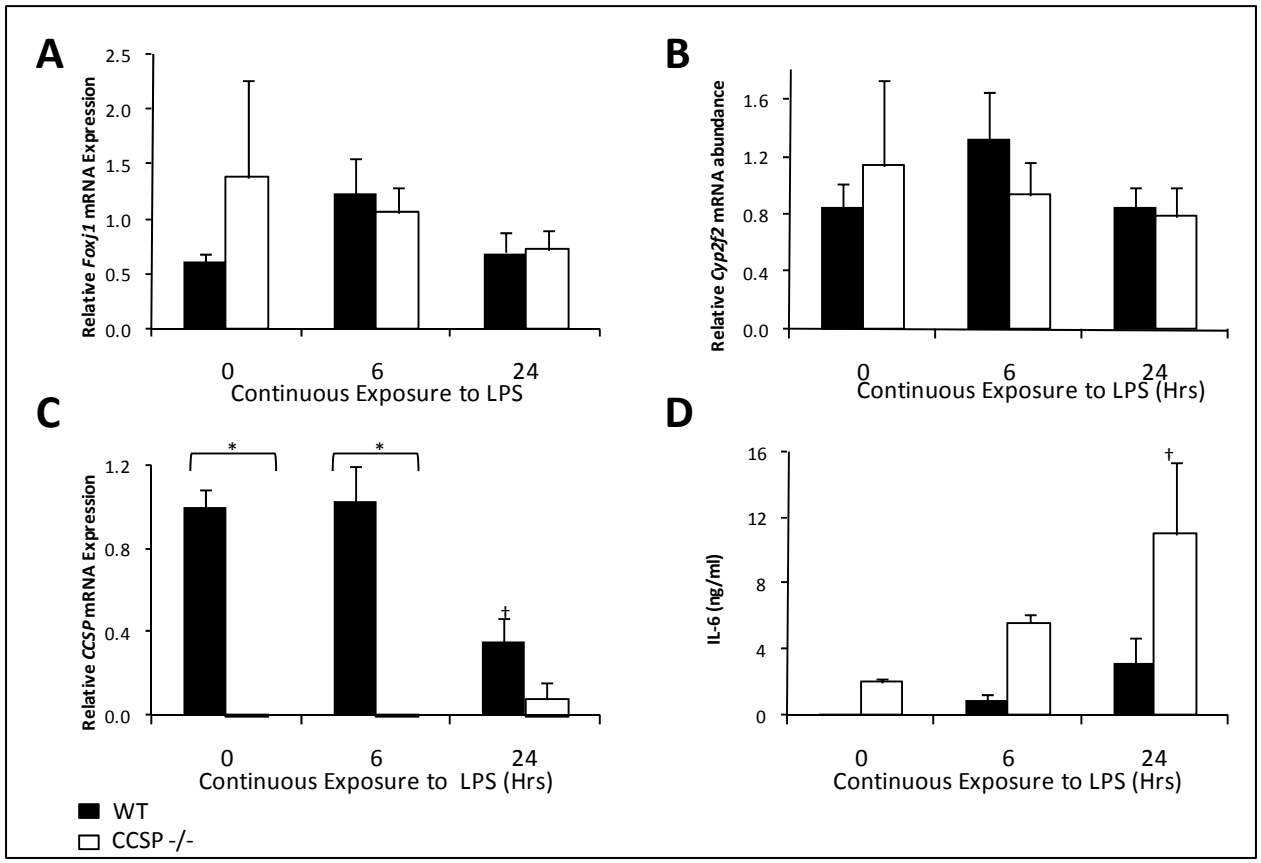

Figure 18. CCSP-/- airway epithelial cells are hyper-responsive to LPS.

Primary cultures of WT and CCSP-/- epithelium were generated and maintained at the air-liquid interface according to established protocol as described in materials in methods (N = 3 per genotype/treatment group). Control group is unexposed to LPS (0). RNA was isolated from each culture for Taqman realtime PCR assessment of (A) FoxJ1, (B) CyP450-2f2, and (C) CCSP expression to interrogate the differentiation status of the epithelium. (D) IL-6 protein secreted into the apical surface fluid was measured using a multiplex immunoassay. Data presented as mean +/- SEM. (* and †: Tukey's *post hoc* p-value <0.05 in comparison of WT and CCSP-/- or comparison to control, respectively; WT: Black, CCSP-/-: White).

To determine whether LPS had direct effects on epithelial cytokine production apical fluid was recovered from cultures and the abundance of pro-inflammatory cytokines and chemokines measured by multiplex immunoassay. LPS stimulated epithelial secretion of IL-6 into apical fluid of cultures from WT and CCSP-/- mice. A trend towards differences between WT and CCSP-/- cultures was observed. Levels of IL-6 present within apical fluid of epithelium from CCSP-/- mice was 6.18 fold and 3.5 fold higher at 6 and 24 hours than that of similarly exposed cultures from WT mice (Figure 18D). These differences did not reach significance due to variability at the 24 hour time point and stringency of the general linear model (GLM). However, a pair-wise comparison using a student's unpaired t-test yielded a statistically significant p-value of 0.001 at the 6 hour timepoint. Additionally, a similar trend in the abundance of KC and RANTES was found (data not shown). Together these data indicate that the CCSP-/- epithelium is intrinsically hyper-responsive to LPS. However, these changes are only weakly associated with the CCSP dependent component of the LPS response. Therefore, the levels of TNF-α secreted into the media were investigated, since this is the most robust difference between genotypes following LPS exposure *in vivo,* as identified by pathway analysis and subsequent protein validation. TNF-α was below the limit of detection in control and LPS exposed WT and CCSP-/- epithelial cultures (data not shown), confirming that the cell types mediating synthesis and secretion of TNF-α are absent within epithelial cultures.

In light of the previous finding of biochemical changes to macrophages of CCSP-/- mice it was determined if there were functional alterations to macrophages of CCSP-/- mice that might account for the observed phenotype described in this study[62]. WT and CCSP-/- macrophages

were isolated by lavage of steady-state lung and exposed to 0.00, 0.39, 0.78, 1.56, 3.13 6.25, 12.5, and 25.00 ng/ml LPS and media harvested for analysis of TNF-α release after 6 hours. Lung macrophages recovered from CCSP-/- mice displayed a robust increase in LPS-elicited TNF-α release compared to similarly exposed macrophages from WT mice (Figure 19A). Levels of TNF-α released into medium of macrophages cultured from CCSP-/- mice was increased over that present in macrophages from WT mice by 1.75-2.6 fold when stimulated by LPS concentrations of 3.1-12.5 ng/ml (Figure 19A). These results indicated that CCSP may moderate the macrophage elicited LPS response.

CCSP deficiency may cause alterations to the LPS recognition machinery on lung macrophages in parallel to the findings following naphthalene induced Clara cell depletion (Figure 13). Determination of mRNA abundance of TLR4 and CD14 in WT and CCSP-/- alveolar macrophages demonstrated no significant difference between genotypes (Figure 19B and C, respectively). As naphthalene induced Clara cell depletion resulted in increased surface expression of TLR4 on lung macrophages, macrophages isolated from steady-state CCSP-/- mice may have a similar alteration to TLR4 distribution. Cells were stained with macrophage marker F4/80 and TLR4 to determine if trafficking had been affected. Confocal microscopy of $F4/80^{+}$ WT and CCSP-/- macrophages (Figure 19D and 19F, respectively) revealed increased TLR4 expression in $F480^{+}$ CCSP-/- macrophages (Figure 19G) compared to WT (Figure 19E). In order to quantify the observed increase in TLR4 expression on CCSP-/- macrophages flow cytometric analysis of WT and CCSP-/- macrophages was performed. Lavaged WT and CCSP-/- cells were stained for F4/80 and TLR4. TLR4 expression was evaluated on $F4/80^{+}$ macrophages and demonstrated that CCSP-/- macrophages have a robust increase in surface

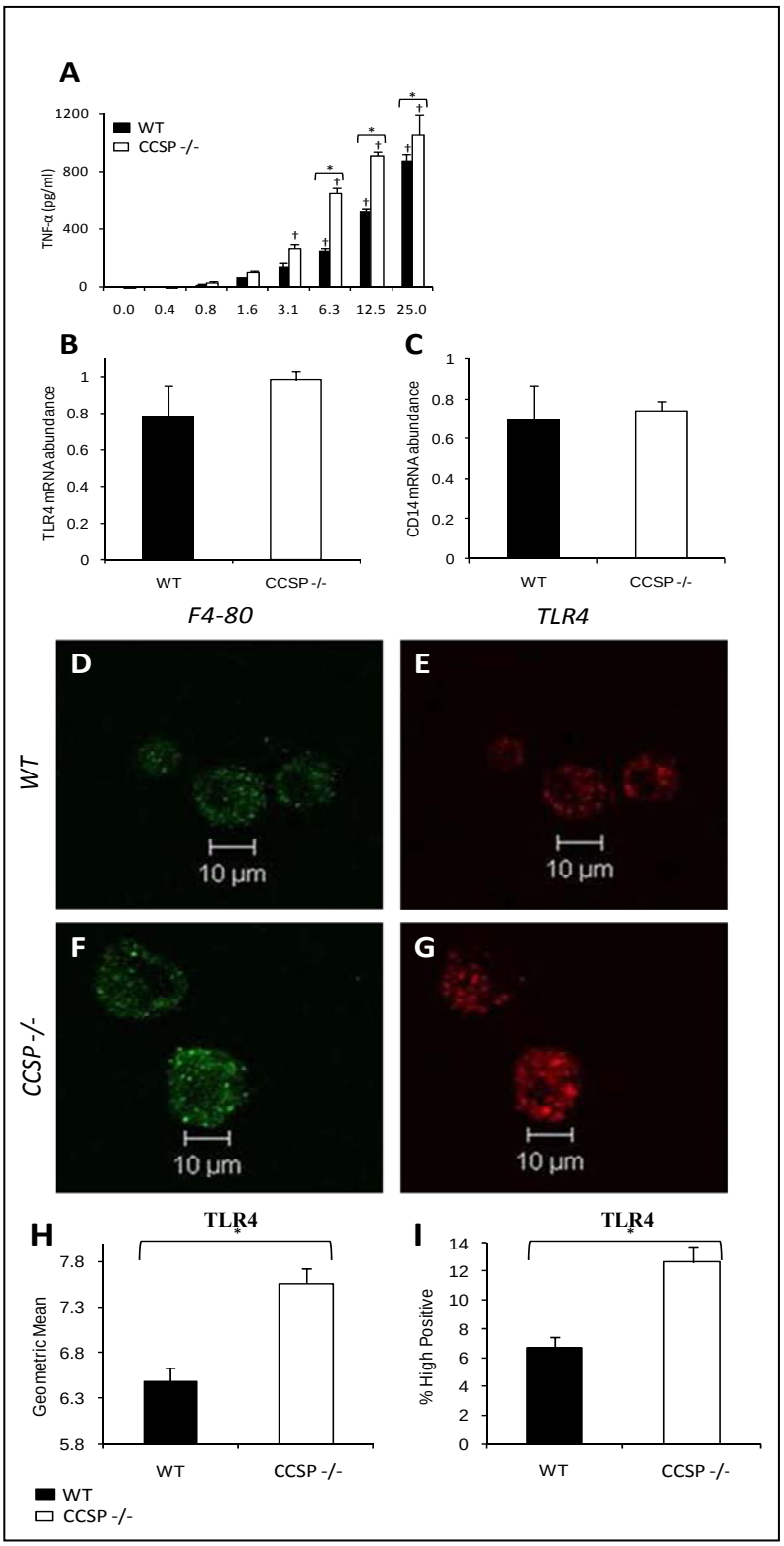

Figure 19. CCSP deficiency augments the macrophage elicited inflammatory response.

Figure 19 Continued.

(A) Primary lung macrophages from WT and CCSP-/- mice were exposed to 0.00, 0.39, 0.78, 1.56, 3.13, 6.25, 12.5, and 25.00 ng/ml *P. Aeruginosa* derived LPS spiked media for six hours (N = 4 per group). TNF-α (pg/ml) was determined in media by a mouse TNF-α sandwich ELISA. (* and †: Tukey's *post hoc* p-value <0.05 in comparison of WT and CCSP-/- or comparison to control, respectively; WT: Black, CCSP-/-: White). (B and C) Realtime PCR analysis of TLR4 and CD14 mRNA abundance in isolated lung macrophages indicates no difference (t-test p-value >0.05) between WT and CCSP-/- in expression of key components of the LPS signaling machinery (N = 3/genotype). BAL cells from WT (D, E) and CCSP-/- (F, G) lungs were stained for the macrophage marker F4/80 (D, F), TLR4 (E, G), and analyzed by confocal microscopy. Flow cytometric analysis of BAL cells from wild-type (Black, N = 5) and CCSP-/- (White, N = 5) lungs were stained for F4/80 and TLR4. TLR4 expression on F4/80 positive macrophages was quantified and presented as geometric mean fluorescent intensity (H, *t-test p-value < 0.001) and percentage of macrophages with high TLR4 expression (I, *t-test p-value < 0.001). Data presented as mean +/- SEM.

TLR4 surface expression represented by the geometric mean of the fluorescence intensity and % of macrophages with high TLR4 surface expression (Figure 19 H and I, respectively). These results confirm that macrophages from CCSP-/- mice are hyper-responsive to LPS and that the increased TLR4 surface expression on macrophages was most likely responsible for the observed increase in TNF-α production in vivo following delivery of aerosolized LPS.

To determine if CCSP directly regulates macrophage responsiveness to LPS in cultured macrophages, fractionated BAL was prepared from WT and CCSP-/- mice according to a previously published protocol[196] and used to test the inhibitory effects of CCSP on macrophage responsiveness. These experiments are discussed in detail in Appendix B.2 Figure 25. Briefly, Raw264.7 macrophages were exposed to LPS and TNF-α measured in the supernatant as an endpoint for macrophage responsiveness. The ability of BAL to modulate this response was further investigated in two separate experiments. In the first experiment, no differences in the potency of LPS were observed following pre-incubation of LPS with fractionated BAL and stimulus of cultured macrophages using BAL/LPS extract.. In the second experiment, pre-treatment of macrophages with fractionated BAL prior to LPS stimulus also didn't affect the LPS elicited inflammatory response (Appendix B. 2 Figure 25). These data suggest that neither CCSP nor other changes to the acellular fraction of airway lining fluid from CCSP-/- mice directly regulate macrophage responsiveness to LPS. Rather, this data support a model in which attenuated Clara cell function results in intrinsic functional differences in the lung macrophage population.

4.5 DISCUSSION

This study provides evidence for anti-inflammatory roles of the airway epithelium and elucidates a mechanism whereby Clara cells may regulate this process. Injured airway epithelium and mice deficient in expression of Clara cell secretory protein (CCSP) respond more robustly to inhaled *P. aeurginosa* lipopolysaccharide (LPS) leading to increased recruitment of PMNs. Through utilization of micrroarray analysis, pathway modeling, and *in vivo* validation it was demonstrated that TNF-α signaling was robustly increased in the CCSP-/- inflammatory response. Functional analysis of macrophages isolated from WT and CCSP-/- lungs revealed a robust increase in LPS responsiveness in the CCSP-/- isolated macrophage compared to WT and was paralleled by increased TLR4 surface abundance on CCSP-/- macrophages at steady-state. The response of cultured macrophages could not be altered *in vitro* with fractionated CCSP enriched BAL indicating that CCSP does not directly regulate macrophage responsiveness. Instead, these data argue that CCSP deficiency causes an intrinsic alteration to lung macrophage behavior.

Recent reports have suggested that the airway epithelium provides a pro-inflammatory role in the innate immune response through modulation of epithelial NF-kB signaling and subsequent secretion of inflammatory cytokines and chemokines [27,35-37]. In contrast, results in this study define normal Clara cell secretory function and the production of CCSP as key negative regulators of the inflammatory response, providing evidence that the airway epithelium

confers anti-inflammatory properties to the lung. Of particular interest is the apparent discrepancy between the findings presented herein and those of Elizur and colleagues describing the effects of acute Clara cell injury on the inflammatory response [27]. In their study, Elizur and colleagues concluded that Clara cells are pro-inflammatory based upon their observation of attenuated TNF-α and KC production in LPS challenged naphthalene injured lung. In contrast, this study demonstrates that Clara cells are anti-inflammatory based upon the observation that PMN recruitment is synergistically increased in LPS challenged naphthalene injured lung. A likely explanation can be attributed to differences in the time at which injured mice are challenged with LPS. In the study by Elizur and colleagues, the protocol indicates mice were exposed to LPS 2.5 hours after injury, which is preceded 1.5 hours earlier by a supra-maximal level of Clara cell secretions in the airway as measured by CCSP protein abundance in BAL (Figure 13A). The overabundance of CCSP delivered into the airway before LPS stimulus may therefore diminish the inflammatory response. In contrast, the protracted loss of Clara cell secretory function results in altering lung macrophage behavior and exacerbating the response to pro-inflammatory stimuli.

These data have important implications regarding regulation of the inflammatory response in normal and diseased airway. In the normal adult airway, Clara cells function to moderate responses to inhaled inflammatory agents, a function that involves paracrine influences of Clara cell secretions on lung macrophages [62]. These data suggest that Clara cell secretory dysfunction that accompanies airway remodeling results in loss of the intrinsic immunosuppressive properties provided by the epithelium leading to exacerbation of the inflammatory response. Furthermore, the exposure of epithelial cells from WT mice to LPS

results in a dramatic decrease in expression of CCSP. This finding is consistent with previous reports demonstrating that in vivo exposure of mice to live *P. aeurginosa* results in decreased expression of CCSP. However, in contrast to the finding of Harrod et al., this study demonstrates that decreased CCSP mRNA abundance can occur independently of TNF-α [195]. When put in the context of these findings from other laboratories these data argue that airway inflammation resulting from acute exposure of normal airways to pro-inflammatory bacterial products is actively suppressed, but that chronic infection leads to decreased Clara cell secretory function and elevated immune-responsiveness that is typical of individuals with chronic lung disease.

The postulated paracrine/endocrine function of CCSP implies recognition by a cell surface receptor. A candidate receptor system has previously been described in the proximal tubule of the kidney in which receptor mediated endocytosis occurs through a megalin/cubilin dependent mechanism. Receptor mediated uptake of CCSP within the proximal convoluted tubule results in its catabolism which has the potential to release bound ligands [197]. However, this receptor/ligand interaction was shown to be specific to the kidney with no evidence for its activity within structural cells or macrophages of the lung. Other candidate receptors have been described previously leading to speculation that CCSP may function as a cytokine [198,199]. Recently another candidate receptor has been identified that mediates interactions with other structurally related members of the secretoglobin family. SCGB3A2 was shown in an expression cloning screen to interact with the macrophage receptor with collagenous structure (MARCO) [200]. Moreover, SCGB3A2 was shown to compete with LPS for interaction with MARCO, suggesting an alternative mechanism by which secretoglobin family members may alter the

macrophage response to LPS. However, these data suggest that a similar mechanism does not operate in the CCSP dependent moderation of LPS elicited lung inflammation, as the CCSP containing fraction of BAL fails to attenuate LPS elicited TNF-α release in cultured macrophages.

The demonstration in the present study that macrophage function is altered in the setting of CCSP deficiency is consistent with the previous description of changes in annexin A1 (ANXA1) post-translational modification (PTM) within macrophages of CCSP-/- mice [62]. ANXA1 has been shown to play a role in modulation of innate immunity through phosphorylation dependent modulation of the subcellular partitioning in phagosomes. However mechanisms by which post-translational modification of ANXA1 modulate this process remains unknown [201,202]. Studies aimed at understanding mechanisms of TNF-α release from macrophages have revealed that secretion occurs exclusively from the phagocytic cup, a subcellular location where TNF-α is brought into close apposition with its activating protease, TNF-α converting enzyme (TACE) [203]. It is possible that the increased surface expression of TLR4 and resultant increase in TNF-α secretion following LPS stimulus may be dependent upon CCSP dependent changes to ANXA1.

The inability of fractionated BAL to modulate macrophage responsiveness to LPS suggests that CCSP does not directly regulate this process. A reasonable explanation is that the macrophage population in the Clara cell depleted and CCSP deficient lung is intrinsically altered compared to the steady-state and WT populations, respectively. A possible explanation is that CCSP-/- results in altered steady-state monocyte/macrophage populations within the lung. Recently, a subpopulation of monocytes has been identified, termed inflammatory monocytes.

These cells can be distinguished based upon the expression of several genetic markers, including ANXA1, and their pro-inflammatory gene signature[204]. Moreover, these cells are required for a robust neutrophilic response to LPS[205]. More recently, Kim and colleagues demonstrated alterations to macrophage subsets in the setting of chronic lung disease. In particular, they identified an increased abundance of alternatively activated macrophages in CLD, in both mouse models as well as patients. These cells contributed directly to the progression of mucus cell metaplasia and epithelial remodeling that is typical of CLD[206]. Additional studies will be necessary to determine if altered Clara cell secretory function impacts the monocyte/macrophage populations within the lungs of CCSP-/- mice.

Chronic lung disease and associated inflammatory exacerbations are a result of complex interactions between the host and environment[207]. This study identifies a mechanism of epithelial:macrophage cross-talk which when perturbed, as in the setting of chronic lung disease, results in an augmented innate inflammatory response to inhaled environmental agents. The precise molecular mechanism by which CCSP or other unidentified Clara cell secreted proteins mediate these immunomodulatory effects will be the subject of future studies.

5.0 CONCLUSIONS AND FUTURE DIRECTIONS

5.1 EPITHELIAL REPARATIVE CAPACITY REGULATES ECM DYNAMICS

5.1.1 Conclusions

In Chapter 3, the hypothesis that airway epithelial reparative capacity moderates ECM dynamics was tested. This hypothesis had long been suggested though it had never been tested *in vivo*. This study demonstrated that airway epithelial injury initiated a robust response from the underlying mesenchyme. Within 4.0 hours of injury mRNA abundance of ECM gene product TNC accumulated in total lung RNA and reached a maximum by 1 day. When repair initiated, TNC mRNA abundance quickly returned to baseline. Immuno-localization of TNC protein during injury and repair indicated an equally dynamic process. TNC quickly accumulated in the subepithelial mesenchyme 1 day after injury and returned to baseline during productive epithelial repair. In contrast, in the setting of unproductive epithelial repair, TNC mRNA and protein abundance aberrantly and chronically accumulate in the lung. These data clearly indicated that mesenchymal remodeling in CLD may be a direct result of attenuated epithelial reparative capacity.

5.1.2 Future Directions

The finding that airway epithelial repair can moderate ECM dynamics illustrates the need to define the molecular pathways regulating proper airway epithelial repair. Currently, few pathways are known that regulate this process, however, recent work has indicated that WNT/CATNNB1[122], TIMP-1[208], MMP-7[209] or STAT3[210] may be regulators of this process. Chapter 3 defines several additional signaling pathways with potential for regulating epithelial repair. TNC has previously been shown to regulate aspects of wound repair including epithelial migration and differentiation[154]. Therefore TNC may play an active role in regulating epithelial repair as an important niche derived protein factor. To test this hypothesis mice deficient for TNC (TNC-/-) will be injured with naphthalene and repair assessed. TNC-/- mice have been imported and breeding initiated to establish an in house experimental colony. Additionally, the mRNA abundance of AREG, a ligand for EGFR shown to mediate repair of injured liver hepatocytes[211,212], was immediately up-regulated following lung injury. This suggests that AREG/EGFR may regulate airway epithelial repair. To test this hypothesis mice deficient for AREG (AREG-/-) will be injured with naphthalene and reparative capacity assessed. AREG-/- mice have been imported and breeding initiated to establish an in house experimental colony. Additionally mice with a floxed allele of EGFR are in the process of being imported. By crossing these mice to a transgenic line in which the CCSP promoter drives expression of CRE, EGFR can be deleted in all CCSP expressing cells of the conducting airway epithelium. These mice will also be injured and repair evaluated. The future studies outlined here will help to define additional regulators of epithelial repair. Given the importance of epithelial repair in

moderating ECM dynamics, these pathways may prove to be useful points of therapeutic intervention in the setting of CLD.

5.2 CLARA CELLS MODERATE THE INFLAMMATORY RESPONSE THROUGH REGULATION OF MACROPHAGE BEHAVIOR

5.2.1 Conclusions

Clara cells are the most abundant secretory cell lining the conducting airway epithelium in mice and an abundant cellular component of bronchiolar airways in human[6,7]. In recent years their role in airway homeostasis has been studied, including epithelial repair and secretion. More recently, studies have sought to determine the role that Clara cells play in regulation of innate immunity and have identified an essential role in transduction of pro-inflammatory signals[28]. Proper moderation of innate immunity and the inflammatory response are critical to lung function due to persistent exposures to environmental agents. As discussed, Clara cell abundance and secretory capacity are severely diminished in the setting of chronic lung disease. Given their role in innate immunity, the persistent inflammation present in CLD, and decreased abundance in inflammatory lung disease, these data suggest that Clara cells may moderate the inflammatory response. This study was designed to test this hypothesis. Results of this study indicated that injury to Clara cells potentiates the inflammatory response. In addition, a mouse model of attenuated Clara cell secretory function (CCSP-/- mice) also demonstrated that Clara cells have immunosuppressive properties. These data implied that Clara cells serve a paracrine

signaling function in the lung to regulate this process. Previous studies indicated that CCSP deficiency caused alterations to the macrophage proteome[62]. Therefore, inflammation and macrophage behavior were assessed in models of diminished Clara cell abundance and secretion. These data indicated that macrophage behavior is altered resulting in increased surface expression of TLR4 and corresponding increased responsiveness to LPS.

5.2.2 Future Directions

Future studies will be directed at elucidating the mechanism by which lung macrophage behavior is altered. There are likely two reasonable mechanisms through which macrophages may have increased surface expression of TLR4 and increased responsiveness to LPS. Clara cells may either 1) directly regulate TLR4 trafficking or 2) regulate the trafficking or differentiation of monocyte and macrophage subpopulations in the lung. The former mechanism is not likely given the inability to affect the responsiveness of macrophages to LPS treated with WT or CCSP-/- lavage. Therefore, the latter represents a more plausible mechanism. Recent data indicate that monocyte populations can be fractionated on cell surface phenotype and their pro-inflammatory gene signature[204]. More recently, alternatively activated macrophages were shown to be increased in the setting of CLD and a driving force for mucus cell metaplasia and epithelial remodeling[206]. Therefore, future studies will be aimed at evaluating the monocyte/macrophage populations in the CCSP-/- lung more thoroughly. This will include microarray analysis of WT and CCSP-/- lung macrophages for comparison to previously published gene signatures of monocyte/macrophage populations as well as FACS analysis using previously identified markers of monocyte/macrophage subsets[213].

5.3 WORK IN PROGRESS

5.3.1 Basic studies to define the behavior of airway progenitor cells in normal and diseased states

Epithelial maintenance is dependent upon a balance between turnover and renewal. If the rate of epithelial turnover is held constant, maintenance is purely a function of progenitor cell self-renewal versus differentiation. There is currently no information in the existing literature that describes the probability with which different progenitor cell types are maintained through self-renewal or whether this property is impacted by divergence from the steady state such as might be the case with acute or chronic lung disease. The existence of multiple progenitor cell types that can be hierarchically organized, such as those of the bronchiolar epithelium, increase the complexity of this question. It is possible, for example, that bronchiolar stem cells are maintained through a highly regulated process involving extrinsic signals from the stem cell niche to ensure long-term maintenance of a stem cell pool of a defined size. The likelihood that stem cells are activated to participate in epithelial maintenance would inevitably be related to longevity of the transit-amplifying progenitor cell pool. For example, if TA cell maintenance occurs through a stochastic mechanism as proposed by Jones and co-workers[68,69], the probability of which is influenced by extrinsic factors such as injury and/or inflammation, the contribution

of stem cells towards epithelial maintenance will be strongly influenced by disease. Major knowledge gaps and experimental rationale are outlined below.

5.3.2 Analysis of airway progenitor cell behavior during normal epithelial maintenance and repair

The utilization of airway epithelial progenitors during normal epithelial maintenance and repair following injury is underappreciated. The most intriguing and fundamental questions are outlined below:

1) How does progenitor cell utilization differ between steady-state maintenance and repair following injury?
2) Are naphthalene resistant cells (vCE, vClara) sequestered through a stochastic mechanism?
3) What is the proliferative latency of the vCE/vClara, and do they contribute to steady-state epithelial maintenance?
4) How does disease state impact progenitor cell utilization and proliferative latency?

To answer these questions, a labeling strategy has been developed in the lab according to a previously published manuscript by Teta and co-workers[80]. Using this approach, successive rounds of proliferation can be monitored by incorporation of halogenated thymidine analogues into DNA when cells traverse S-phase of the cell cycle and immuno-localized with antibodies specific to each thymidine derivative. Antibody/antigen specificity and evaluation of labeling efficiency are presented in figures 20 and 21, respectively. Preliminary evidence does indicate the airway epithelial progenitor cell utilization differs greatly compared to the intestine at steady-state (Figures 22 and 23). At steady-state, epithelial proliferation is randomly distributed throughout the airway and does not utilize an obligate progenitor population. This is demonstrated by the lack of cells undergoing repeated rounds of proliferation. Interestingly,

activation of the stem cell compartment following airway epithelial injury does indicate that progenitor cells lining the conducting airway epithelium do have the capacity for successive rounds of proliferation with a marked reduction in the latency period. These preliminary data indicate that the airway epithelium is maintained and repaired through two different modes of progenitor cell utilization. Experiments are ongoing to more thoroughly investigate the questions outlined above and are expected to reach completion by June 2009.

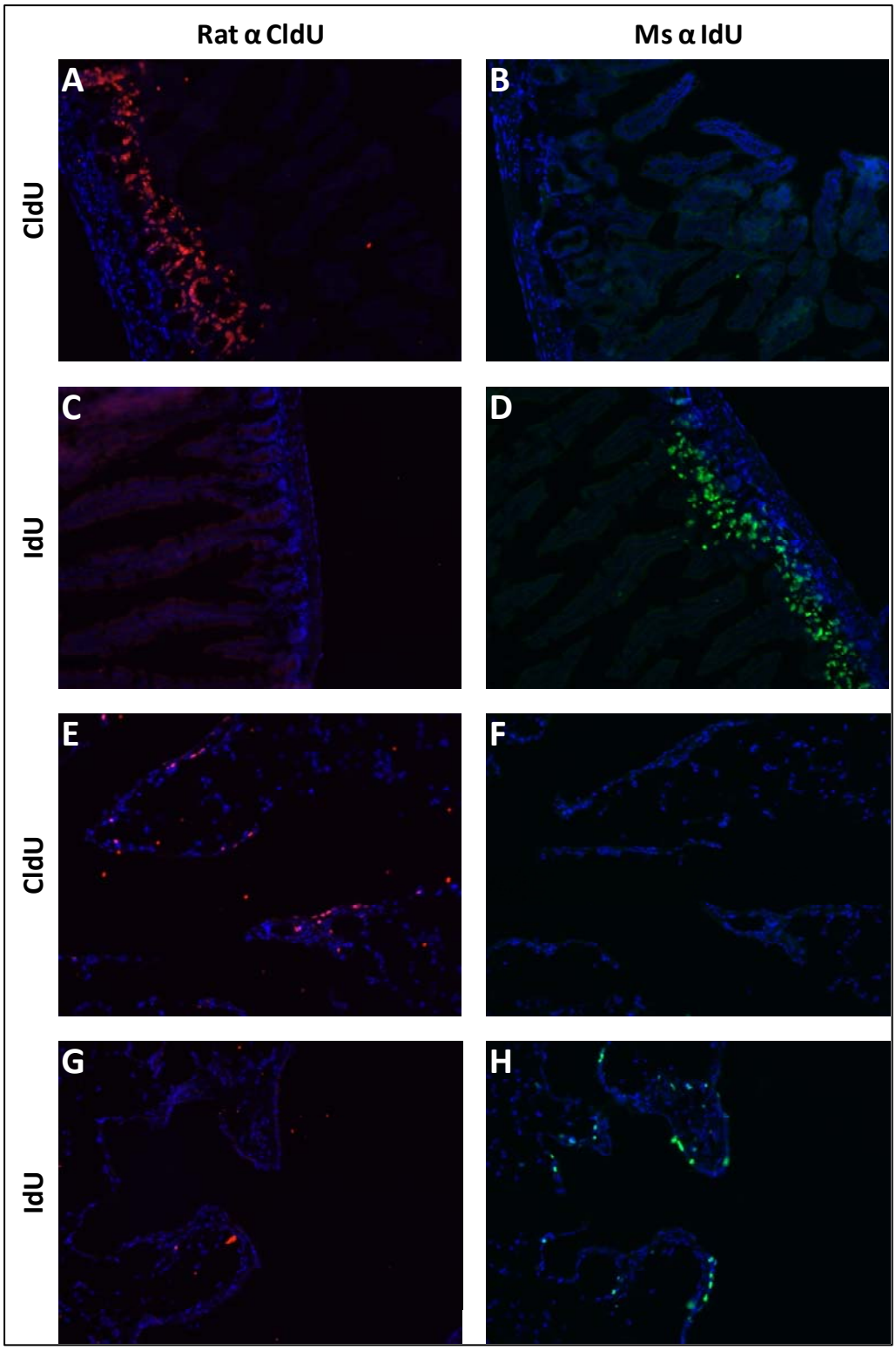

Figure 20. Determination of antibody immunoreactivity and specificity in intestinal and airway epithelium labeled with halogenated thymidine derivatives.

Figure 20 Continued.

WT mice were injected with 0.25 mg of CldU (A, B, E, F) or IdU (C, D, G, H) reconstituted in sterile pyrogenic free saline in the intraperitoneal cavity and sacrificed following a 2.0 hour chase. (A-D) The intestinal epithelium was formalin fixed, cryo-preserved, sectioned at 5um, and stained with antibodies raised against CldU (A,C) or IdU (B, D) (pseudo-colored red or green, respectively, and DAPI nuclear dye pseudo-colored blue). Note both (A) CldU and (D) IdU injections and immuno-staining revealed extensive epithelial proliferation in the intestinal crypts. IdU immunoreactivity in CldU injected mice (B) and CldU immunoreactivity in IdU injected mice (C) was unremarkable, indicating the specificity of the antibody/antigen complex. (E-H) To test the specificity in lung, mice were first exposed to naphthalene to increase the proliferative fraction of airway epithelium. Lungs were harvested 3 days after injury, inflation fixed, cryopreserved, sectioned at 5um, and stained with antibodies raised against CldU (E,G) or IdU (F, H) (pseudo-colored red or green, respectively; and DAPI nuclear dye, blue). Note both (E) CldU and (E) IdU injections and immuno-staining revealed extensive airway and alveolar epithelial proliferation as well as proliferation in the underlying mesenchyme. IdU immunoreactivity in CldU injected mice (F) and CldU immunoreactivity in IdU injected mice (G) was unremarkable, indicating the specificity of the antibody/antigen complex. Representative images at 200X.

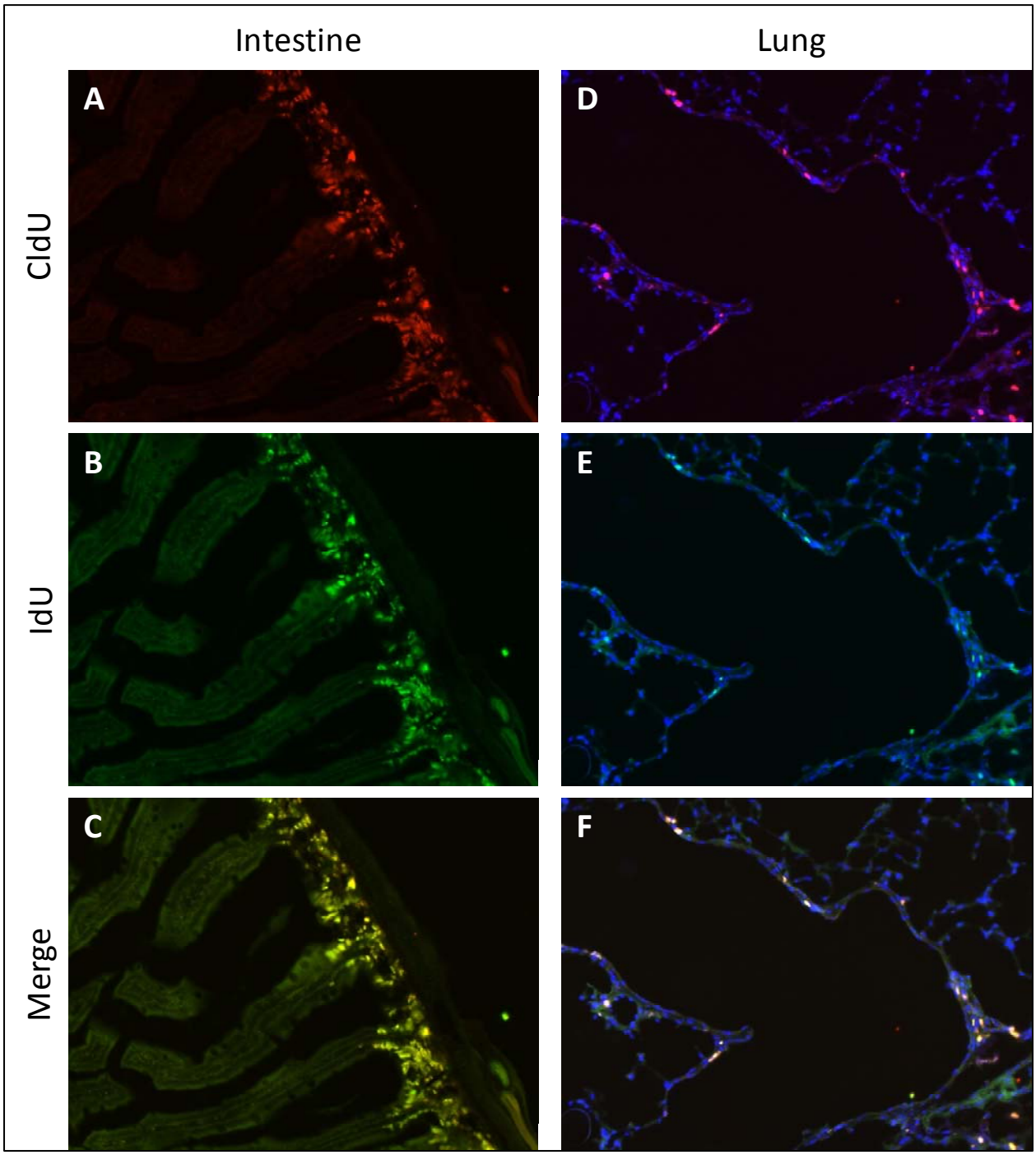

Figure 21. IdU and CldU label equivalent populations of proliferative intestinal or lung epithelial cells.

WT mice were injected with 0.25 mg of CldU and IdU reconstituted in sterile pyrogenic free saline in the intraperitoneal cavity and sacrificed following a 2.0 hour chase. (A-C) Intestine was formalin fixed, cryopreserved,

Figure 21 Continued.

sectioned at 5um, and immuno-stained for CldU and IdU. (A) CldU pseudo-colored red, (B) IdU pseudo-colored green, and (C) merged image pseudo-colored yellow demonstrate that CldU and IdU label equivalent populations of intestinal crypt epithelial cells traversing the S-phase of the cell cycle. (D-F) Mice were exposed to naphthalene to increase the proliferative pool of the epithelium, injected with 0.25mg CldU and IdU 3 days after injury, and sacrificed following a 2.0 hour chase. The lung was harvested, formalin fixed, cryopreserved, sectioned at 5um, and immuno-stained for CldU and IdU. (D) CldU pseudo-colored red, (E) IdU pseudo-colored green, and (F) merged image pseudo-colored yellow demonstrate that CldU and IdU label equivalent populations of airway epithelial cells, alveolar epithelial cells, and mesenchymal cells traversing the S-phase of the cell cycle. Representative images at 200X.

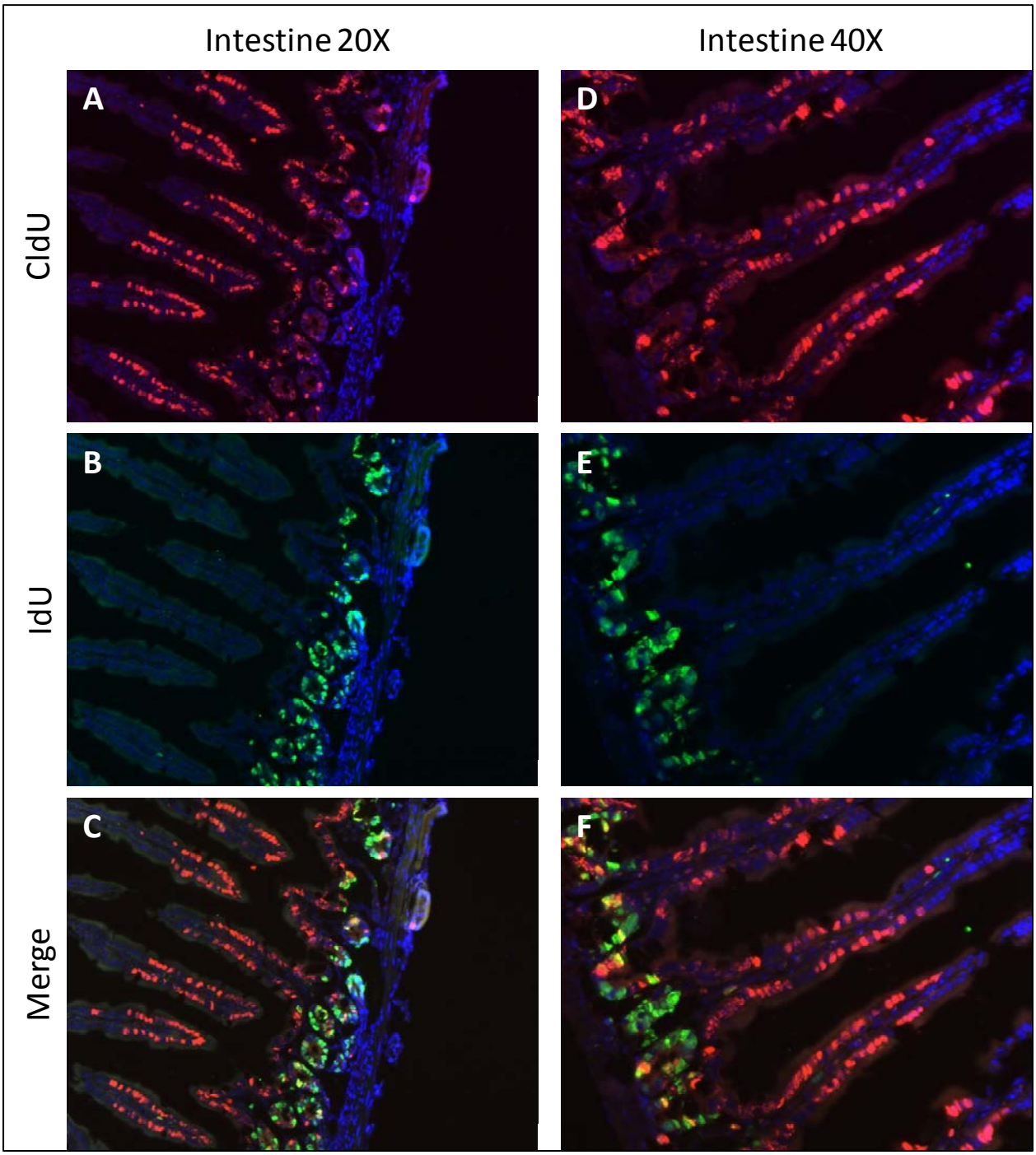

Figure 22. Proliferative latency of progenitor cells in the intestinal epithelium.

Mice were injected with 0.25 mg of CldU, chased for 2 days, injected with 0.25mg of IdU, and sacrificed after a 2 hour chase. Intestine was harvested, formalin fixed, cryopreserved, sectioned at 5um, and immuno-stained for CldU (A, D; pseudo-colored red), IdU (B, E; pseudo-colored green). Merged images are presented in panels C

Figure 22 Continued.

and F. Representative images at 200X (A-C) and 400X (D-F). Note the high degree of proliferation throughout the intestinal crypt and villus. This approach clearly demonstrates that cells proliferate in the intestinal crypt, and migrate up the intestinal villus where they continue to proliferate (note the label dilution that occurs between the migrating tip of the CldU positive epithelial cells and the intestinal crypt). The highly proliferative population of epithelial cells migrating up the intestinal villus is referred to as an obligate transit-amplifying cell. Additionally a subset of cells in the crypt proliferates rapidly, located near the +4 position of the crypt (F, marked by *arrow)*. This is a putative stem cell location within the crypt characterized by Lgr5 expression and short proliferative latency.

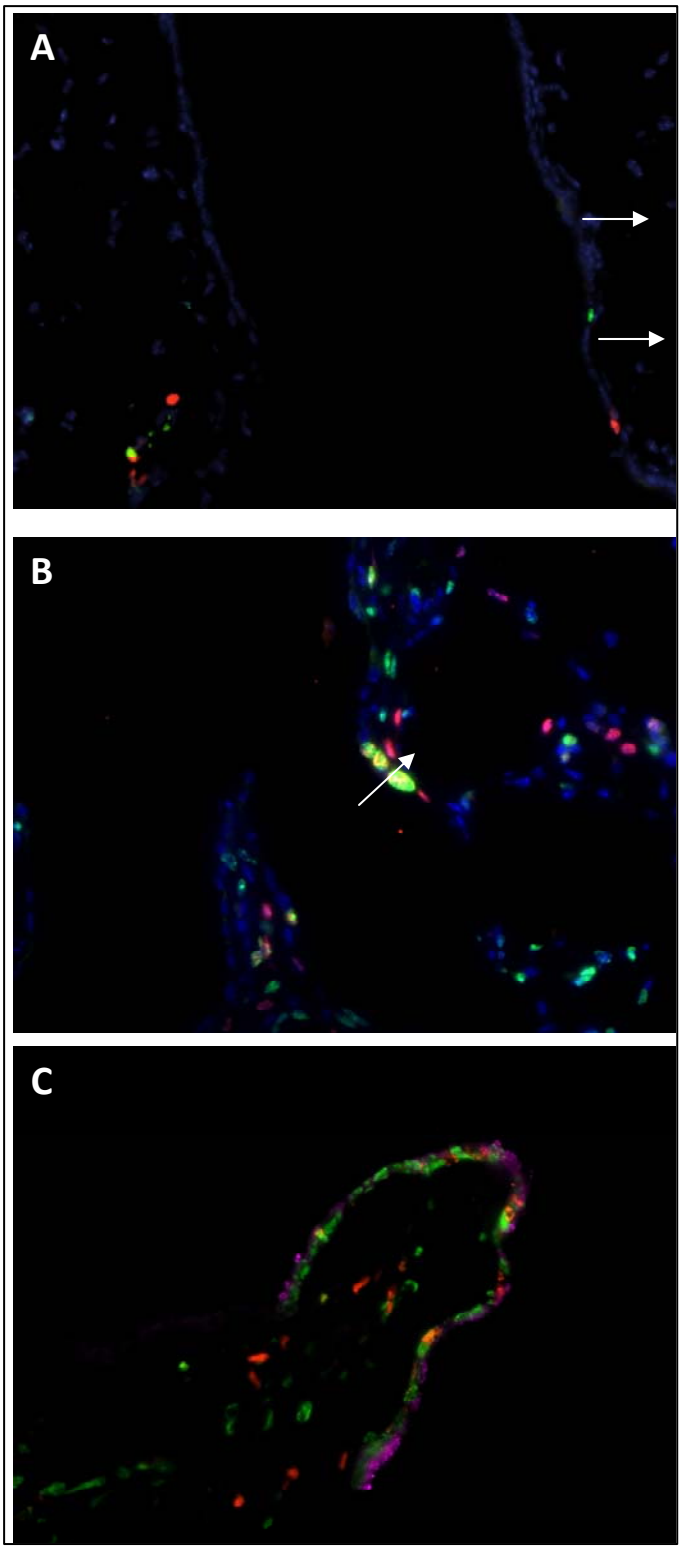

Figure 23. Utilization of progenitor cells in the conducting airway epithelium during steady-state maintenance and repair.

Figure 23 Continued.

(A) WT mice were injected every 12 hours with 0.25mg CldU for 3 days followed by IdU injections every 12 hours for an additional 3 days. Lungs were harvested, formalin fixed, cryopreserved, sectioned at 5um, and immuno-stained for CldU (pseudo-colored red) and IdU (pseudo-colored green). A merged image is presented and representative at 400X. Note the low levels of proliferation in the airway epithelium, and high degree of proliferative latency (lack of cells undergoing proliferation >1, as indicated by a lack of CldU/IdU positive epithelium). Also, proliferation is not defined to a specific region of the airway epithelium. This is in stark contrast to the intestinal epithelium (Figure 22). To test if this mode of progenitor cell utilization changes as a function of injury, WT mice were injected with naphthalene and (B) CldU for 3 days every 12 hours followed by IdU for 1 day every 12 hours or (C) CldU for 3 days every 12 hours followed by IdU for 3 days every 12 hours. Lung tissue was harvested, formalin fixed, cryopreserved, sectioned at 5um, and immuno-stained for CldU (pseudo-colored red), IdU (pseudo-colored green), and CCSP (pseudo-colored magenta). Sections were also stained with the nuclear dye DAPI (pseudo-colored (B) blue, and (C) grey). Merged images are presented and representative of 400X fields. In panel B, note the increased proliferation of the airway epithelial cells that are located at the BADJ and have undergone successive rounds of proliferation as indicated by their immuno-reactivity to both CldU and IdU (yellow, arrow). In panel C, epithelial repair has advanced as evidenced by the appearance of epithelial cells immuno-reactive for the Clara cell specific antigen CCSP and dilution of CldU. Collectively, these data demonstrate that airway epithelial progenitor cell utilization differs markedly from steady-state maintenance both in the latency period between successive rounds of proliferation and the organization of highly proliferative cells to defined microenvironments within the airway.

5.4 FINAL THOUGHTS

The conducting airway epithelium fulfills a myriad of important functions that serve to modulate and maintain lung homeostasis. In order to develop successful treatment strategies for CLD, studies designed to elucidate the mechanisms underlying development and progression of CLD are necessary. In this dissertation, cellular and molecular mechanisms are identified that affect aspects of CLD including uncontrolled ECM deposition, mesenchymal remodeling, and lung inflammation. This work significantly advances the current views of the airway epithelium and the role it plays in normal lung homeostasis and disease.

APPENDIX A

CHAPTER 2 SUPPLEMENTARY MATERIAL

A.1 SUPPLEMENTARY TABLES: PRODUCTIVE REPAIR GENE SIGNATURE

Table 1. Productive Repair Gene Signature (Node 89)

			Fold Change Relative to Control (0)				
LLID	Symbol	Name	0	1	2	3	6
17750	Mt2	Metallothionein 2	1.0	42.8	11.4	7.4	6.5
16156	Il11	Interleukin 11	1.0	17.7	6.1	4.4	2.4
55948	Sfn	Stratifin	1.0	11.7	4.4	3.4	2.5
12740	Cldn4	Claudin 4	1.0	12.2	5.3	2.9	2.9
57875	Angptl4	Angiopoietin-like 4	1.0	7.5	3.6	2.4	1.7
12575		Cyclin-dependent kinase inhibitor 1A (P21)	1.0	9.7	2.8	2.7	2.4
20698	Sphk1	Sphingosine kinase 1	1.0	10.9	3.7	3.7	2.7
***27279**	***Tnfrsf12a**	***Tumor necrosis factor receptor superfamily, member 12a**	***1.0**	***9.6**	***4.4**	***3.5**	***2.9**
23886	Gdf15	Growth differentiation factor 15	1.0	8.5	3.2	2.3	2.8
20648	Snta1	Syntrophin, acidic 1	1.0	3.6	3.0	3.5	2.8
170706	Tmem37	Transmembrane protein 37	1.0	5.1	3.2	3.4	2.6
17869	Myc	Myelocytomatosis oncogene	1.0	5.5	4.2	3.6	3.1
66166	S100a14	S100 calcium binding protein A14	1.0	6.9	4.2	4.3	3.2
20361	Sema7a	Sema domain, immunoglobulin domain (Ig), and GPI membrane anchor, (semaphorin) 7A	1.0	5.6	3.5	3.5	2.4
66214	1190002H23Rik	RIKEN cDNA 1190002H23 gene	1.0	6.2	3.5	3.4	2.0
104009	Qsox1	Quiescin Q6 sulfhydryl oxidase 1	1.0	6.5	3.5	3.2	2.2
214855	Arid5a	AT rich interactive domain 5A (Mrf1 like)	1.0	5.5	3.0	2.8	2.6
18654	Pgf	Placental growth factor	1.0	5.2	3.2	2.7	1.9
***18791**	***Plat**	***Plasminogen activator, tissue**	***1.0**	***5.5**	***2.8**	***2.7**	***1.8**
15368	Hmox1	Heme oxygenase (decycling) 1	1.0	4.6	2.8	2.7	2.3
***11647**	***Alpl**	***Alkaline phosphatase, liver/bone/kidney**	***1.0**	***5.1**	***2.4**	***2.4**	***1.9**
57266	Cxcl14	Chemokine (C-X-C motif) ligand 14	1.0	7.4	3.2	3.1	1.8
22223	Uchl1	Ubiquitin carboxy-terminal hydrolase L1	1.0	7.0	3.4	3.0	1.9
***18793**	***Plaur**	***Plasminogen activator, urokinase receptor**	***1.0**	***7.1**	***3.6**	***3.1**	***2.4**
94242	Tinagl	Tubulointerstitial nephritis antigen-like	1.0	8.2	3.7	3.5	2.8
20295	Ccl17	Chemokine (C-C motif) ligand 17	1.0	9.0	3.2	5.2	2.6
14229	Fkbp5	FK506 binding protein 5	1.0	6.9	3.3	4.0	1.6
20296	Ccl2	Chemokine (C-C motif) ligand 2	1.0	6.6	4.9	5.5	1.9
19288	Ptx3	Pentraxin related gene	1.0	9.3	7.4	4.9	2.7
12642	Ch25h	Cholesterol 25-hydroxylase	1.0	10.8	8.0	5.5	3.6
21816	Tgm1	Transglutaminase 1, K polypeptide	1.0	8.8	7.4	6.3	4.0
67951	Tubb6	Tubulin, beta 6	1.0	5.0	5.0	4.4	2.3
20293	Ccl12	Chemokine (C-C motif) ligand 12	1.0	6.3	5.3	4.4	2.3
20716		Serine (or cysteine) peptidase inhibitor, clade A, member 3N	1.0	8.6	7.2	4.8	2.7

18212	Ntrk2	Neurotrophic tyrosine kinase, receptor, type 2	1.0	4.3	6.2	3.4	1.6
***21923**	**TNC**	***Tenascin C***	***1.0***	***3.8***	***4.8***	***2.9***	***1.8***
18405	Orm1	Orosomucoid 1	1.0	3.7	5.0	3.9	1.8
20308	Ccl9	Chemokine (C-C motif) ligand 9	1.0	2.9	3.9	3.8	1.8
11813		Apolipoprotein C-II	1.0	3.3	3.8	4.5	2.3
11847	Arg2	Arginase type II	1.0	2.8	3.3	3.8	1.6
11846	Arg1	Arginase 1, liver	1.0	2.3	3.6	3.4	1.4
76574	Mfsd2	Major facilitator superfamily domain containing 2	1.0	2.3	2.7	3.5	3.4
12796	Camp	Cathelicidin antimicrobial peptide	1.0	3.5	2.0	3.0	3.3
59083	Fetub	Fetuin beta	1.0	2.5	3.2	2.9	2.4
234199	Fgl1	Fibrinogen-like protein 1	1.0	2.9	3.6	2.7	2.0
57814	Kcne4	Potassium voltage-gated channel, Isk-related subfamily, gene 4	1.0	3.1	3.2	3.1	1.7
11486	Ada	Adenosine deaminase	1.0	4.7	2.5	2.9	1.6
11625	Ahsg	Alpha-2-HS-glycoprotein	1.0	6.9	4.0	3.1	2.4
14121	Fbp1	Fructose bisphosphatase 1	1.0	5.9	3.6	3.0	3.5
14325		Ferritin light chain 1	1.0	3.1	3.0	2.5	2.8
20302	Ccl3	Chemokine (C-C motif) ligand 3	1.0	3.6	3.3	2.7	2.3
116903	Calcb	Calcitonin-related polypeptide, beta	1.0	4.7	2.9	2.1	1.7
13654	Egr2	Early growth response 2	1.0	3.6	3.3	2.4	1.9
23882	Gadd45g	Growth arrest and DNA-damage-inducible 45 gamma	1.0	3.9	2.5	2.7	2.1
17395	Mmp9	Matrix metallopeptidase 9	1.0	4.0	2.1	2.9	1.9
16012	Igfbp6	Insulin-like growth factor binding protein 6	1.0	3.4	2.3	2.9	2.1
14622	Gjb5	Gap junction protein, beta 5	1.0	4.3	3.9	3.9	1.9
21930	Tnfaip6	Tumor necrosis factor alpha induced protein 6	1.0	4.4	3.2	3.7	2.0
26366	Ceacam10	CEA-related cell adhesion molecule 10	1.0	3.0	1.8	3.5	2.8
14204		Interleukin 4 induced 1	1.0	3.0	2.1	3.3	2.8
66277	Klf15	Kruppel-like factor 15	1.0	3.2	1.8	3.1	2.2
15945	Cxcl10	Chemokine (C-X-C motif) ligand 10	1.0	2.7	2.0	3.8	2.1
20568	Slpi	Secretory leukocyte peptidase inhibitor	1.0	4.1	3.4	5.2	3.1
74747	Ddit4	DNA-damage-inducible transcript 4	1.0	3.5	3.2	4.3	3.2
18029	Nfic	Nuclear factor I/C	1.0	2.2	2.3	2.8	2.3
69665	2310043J07Rik	RIKEN cDNA 2310043J07 gene	1.0	2.6	2.5	2.6	2.2
224619	Traf7	Tnf receptor-associated factor 7	1.0	3.3	2.7	3.1	3.0
19229	Ptk2b	PTK2 protein tyrosine kinase 2 beta	1.0	2.0	1.9	1.5	2.1
76905	Lrg1	Leucine-rich alpha-2-glycoprotein 1	1.0	7.5	7.4	7.9	8.1
19152	Prtn3	Proteinase 3	1.0	4.3	4.4	8.2	3.2
70835	Prss22	Protease, serine, 22	1.0	3.8	4.7	4.1	2.5
14620	Gjb3	Gap junction protein, beta 3	1.0	5.4	5.5	5.6	3.8
19734	Rgs16	Regulator of G-protein signaling 16	1.0	5.4	4.9	5.4	4.3
16000	Igf1	Insulin-like growth factor 1	1.0	1.7	5.7	4.9	1.2
18406	Orm2	Orosomucoid 2	1.0	3.9	8.0	8.0	2.9
13717	Eln	Elastin	1.0	3.0	5.6	9.6	3.6
20202	S100a9	S100 calcium binding protein A9 (calgranulin B)	1.0	4.5	2.3	4.5	1.7
76770	2010005H15Rik	RIKEN cDNA 2010005H15 gene	1.0	5.0	3.6	5.0	2.1
20201	S100a8	S100 calcium binding protein A8 (calgranulin A)	1.0	7.0	3.6	5.1	2.7
53608	Map3k6	Mitogen-activated protein kinase kinase kinase 6	1.0	7.6	2.6	3.7	1.6
85031	Pla1a	Phospholipase A1 member A	1.0	8.9	6.2	3.0	1.4
20306	Ccl7	Chemokine (C-C motif) ligand 7	1.0	7.2	5.5	6.0	1.3
20753	Sprr1a	Small proline-rich protein 1A	1.0	13.7	10.4	10.7	3.1
20310	Cxcl2	Chemokine (C-X-C motif) ligand 2	1.0	12.6	8.2	13.7	5.3
14825	Cxcl1	Chemokine (C-X-C motif) ligand 1	1.0	10.5	7.9	9.8	3.8
***11839**	**AREG**	***Amphiregulin***	***1.0***	***5.6***	***9.9***	***8.6***	***6.4***
68891	Cd177	CD177 antigen	1.0	2.3	3.5	10.7	32.5
17840		Major urinary protein 1	1.0	81.6	5.1	9.4	4.9
21857	Timp1	Tissue inhibitor of metalloproteinase 1	1.0	23.7	36.0	23.1	5.6
20210	Saa3	Serum amyloid A 3	1.0	30.5	39.7	71.1	11.3

*Denotes realtime validation.

Table 2. Productive Repair Gene Signature (Node 176)

.

			Fold Change Relative to Control (0)				
LLID	Symbol	Name	0	1	2	3	6
107585	Dio3	Deiodinase, iodothyronine type III	1.0	3.7	3.1	2.3	1.2
16948	Lox	Lysyl oxidase	1.0	4.4	2.5	2.2	1.0
20700		Serine (or cysteine) peptidase inhibitor, clade A, member 1a	1.0	4.9	2.3	1.8	1.2
14066	F3	Coagulation factor III	1.0	4.1	2.2	2.0	1.1
20700		Serine (or cysteine) peptidase inhibitor, clade A, member 1a	1.0	3.7	2.3	2.1	1.5
11815	Apod	Apolipoprotein D	1.0	5.0	1.4	1.7	1.2
70544	5730437N04Rik	RIKEN cDNA 5730437N04 gene	1.0	3.9	1.7	1.7	1.5
271424	Ihpk3	Inositol hexaphosphate kinase 3	1.0	3.3	1.7	1.7	1.4
21859	Timp3	Tissue inhibitor of metalloproteinase 3	1.0	3.2	1.9	1.7	1.3
171531	Mlph	Melanophilin	1.0	2.8	1.7	1.5	1.3
69863	1810054D07Rik	RIKEN cDNA 1810054D07 gene	1.0	4.5	2.4	1.8	1.5
240913	Adamts4	A disintegrin-like and metallopeptidase (reprolysin type) with thrombospondin type 1 motif, 4	1.0	5.4	2.8	2.0	1.4
17454	Mov10	Moloney leukemia virus 10	1.0	4.1	1.9	2.1	3.0
14469	Gbp2	Guanylate binding protein 2	1.0	3.0	1.3	1.2	1.7
17932	Myt1	Myelin transcription factor 1	1.0	2.9	1.4	1.3	1.8
11606	Agt	Angiotensinogen (serpin peptidase inhibitor, clade A, member 8)	1.0	3.5	1.3	1.7	2.0
11536	Gpr182	G protein-coupled receptor 182	1.0	3.4	1.5	1.5	2.3
13614	Edn1	Endothelin 1	1.0	4.2	1.7	1.6	2.2
71839	Osgin1	Oxidative stress induced growth inhibitor 1	1.0	5.4	1.5	1.6	1.7
18787	Serpine1	Serine (or cysteine) peptidase inhibitor, clade E, member 1	1.0	7.3	2.7	1.9	2.5
433772		Hypothetical LOC433772	1.0	5.5	2.0	1.6	2.8
75146	Tmem180	Transmembrane protein 180	1.0	7.3	2.4	2.0	4.3
18784	Pla2g5	Phospholipase A2, group V	1.0	5.3	1.3	1.2	1.4
20209	Saa2	Serum amyloid A 2	1.0	5.7	1.2	1.3	1.1
14411	Slc6a12	Solute carrier family 6 (neurotransmitter transporter, betaine/GABA), member 12	1.0	6.0	1.3	1.1	1.2
23801	Aloxe3	Arachidonate lipoxygenase 3	1.0	2.5	1.3	1.1	1.2
73679	Tex19.1	Testis expressed gene 19.1	1.0	3.3	1.3	1.1	1.3
78593	Nrip3	Nuclear receptor interacting protein 3	1.0	3.1	1.7	1.2	1.2
18491	Pappa	Pregnancy-associated plasma protein A	1.0	2.8	1.8	1.4	1.4
17133	Maff	V-maf musculoaponeurotic fibrosarcoma oncogene family, protein F (avian)	1.0	3.2	1.5	1.6	1.5
68760	Synpo2l	Synaptopodin 2-like	1.0	3.3	1.0	1.6	1.7
58522	Trim54	Tripartite motif-containing 54	1.0	3.6	0.9	1.3	1.3
17067	Ly6c1	Lymphocyte antigen 6 complex, locus C1	1.0	3.1	1.6	1.5	1.3
15547	Htf9c	HpaII tiny fragments locus 9c	1.0	2.4	1.2	1.0	1.4
328801	Zfp414	Zinc finger protein 414	1.0	1.5	1.1	1.0	1.5
70617	5730508B09Rik	RIKEN cDNA 5730508B09 gene	1.0	1.7	1.8	1.2	1.2
76714		RIKEN cDNA 1700040G22 gene	1.0	2.2	1.8	1.2	1.3
104174	Gldc	Glycine decarboxylase	1.0	2.6	1.6	1.2	1.3
213393	8430408G22Rik	RIKEN cDNA 8430408G22 gene	1.0	4.0	2.1	1.4	1.5
17071	Ly6f	Lymphocyte antigen 6 complex, locus F	1.0	3.5	1.9	1.5	1.0
228765	Sdcbp2	Syndecan binding protein (syntenin) 2	1.0	4.0	2.2	1.5	1.2
20717		Serine (or cysteine) peptidase inhibitor, clade A, member 3M	1.0	3.4	2.4	1.7	1.2
69852	Tcf23	Transcription factor 23	1.0	8.2	2.6	1.5	1.3
193740	Hspa1a	Heat shock protein 1A	1.0	7.6	1.0	1.2	2.5
81702	Ankrd17	Ankyrin repeat domain 17	1.0	1.0	0.6	0.6	1.0
11426	Macf1	Microtubule-actin crosslinking factor 1	1.0	1.2	0.7	0.7	0.9
56542	Ick	Intestinal cell kinase	1.0	1.6	0.9	0.7	0.7
67118	Bfar	RIKEN cDNA 3110001I22 gene	1.0	3.0	1.2	0.8	0.9
16009	Igfbp3	Insulin-like growth factor binding protein 3	1.0	3.7	0.9	0.9	0.9
70422	Ints2	Integrator complex subunit 2	1.0	1.9	1.1	0.8	1.1
66743	4931406I20Rik	RIKEN cDNA 4931406I20 gene	1.0	2.0	1.1	0.9	1.2
16535		Potassium voltage-gated channel, subfamily Q, member 1	1.0	1.6	1.4	1.0	1.5
27643	Ubl4	Ubiquitin-like 4	1.0	1.7	1.4	1.1	1.4
57248	Ly6i	Lymphocyte antigen 6 complex, locus I	1.0	2.3	1.6	1.0	1.0
85031	Pla1a	Phospholipase A1 member A	1.0	2.3	1.6	1.1	1.0
18049	Ngf	Nerve growth factor	1.0	2.3	1.3	1.1	1.1
56365	Clcnkb	Chloride channel Kb	1.0	2.2	1.2	1.0	1.0
14724	Gp1bb	Glycoprotein Ib, beta polypeptide	1.0	2.1	0.8	1.2	1.5
16399	Itga2b	Integrin alpha 2b	1.0	2.1	1.1	1.6	1.4
69573	2310016C08Rik	RIKEN cDNA 2310016C08 gene	1.0	2.7	1.3	1.7	1.3
93960	Nkd1	Naked cuticle 1 homolog (Drosophila)	1.0	2.6	1.4	1.7	1.5

56744	Pf4	Platelet factor 4	1.0	2.4	1.2	1.5	1.4
15476	Hs3st1	Heparan sulfate (glucosamine) 3-O-sulfotransferase 1	1.0	2.6	1.4	1.6	1.6
66922	Rras2	Related RAS viral (r-ras) oncogene homolog 2	1.0	2.7	1.8	2.0	1.2
110454	Ly6a	Lymphocyte antigen 6 complex, locus A	1.0	2.2	1.6	1.6	1.0
66871	Cpne8	Copine VIII	1.0	2.1	1.7	2.2	1.5
13388	Dll1	Delta-like 1 (Drosophila)	1.0	2.5	1.7	2.2	1.5
80981		ADP-ribosylation factor-like 4D	1.0	2.8	1.6	2.1	1.7
30933	Tor2a	Torsin family 2, member A	1.0	2.4	1.7	1.8	1.6
20393	Sgk1	Serum/glucocorticoid regulated kinase 1	1.0	2.3	2.0	1.9	1.4
434325	BC033932	CDNA sequence BC033932	1.0	2.6	2.2	2.3	1.7
***74155**	***Errfi1**	***ERBB receptor feedback inhibitor 1**	***1.0**	***2.3**	***2.0**	***2.1**	***1.6**
16007	Cyr61	Cysteine rich protein 61	1.0	2.8	2.0	2.0	2.2
170776	Cd209c	CD209c antigen	1.0	2.8	2.1	1.9	2.1
19252	Dusp1	Dual specificity phosphatase 1	1.0	2.5	1.6	2.0	2.5
11910	Atf3	Activating transcription factor 3	1.0	3.2	2.0	2.1	2.3
15511	Hspa1b	Heat shock protein 1B	1.0	3.6	1.1	1.4	2.8
18212	Ntrk2	Neurotrophic tyrosine kinase, receptor, type 2	1.0	3.2	1.6	1.1	2.5
17169	Mark3	MAP/microtubule affinity-regulating kinase 3	1.0	1.9	0.9	0.7	1.8
17169	Mark3	MAP/microtubule affinity-regulating kinase 3	1.0	1.9	0.9	0.9	1.9
68724	Arl8a	ADP-ribosylation factor-like 8A	1.0	1.8	1.0	0.8	2.0
20658	Son	Son cell proliferation protein	1.0	2.0	1.1	1.1	2.3
12739	Cldn3	Claudin 3	1.0	2.5	1.7	1.5	2.9
18491	Pappa	Pregnancy-associated plasma protein A	1.0	1.6	1.2	0.9	1.7
231532	Arhgap24	Rho GTPase activating protein 24	1.0	1.8	1.1	0.9	1.8
232449	Dera	2-deoxyribose-5-phosphate aldolase homolog (C. elegans)	1.0	1.4	1.0	0.8	1.7
100689	Spon2	Spondin 2, extracellular matrix protein	1.0	1.7	1.3	1.0	2.2
14760	Gpr19	G protein-coupled receptor 19	1.0	1.5	1.6	1.0	2.0

*****Denotes realtime validation.

Table 3. Productive Repair Gene Signature (Node 534)

			Fold Change Relative to Control (0)				
LLID	Symbol	Name	0	1	2	3	6
18111		Neuronatin	1.0	1.2	2.5	3.7	2.6
93721	Cpn1	Carboxypeptidase N, polypeptide 1	1.0	0.9	2.2	2.9	2.2
15223	Foxj1	Forkhead box J1	1.0	1.3	2.6	3.8	3.5
12654	Chi3l1	Chitinase 3-like 1	1.0	1.5	3.3	4.8	4.3
64136	Sdf2l1	Stromal cell-derived factor 2-like 1	1.0	2.1	3.7	4.5	2.9
100689	Spon2	Spondin 2, extracellular matrix protein	1.0	2.1	2.8	4.4	2.6
77914	Krtap17-1	Keratin associated protein 17-1	1.0	2.4	1.9	4.8	3.2
81007	Defb5	Defensin beta 5	1.0	2.4	2.5	3.5	2.8
76507	Abp1	Amiloride binding protein 1 (amine oxidase, copper-containing)	1.0	1.4	2.9	3.3	4.6
71780	Isyna1	Myo-inositol 1-phosphate synthase A1	1.0	1.8	3.3	4.9	3.9
12709	Ckb	Creatine kinase, brain	1.0	1.5	3.5	4.2	3.3
26561	Mmp23	Matrix metallopeptidase 23	1.0	1.3	3.2	4.9	3.3
67305	Gpx7	Glutathione peroxidase 7	1.0	1.5	2.6	4.3	2.5
52377	Rcn3	Reticulocalbin 3, EF-hand calcium binding domain	1.0	1.0	2.8	3.8	2.4
99543	Olfml3	Olfactomedin-like 3	1.0	1.2	2.9	3.7	2.3
27078	B9d1	B9 protein domain 1	1.0	1.0	2.3	3.1	2.2
77889	Lbh	Limb-bud and heart	1.0	1.4	3.2	3.8	2.6
17534	Mrc2	Mannose receptor, C type 2	1.0	0.9	3.0	3.6	3.1
72080	2010317E24Rik	RIKEN cDNA 2010317E24 gene	1.0	1.1	3.2	4.1	2.2
17218	Mcm5	Minichromosome maintenance deficient 5, cell division cycle 46 (S. cerevisiae)	1.0	1.5	3.5	4.4	2.4
209027	Pycr1	Pyrroline-5-carboxylate reductase 1	1.0	1.4	4.3	4.9	2.8
20377	Sfrp1	Secreted frizzled-related protein 1	1.0	1.6	3.9	5.5	3.0
66929	Asf1b	ASF1 anti-silencing function 1 homolog B (S. cerevisiae)	1.0	1.7	4.1	4.9	3.0
66570	Cenpm	Centromere protein M	1.0	1.8	4.9	5.6	3.2
14962	Cfb	Complement factor B	1.0	2.1	3.6	5.5	2.7
53867	Col5a3	Collagen, type V, alpha 3	1.0	2.5	5.4	4.6	2.6
***16852**	***Lgals1**	***Lectin, galactose binding, soluble 1**	***1.0***	***2.4***	***5.4***	***5.0***	***2.8***
19216	Ptger1	Prostaglandin E receptor 1 (subtype EP1)	1.0	1.7	5.2	5.8	4.0
71878	2310007D09Rik	RIKEN cDNA 2310007D09 gene	1.0	2.3	4.3	4.9	2.5
12822	Col18a1	Collagen, type XVIII, alpha 1	1.0	2.5	4.5	5.5	3.4
12831	Col5a1	Collagen, type V, alpha 1	1.0	2.0	4.6	5.9	3.3
17216	Mcm2	Minichromosome maintenance deficient 2 mitotin (S. cerevisiae)	1.0	2.1	4.2	5.1	2.9
54124	Cks1b	CDC28 protein kinase 1b	1.0	2.8	4.6	5.4	3.2
20204	Prrx2	Paired related homeobox 2	1.0	3.3	5.3	6.4	2.9
272551	Gins2	GINS complex subunit 2 (Psf2 homolog)	1.0	2.1	5.9	6.5	3.5
107995	Cdc20	Cell division cycle 20 homolog (S. cerevisiae)	1.0	2.1	5.4	7.5	4.5
70218	3000004C01Rik	RIKEN cDNA 3000004C01 gene	1.0	1.4	5.7	7.0	4.3
20256	Clec11a	C-type lectin domain family 11, member a	1.0	1.3	3.7	5.8	3.4
12843	Col1a2	Collagen, type I, alpha 2	1.0	1.0	3.5	5.8	3.7
20307	Ccl8	Chemokine (C-C motif) ligand 8	1.0	2.7	5.8	12.1	7.6
12842	Col1a1	Collagen, type I, alpha 1	1.0	1.4	6.6	9.0	6.4
12534	Cdc2a	Cell division cycle 2 homolog A (S. pombe)	1.0	1.3	8.3	9.9	5.3
14793	Cdca3	Cell division cycle associated 3	1.0	1.3	6.4	8.0	3.9
11799	Birc5	Baculoviral IAP repeat-containing 5	1.0	1.2	6.0	7.0	3.7
21877	Tk1	Thymidine kinase 1	1.0	1.1	5.9	7.2	3.4
12442	Ccnb2	Cyclin B2	1.0	0.9	5.1	6.9	2.9
59288		Dynactin 5	1.0	0.9	4.2	5.6	2.8
20877	Aurkb	Aurora kinase B	1.0	0.9	3.3	4.1	2.3
20878	Aurka	Aurora kinase A	1.0	1.2	3.9	4.8	3.2
52276	Cdca8	Cell division cycle associated 8	1.0	1.2	3.6	4.4	2.7
17865	Mybl2	Myeloblastosis oncogene-like 2	1.0	1.1	3.4	3.8	2.2
110033	Kif22	Kinesin family member 22	1.0	1.1	2.9	3.4	1.8
17121	Mxd3	Max dimerization protein 3	1.0	0.9	2.8	3.1	2.1
16580	Kifc1	Kinesin family member C1	1.0	1.3	3.3	2.7	2.3
106795	Tcf19	Transcription factor 19	1.0	1.3	3.3	3.6	2.3
12759	Clu	Clusterin	1.0	1.3	3.2	3.1	2.5
269224	Pask	PAS domain containing serine/threonine kinase	1.0	1.2	3.9	3.8	2.5
68298	Ncapd2	Non-SMC condensin I complex, subunit D2	1.0	0.8	2.9	2.9	1.9
68588	Cthrc1	Collagen triple helix repeat containing 1	1.0	0.7	3.8	4.4	1.8
12832	Col5a2	Collagen, type V, alpha 2	1.0	1.2	3.8	4.2	2.0
20377	Sfrp1	Secreted frizzled-related protein 1	1.0	1.3	4.4	5.8	2.2

*Denotes realtime validation.

A.2 SUPPLEMENTARY TABLES: UNPRODUCTIVE REPAIR GENE SIGNATURE

Table 4. Unproductive Repair Gene Signature (Node 278)

			Fold Change Retive to Control (0)			
LLID	Symbol	Name	0	3	6	9
20753	Sprr1a	Small proline-rich protein 1A	1.0	2.0	44.0	72.6
20210	Saa3	Serum amyloid A 3	1.0	5.7	32.6	39.3
17394	Mmp8	Matrix metallopeptidase 8	1.0	1.7	2.2	11.7
17381	Mmp12	Matrix metallopeptidase 12	1.0	0.9	3.0	6.7
17392	Mmp3	Matrix metallopeptidase 3	1.0	0.8	3.6	7.8
12661	Chl1	Cell adhesion molecule with homology to L1CAM	1.0	1.0	2.4	10.2
231293	C130090K23Rik	RIKEN cDNA C130090K23 gene	1.0	1.0	2.4	12.7
74175	Crct1	Cysteine-rich C-terminal 1	1.0	1.0	2.1	37.9
78593	Nrip3	Nuclear receptor interacting protein 3	1.0	1.3	6.9	8.8
21923*	**TNC**	***Tenascin C***	***1.0***	***0.9***	***6.5***	***8.6***
20306	Ccl7	Chemokine (C-C motif) ligand 7	1.0	1.8	8.9	8.2
85031	Pla1a	Phospholipase A1 member A	1.0	1.8	7.0	11.8
21825	Thbs1	Thrombospondin 1	1.0	2.0	6.7	8.6
21816	Tgm1	Transglutaminase 1, K polypeptide	1.0	2.5	9.3	10.0
18405	Orm1	Orosomucoid 1	1.0	2.8	6.8	8.5
77522	D630002J15Rik	RIKEN cDNA D630002J15 gene	1.0	2.5	5.5	6.6
20296	Ccl2	Chemokine (C-C motif) ligand 2	1.0	2.0	5.4	5.6
20717		Serine (or cysteine) peptidase inhibitor, clade A, member 3M	1.0	1.7	5.2	7.9
15945	Cxcl10	Chemokine (C-X-C motif) ligand 10	1.0	2.1	5.3	8.5
12740	Cldn4	Claudin 4	1.0	2.7	5.9	18.2
20716		Serine (or cysteine) peptidase inhibitor, clade A, member 3N	1.0	2.5	10.3	16.6
21857	Timp1	Tissue inhibitor of metalloproteinase 1	1.0	2.7	17.7	21.2
68891	Cd177	CD177 antigen	1.0	11.2	21.9	29.1
11839*	**AREG**	***Amphiregulin***	***1.0***	***5.7***	***13.7***	***12.9***
23886	Gdf15	Growth differentiation factor 15	1.0	7.5	14.5	14.0
12575		12575 Cyclin-dependent kinase inhibitor 1A (P21)	1.0	5.7	9.1	10.2
76507	Abp1	Amiloride binding protein 1 (amine oxidase, copper-containing)	1.0	4.8	5.6	4.7
56742	Psrc1	Proline/serine-rich coiled-coil 1	1.0	4.1	5.7	6.4
20310	Cxcl2	Chemokine (C-X-C motif) ligand 2	1.0	3.1	5.5	8.3
12534	Cdc2a	Cell division cycle 2 homolog A (S. pombe)	1.0	3.0	6.4	6.8
20307	Ccl8	Chemokine (C-C motif) ligand 8	1.0	4.5	6.9	8.0
17750	Mt2	Metallothionein 2	1.0	3.9	10.8	13.5
20730	Spink3	Serine peptidase inhibitor, Kazal type 3	1.0	6.5	17.6	3.7
14120	Fbp2	Fructose bisphosphatase 2	1.0	1.1	4.2	4.9
16668	Krt18	Keratin 18	1.0	1.6	4.3	6.1
66166	S100a14	S100 calcium binding protein A14	1.0	1.7	4.4	5.5
17869	Myc	Myelocytomatosis oncogene	1.0	1.9	4.4	5.1
69908	Rab3b	RAB3B, member RAS oncogene family	1.0	2.4	4.9	4.3
21950	Tnfsf9	Tumor necrosis factor (ligand) superfamily, member 9	1.0	2.4	4.7	4.2
16156	Il11	Interleukin 11	1.0	1.6	4.5	3.9
100952	Emilin1	Elastin microfibril interfacer 1	1.0	1.6	3.7	3.8
13929	Amz2	Archaelysin family metallopeptidase 2	1.0	1.7	3.7	3.7
13121	Cyp51	Cytochrome P450, family 51	1.0	1.3	2.6	3.1
51797	Ctps	Cytidine 5'-triphosphate synthase	1.0	1.3	2.8	3.6
16782	Lamc2	Laminin, gamma 2	1.0	1.4	2.9	3.7
76905	Lrg1	Leucine-rich alpha-2-glycoprotein 1	1.0	2.9	6.0	6.5
20293	Ccl12	Chemokine (C-C motif) ligand 12	1.0	2.5	5.2	5.6
12450	Ccng1	Cyclin G1	1.0	2.8	5.4	6.4
11847	Arg2	Arginase type II	1.0	2.5	4.1	5.5
12842	Col1a1	Collagen, type I, alpha 1	1.0	1.9	3.8	4.8
103988	Gck	Glucokinase	1.0	2.0	4.5	5.2
16691	Krt8	Keratin 8	1.0	2.0	4.6	5.4
55948	Sfn	Stratifin	1.0	2.5	5.8	6.4
27279*	***Tnfrsf12a***	***Tumor necrosis factor receptor superfamily, member 12a***	***1.0***	***2.5***	***6.5***	***6.8***
12642	Ch25h	Cholesterol 25-hydroxylase	1.0	2.5	7.4	5.8
20295	Ccl17	Chemokine (C-C motif) ligand 17	1.0	2.0	7.5	5.3
14825	Cxcl1	Chemokine (C-X-C motif) ligand 1	1.0	2.7	5.3	5.1
14620	Gjb3	Gap junction protein, beta 3	1.0	2.2	5.2	6.3
20297	Ccl20	Chemokine (C-C motif) ligand 20	1.0	2.0	5.3	5.7
19734	Rgs16	Regulator of G-protein signaling 16	1.0	1.8	6.1	4.6
66929	Asf1b	ASF1 anti-silencing function 1 homolog B (S. cerevisiae)	1.0	1.9	5.3	4.2
54124	Cks1b	CDC28 protein kinase 1b	1.0	2.2	5.0	4.0
272551	Gins2	GINS complex subunit 2 (Psf2 homolog)	1.0	2.3	6.2	4.9
21877	Tk1	Thymidine kinase 1	1.0	2.1	5.5	5.2
14793	Cdca3	Cell division cycle associated 3	1.0	1.9	5.1	5.8

70835	Prss22	Protease, serine, 22	1.0	2.1	5.2	4.8
11799	Birc5	Baculoviral IAP repeat-containing 5	1.0	2.2	5.1	5.6
70218	3000004C01Rik	RIKEN cDNA 3000004C01 gene	1.0	2.6	4.5	5.3
107995	Cdc20	Cell division cycle 20 homolog (S. cerevisiae)	1.0	2.4	3.9	4.9
20878	Aurka	Aurora kinase A	1.0	2.0	3.9	4.6
12442	Ccnb2	Cyclin B2	1.0	1.8	3.9	5.3
72391	Cdkn3	Cyclin-dependent kinase inhibitor 3	1.0	1.5	4.0	6.6
74041	4632434I11Rik	RIKEN cDNA 4632434I11 gene	1.0	1.3	4.0	6.5
16644	Kng1	Kininogen 1	1.0	1.6	3.1	6.5
56710	Dbc1	Deleted in bladder cancer 1 (human)	1.0	1.5	2.9	6.4
71934	Car13	Carbonic anhydrase 13	1.0	1.5	3.0	5.0
14187		Aldo-keto reductase family 1, member B8	1.0	1.2	2.6	4.8
16426	Itih3	Inter-alpha trypsin inhibitor, heavy chain 3	1.0	1.4	2.7	4.7
171180	Syt12	Synaptotagmin XII	1.0	1.6	3.3	4.6
20754	Sprr1b	Small proline-rich protein 1B	1.0	1.5	3.2	4.5
53867	Col5a3	Collagen, type V, alpha 3	1.0	1.5	3.0	3.8
240913	Adamts4	A disintegrin-like and metallopeptidase (reprolysin type) with thrombospondin type 1 motif, 4	1.0	1.4	3.0	4.0
14066	F3	Coagulation factor III	1.0	1.7	3.3	4.0
384009	Glipr2	GLI pathogenesis-related 2	1.0	1.9	3.5	3.8
60411	Cenpk	Centromere protein K	1.0	1.5	3.5	4.2
70645	Oip5	Opa interacting protein 5	1.0	1.6	3.3	3.6
66198	Them5	Thioesterase superfamily member 5	1.0	2.3	3.7	7.7
14229	Fkbp5	FK506 binding protein 5	1.0	2.2	3.0	5.7
11486	Ada	Adenosine deaminase	1.0	1.8	2.8	6.0
16948	Lox	Lysyl oxidase	1.0	1.8	3.1	6.2
20288	Msr1	Macrophage scavenger receptor 1	1.0	1.5	2.4	4.7
69863	1810054D07Rik	RIKEN cDNA 1810054D07 gene	1.0	1.4	2.4	5.2
14130	Fcgr2b	Fc receptor, IgG, low affinity IIb	1.0	0.9	2.3	5.4
51944	D2Ertd750e	DNA segment, Chr 2, ERATO Doi 750, expressed	1.0	1.0	2.2	5.3
12630	Cfi	Complement component factor i	1.0	1.3	2.9	8.4
72119	Tpx2	TPX2, microtubule-associated protein homolog (Xenopus laevis)	1.0	1.2	3.1	5.3
70466	Ckap2l	Cytoskeleton associated protein 2-like	1.0	1.1	2.5	4.5
76131	Depdc1a	DEP domain containing 1a	1.0	1.0	2.8	4.6
55985	Cxcl13	Chemokine (C-X-C motif) ligand 13	1.0	1.4	2.8	7.7
13717	Eln	Elastin	1.0	2.1	4.8	8.9
66442	Spc25	SPC25, NDC80 kinetochore complex component, homolog (S. cerevisiae)	1.0	1.0	2.6	2.9
108907	Nusap1	Nucleolar and spindle associated protein 1	1.0	0.9	2.2	2.8
21789	Tfpi2	Tissue factor pathway inhibitor 2	1.0	0.9	2.3	3.0
70385	Ccdc99	Coiled-coil domain containing 99	1.0	0.9	2.1	3.1
192200	Wfdc12	WAP four-disulfide core domain 12	1.0	0.6	2.0	4.5
79201	Tnfrsf23	Tumor necrosis factor receptor superfamily, member 23	1.0	1.1	2.7	5.5
19417	Rasgrf1	RAS protein-specific guanine nucleotide-releasing factor 1	1.0	1.1	3.3	4.6
13123	Cyp7b1	Cytochrome P450, family 7, subfamily b, polypeptide 1	1.0	0.9	3.2	4.8
11752	Anxa8	Annexin A8	1.0	1.1	3.7	5.3
52033	Pbk	PDZ binding kinase	1.0	1.6	5.6	4.8
12448	Ccne2	Cyclin E2	1.0	1.0	3.8	2.9
18973	Pole	Polymerase (DNA directed), epsilon	1.0	0.9	3.3	3.6
17219	Mcm6	Minichromosome maintenance deficient 6 (MIS5 homolog, S. pombe) (S. cerevisiae)	1.0	1.1	2.9	3.2
15366	Hmmr	Hyaluronan mediated motility receptor (RHAMM)	1.0	1.2	3.0	4.5
110033	Kif22	Kinesin family member 22	1.0	1.2	2.8	3.8
13605	Ect2	Ect2 oncogene	1.0	1.1	2.4	4.0
23921	Sh2b2	SH2B adaptor protein 2	1.0	1.9	2.7	3.6
69028	Mitd1	MIT, microtubule interacting and transport, domain containing 1	1.0	1.4	2.3	3.7
57266	Cxcl14	Chemokine (C-X-C motif) ligand 14	1.0	1.4	2.7	4.6
18802	Plcd4	Phospholipase C, delta 4	1.0	1.7	2.7	3.9
57875	Angptl4	Angiopoietin-like 4	1.0	2.5	3.2	3.4
12428	Ccna2	Cyclin A2	1.0	1.4	4.1	4.7
19366	Rad54l	RAD54 like (S. cerevisiae)	1.0	1.5	4.2	3.9
26886	Cenph	Centromere protein H	1.0	1.2	3.9	4.2
12544	Cdc45l	Cell division cycle 45 homolog (S. cerevisiae)-like	1.0	1.5	3.6	3.2
20135	Rrm2	Ribonucleotide reductase M2	1.0	1.5	3.3	2.6
22171	Tyms	Thymidylate synthase	1.0	1.2	3.3	2.6
16772	Lama1	Laminin, alpha 1	1.0	1.0	2.4	3.5
78354	2210407C18Rik	RIKEN cDNA 2210407C18 gene	1.0	1.0	2.5	4.0
12267	C3ar1	Complement component 3a receptor 1	1.0	1.2	2.0	4.9
54159	Ear5	Eosinophil-associated, ribonuclease A family, member 5	1.0	1.2	2.0	4.1
85031	Pla1a	Phospholipase A1 member A	1.0	1.2	2.0	4.1
18491	Pappa	Pregnancy-associated plasma protein A	1.0	1.3	1.9	4.3
18491	Pappa	Pregnancy-associated plasma protein A	1.0	0.9	1.4	3.9
11846	Arg1	Arginase 1, liver	1.0	1.2	1.6	5.5
17167	Marco	Macrophage receptor with collagenous structure	1.0	1.1	1.2	6.0
68774	Ms4a6d	Membrane-spanning 4-domains, subfamily A, member 6D	1.0	1.3	1.9	4.7
14727	Gp49a	Glycoprotein 49 A	1.0	1.2	1.7	4.4

12768	Ccr1	Chemokine (C-C motif) receptor 1	1.0	1.4	2.3	5.5
13038	Ctsk	Cathepsin K	1.0	1.4	2.1	5.3
216725	Adamts2	A disintegrin-like and metallopeptidase (reprolysin type) with thrombospondin type 1 motif, 2	1.0	1.5	1.9	4.5
18212	Ntrk2	Neurotrophic tyrosine kinase, receptor, type 2	1.0	1.2	4.6	2.8
17865	Mybl2	Myeloblastosis oncogene-like 2	1.0	1.6	3.8	3.1
106795	Tcf19	Transcription factor 19	1.0	1.7	3.8	3.4
16000	Igf1	Insulin-like growth factor 1	1.0	1.4	3.3	3.6
66311	2610036L11Rik	RIKEN cDNA 2610036L11 gene	1.0	1.9	3.5	3.5
16852*	***Lgals1***	***Lectin, galactose binding, soluble 1***	***1.0***	***2.0***	***3.8***	***3.3***
66570	Cenpm	Centromere protein M	1.0	2.0	3.8	3.6
17218	Mcm5	Minichromosome maintenance deficient 5, cell division cycle 46 (S. cerevisiae)	1.0	1.9	4.4	2.8
19216	Ptger1	Prostaglandin E receptor 1 (subtype EP1)	1.0	2.0	3.9	2.1
17216	Mcm2	Minichromosome maintenance deficient 2 mitotin (S. cerevisiae)	1.0	1.8	4.0	2.5
14121	Fbp1	Fructose bisphosphatase 1	1.0	2.1	3.9	2.1
269224	Pask	PAS domain containing serine/threonine kinase	1.0	2.3	4.7	4.3
67951	Tubb6	Tubulin, beta 6	1.0	2.0	4.5	3.9
110749	Chaf1b	Chromatin assembly factor 1, subunit B (p60)	1.0	1.7	3.7	2.6
20877	Aurkb	Aurora kinase B	1.0	1.7	3.0	3.3
69784	1500009L16Rik	RIKEN cDNA 1500009L16 gene	1.0	1.9	2.9	3.8
76835		RIKEN cDNA 2900052L18 gene	1.0	1.7	2.4	3.6
18791*	***Plat***	***Plasminogen activator, tissue***	***1.0***	***1.9***	***3.6***	***3.5***
67177	Cdt1	Chromatin licensing and DNA replication factor 1	1.0	1.8	3.1	3.0
15484	Hsd11b2	Hydroxysteroid 11-beta dehydrogenase 2	1.0	1.9	3.2	2.9
268930	Pkmyt1	Protein kinase, membrane associated tyrosine/threonine 1	1.0	1.5	2.5	2.2
209027	Pycr1	Pyrroline-5-carboxylate reductase 1	1.0	1.6	2.6	2.3
21915	Dtymk	Deoxythymidylate kinase	1.0	1.8	2.7	2.5
17220	Mcm7	Minichromosome maintenance deficient 7 (S. cerevisiae)	1.0	1.7	3.0	2.4
72151	Rfc5	Replication factor C (activator 1) 5	1.0	1.9	3.4	2.8
18102	Nme1	Non-metastatic cells 1, protein (NM23A) expressed in	1.0	2.0	3.3	2.9
56454	Aldh18a1	Aldehyde dehydrogenase 18 family, member A1	1.0	1.8	2.7	2.7
72512	Tmem173	Transmembrane protein 173	1.0	1.7	2.9	2.9
214425	Cilp	Cartilage intermediate layer protein, nucleotide pyrophosphohydrolase	1.0	1.6	2.8	3.1
14156	Fen1	Flap structure specific endonuclease 1	1.0	1.7	2.8	2.8
12831	Col5a1	Collagen, type V, alpha 1	1.0	1.7	2.5	3.0
20204	Prrx2	Paired related homeobox 2	1.0	1.6	2.7	3.2
19288	Ptx3	Pentraxin related gene	1.0	1.4	2.5	2.3
234199	Fgl1	Fibrinogen-like protein 1	1.0	1.4	2.7	2.6
14086	Fscn1	Fascin homolog 1, actin bundling protein (Strongylocentrotus purpuratus)	1.0	1.5	2.5	2.5
66183	1110032A04Rik	RIKEN cDNA 1110032A04 gene	1.0	1.9	2.7	2.7
12822	Col18a1	Collagen, type XVIII, alpha 1	1.0	2.0	2.9	2.5
14705	Bscl2	Bernardinelli-Seip congenital lipodystrophy 2 homolog (human)	1.0	1.8	2.2	2.2
56264		Carboxypeptidase X 1 (M14 family)	1.0	1.7	2.0	2.3
68678	Smtnl1	Smoothelin-like 1	1.0	1.8	2.2	2.8
23795	Agr2	Anterior gradient 2 (Xenopus laevis)	1.0	1.4	2.8	3.1
71860	Wdr16	WD repeat domain 16	1.0	1.7	2.5	3.0
20377	Sfrp1	Secreted frizzled-related protein 1	1.0	2.1	2.4	3.0
12332	Capg	Capping protein (actin filament), gelsolin-like	1.0	2.2	2.7	3.5
51800	Bok	Bcl-2-related ovarian killer protein	1.0	2.3	3.4	3.6
12833	Col6a1	Collagen, type VI, alpha 1	1.0	1.8	2.7	2.8
12843	Col1a2	Collagen, type I, alpha 2	1.0	1.6	2.2	2.9
104009	Qsox1	Quiescin Q6 sulfhydryl oxidase 1	1.0	2.1	2.9	3.4
22351	Vill	Villin-like	1.0	1.9	2.4	2.9
16669	Krt19	Keratin 19	1.0	2.1	2.7	3.1
14226	Fkbp1b	FK506 binding protein 1b	1.0	2.5	2.8	3.8
170706	Tmem37	Transmembrane protein 37	1.0	2.3	2.8	4.1
20377	Sfrp1	Secreted frizzled-related protein 1	1.0	2.2	2.7	3.9
16580	Kifc1	Kinesin family member C1	1.0	2.1	2.9	2.6
12447	Ccne1	Cyclin E1	1.0	1.7	2.4	2.3
78906	9130017N09Rik	RIKEN cDNA 9130017N09 gene	1.0	2.0	2.5	2.5
66422	2410015N17Rik	RIKEN cDNA 2410015N17 gene	1.0	2.0	3.0	2.6
12070	Ngfrap1	Nerve growth factor receptor (TNFRSF16) associated protein 1	1.0	2.1	2.8	2.6
16176	Il1b	Interleukin 1 beta	1.0	2.2	2.3	2.6
14972		Histocompatibility 2, K1, K region	1.0	1.8	2.2	1.9
18971	Pold1	Polymerase (DNA directed), delta 1, catalytic subunit	1.0	1.9	2.5	1.4
77889	Lbh	Limb-bud and heart	1.0	1.8	2.7	1.4
217847	Serpina10	Serine (or cysteine) peptidase inhibitor, clade A (alpha-1 antiproteinase, antitrypsin), member 10	1.0	1.9	3.1	1.6
27273	Pdk4	Pyruvate dehydrogenase kinase, isoenzyme 4	1.0	1.9	2.8	2.5
52276	Cdca8	Cell division cycle associated 8	1.0	1.7	3.0	3.0
68298	Ncapd2	Non-SMC condensin I complex, subunit D2	1.0	1.6	2.7	3.1
66336	Cenpp	Centromere protein P	1.0	1.3	2.5	2.5
15201	Hells	Helicase, lymphoid specific	1.0	1.1	2.5	2.2

67141	Fbxo5	F-box protein 5	1.0	1.2	2.3	2.3
23834	Cdc6	Cell division cycle 6 homolog (S. cerevisiae)	1.0	1.1	2.7	2.2
27357	Gyg	Glycogenin	1.0	1.2	2.4	2.2
13361	Dhfr	Dihydrofolate reductase	1.0	1.5	2.9	2.3
67196	Ube2t	Ubiquitin-conjugating enzyme E2T (putative)	1.0	1.9	3.1	2.5
76843	Dtl	Denticleless homolog (Drosophila)	1.0	1.7	2.7	2.3
17067	Ly6c1	Lymphocyte antigen 6 complex, locus C1	1.0	1.8	3.1	3.0
17215	Mcm3	Minichromosome maintenance deficient 3 (S. cerevisiae)	1.0	1.1	2.4	2.1
26557	Homer2	Homer homolog 2 (Drosophila)	1.0	1.3	2.6	2.4
319554	Idi1	Isopentenyl-diphosphate delta isomerase	1.0	1.3	2.5	2.2
13346	Des	Desmin	1.0	1.5	2.1	1.5
13653	Egr1	Early growth response 1	1.0	1.6	2.8	1.6
11468	Actg2	Actin, gamma 2, smooth muscle, enteric	1.0	1.7	2.6	1.5
67711	Nsmce1	Non-SMC element 1 homolog (S. cerevisiae)	1.0	1.7	2.1	1.6
66548	Adamtsl5	ADAMTS-like 5	1.0	1.7	2.3	1.5
19342		RAB4B, member RAS oncogene family	1.0	1.9	2.0	1.8
11490	Adam15	A disintegrin and metallopeptidase domain 15 (metargidin)	1.0	1.7	2.1	1.9
103733	Tubg1	Tubulin, gamma 1	1.0	1.7	2.2	1.8
110074	Dut	Deoxyuridine triphosphatase	1.0	1.9	2.5	2.0
20382	Sfrs2	Splicing factor, arginine/serine-rich 2 (SC-35)	1.0	1.7	2.3	1.9
108115	Slco4a1	Solute carrier organic anion transporter family, member 4a1	1.0	2.2	3.1	2.3
15200	Hbegf	Heparin-binding EGF-like growth factor	1.0	2.0	3.2	2.3
11535	Adm	Adrenomedullin	1.0	2.1	3.1	2.2
16007	Cyr61	Cysteine rich protein 61	1.0	1.9	2.8	1.9
12817	Col13a1	Collagen, type XIII, alpha 1	1.0	1.9	3.0	1.8
16404	Itga7	Integrin alpha 7	1.0	1.9	3.1	1.7
12406	Serpinh1	Serine (or cysteine) peptidase inhibitor, clade H, member 1	1.0	1.8	2.3	1.3
76574	Mfsd2	Major facilitator superfamily domain containing 2	1.0	1.5	2.1	1.4
75495	1700010A17Rik	RIKEN cDNA 1700010A17 gene	1.0	1.9	2.0	1.2
14613	Gja5	Gap junction membrane channel protein alpha 5	1.0	1.6	2.3	1.3
54525	Syt7	Synaptotagmin VII	1.0	1.5	2.3	1.2
223646	Naprt1	Nicotinate phosphoribosyltransferase domain containing 1	1.0	1.6	2.1	1.6
67169	Nradd	Neurotrophin receptor associated death domain	1.0	1.7	2.2	1.6
18218	Dusp8	Dual specificity phosphatase 8	1.0	2.0	2.4	1.4
13710	Elf3	E74-like factor 3	1.0	2.0	1.9	1.2
18011	Neurl	Neuralized-like homolog (Drosophila)	1.0	2.4	2.6	2.3
20256	Clec11a	C-type lectin domain family 11, member a	1.0	2.2	2.6	2.1
71780	Isyna1	Myo-inositol 1-phosphate synthase A1	1.0	2.3	2.5	1.8
18111		Neuronatin	1.0	2.1	2.1	1.8
114663	Impa2	Inositol (myo)-1(or 4)-monophosphatase 2	1.0	1.9	2.6	2.1
12580	Cdkn2c	Cyclin-dependent kinase inhibitor 2C (p18, inhibits CDK4)	1.0	1.8	2.6	2.0
17766	Nudt1	Nudix (nucleoside diphosphate linked moiety X)-type motif 1	1.0	1.8	2.3	1.9
22256	Ung	Uracil DNA glycosylase	1.0	1.7	2.3	1.7
11806	Apoa1	Apolipoprotein A-I	1.0	1.8	2.8	1.4
20941	Svs4	Seminal vesicle secretory protein 4	1.0	1.5	1.9	2.2
20308	Ccl9	Chemokine (C-C motif) ligand 9	1.0	2.4	3.1	5.2
29870	Gtse1	G two S phase expressed protein 1	1.0	3.3	4.8	6.0
20698	Sphk1	Sphingosine kinase 1	1.0	2.8	3.1	4.3
18793*	***Plaur***	***Plasminogen activator, urokinase receptor***	***1.0***	***2.5***	***3.1***	***3.4***
94242	Tinagl	Tubulointerstitial nephritis antigen-like	1.0	2.5	4.2	3.5
20361	Sema7a	Sema domain, immunoglobulin domain (Ig), and GPI membrane anchor, (semaphorin) 7A	1.0	2.5	3.8	3.7
116903	Calcb	Calcitonin-related polypeptide, beta	1.0	2.6	3.1	3.2
59083	Fetub	Fetuin beta	1.0	2.9	3.2	4.3
26366	Ceacam10	CEA-related cell adhesion molecule 10	1.0	3.3	2.7	4.3
19152	Prtn3	Proteinase 3	1.0	3.7	3.4	4.8
17071	Ly6f	Lymphocyte antigen 6 complex, locus F	1.0	2.8	2.6	4.6
17474	Clec4d	C-type lectin domain family 4, member d	1.0	2.9	2.1	3.9
12765	Il8rb	Interleukin 8 receptor, beta	1.0	3.0	2.4	4.6
58203	Zbp1	Z-DNA binding protein 1	1.0	2.7	2.9	3.3
17314	Mgmt	O-6-methylguanine-DNA methyltransferase	1.0	2.8	3.2	3.1
11910	Atf3	Activating transcription factor 3	1.0	3.2	4.5	3.5
27280	Phlda3	Pleckstrin homology-like domain, family A, member 3	1.0	3.2	4.0	3.4
18406	Orm2	Orosomucoid 2	1.0	4.7	4.9	4.3
74747	Ddit4	DNA-damage-inducible transcript 4	1.0	3.7	2.7	2.8
77914	Krtap17-1	Keratin associated protein 17-1	1.0	3.6	3.2	2.6
223921	Aaas	Achalasia, adrenocortical insufficiency, alacrimia	1.0	2.7	3.3	2.9
12609	Cebpd	CCAAT/enhancer binding protein (C/EBP), delta	1.0	3.3	4.0	2.5
76770	2010005H15Rik	RIKEN cDNA 2010005H15 gene	1.0	6.4	2.7	7.4
20202	S100a9	S100 calcium binding protein A9 (calgranulin B)	1.0	5.9	2.8	5.1
20201	S100a8	S100 calcium binding protein A8 (calgranulin A)	1.0	6.1	2.6	5.1

*Denotes realtime validation.

A.3 SUPPLEMENTARY FIGURES

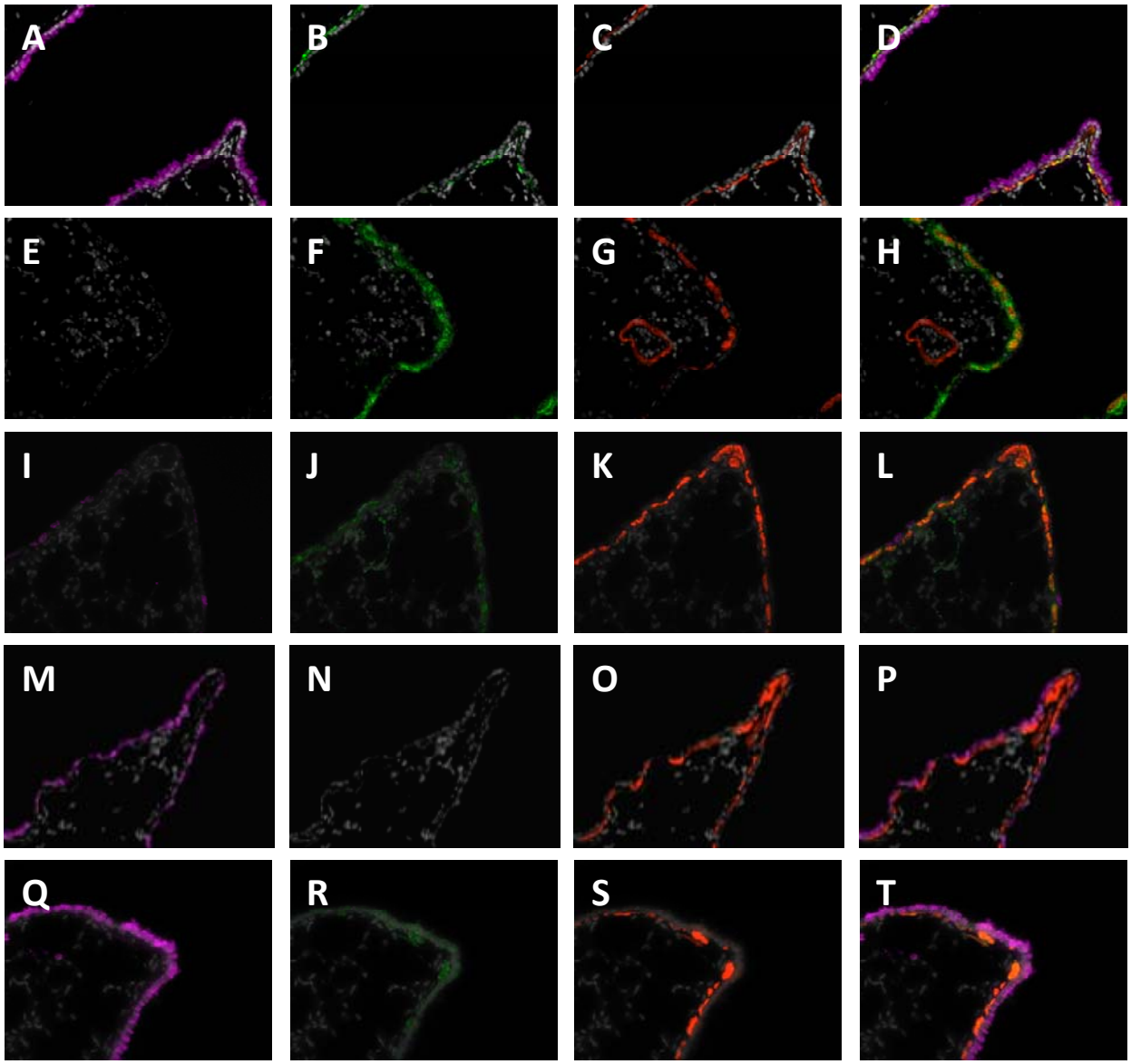

Figure 24. Epithelial repair is associated with matrix remodeling leading to restoration of steady-state levels and distribution.

Figure 24 Continued.

CCSP, TNC, and α-SMA were immuno-localized on formalin fixed and cryo-preserved lung tissue isolated from (A-D) Control mice and (E-H) 1, (I-L) 3, (M-P) 5, and (Q-T) 30 days after naphthalene injury. Pseudo-colored images of DAPI (Grey) merged with CCSP (A, E, I, M, Q; Magenta), TNC (B, F, J, N, R; Green), or α-SMA (C, G, K, O, S; Red). (D, H, L, P, T) 4-color merged images of tissue from Control, 1, 3, 5, and 30 days post injury. Images are representative of the proximal airway epithelium at 400X.

APPENDIX B

SUPPLEMENTARY MATERIALS (CHAPTER 3)

B.1 SUPPLEMENTARY TABLES

Table 5. CCSP independent and LPS responsive alterations to gene expression.

			Wild-type Fold-Change*				CCSP-/- Fold Change*			
Row	Acc Num	Name	C	1.5	6	12	C	1.5	6	12
1	AK015155	RIKEN cDNA 4930415O20 gene	1.0	3.1	6.1	2.6	1.0	2.2	4.6	2.9
2	NM_133712	Kallikrein related-peptidase 10	1.0	2.9	5.9	1.9	1.0	2.6	2.9	1.9
3	AK016757	Ankyrin repeat domain 45	1.0	1.2	3.1	2.5	1.0	1.1	1.5	1.2
4	BB022508	Gap junction membrane channel protein alpha 5	1.0	1.5	2.7	1.6	1.0	2.1	3.0	1.4
5	NM_011331	Chemokine (C-C motif) ligand 12	1.0	3.1	3.8	1.6	1.0	2.5	2.5	1.1
6	NM_146963	Olfactory receptor 45	1.0	1.5	2.1	1.0	1.0	0.7	2.0	1.4
7	NM_133362	Erythroid differentiation regulator 1	1.0	1.6	2.7	1.3	1.0	1.5	2.3	0.9
8	NM_022435	Trans-acting transcription factor 5	1.0	1.2	2.2	1.5	1.0	1.8	3.2	1.1
9	AK002567	Metallothionein 2	1.0	1.0	1.7	0.5	1.0	1.6	2.7	1.1
10	NM_145357	cDNA sequence BC023105	1.0	0.7	2.3	0.8	1.0	1.2	2.1	1.4
11	NM_008331	Interferon-induced protein with tetratricopeptide repeats 1	1.0	0.8	2.7	1.5	1.0	1.4	1.3	1.6
12	NM_008599	Chemokine (C-X-C motif) ligand 9	1.0	1.4	2.5	1.5	1.0	1.6	1.2	2.0
13	BB185036	Transcribed locus	1.0	2.1	2.6	1.5	1.0	1.9	0.7	1.8
14	AF285585	Ring finger protein 17	1.0	2.1	3.4	4.9	1.0	1.6	0.8	1.5
15	Z31361	Vasoactive intestinal polypeptide	1.0	1.8	3.5	1.8	1.0	1.0	0.5	1.1
16	BB383444	Mitogen-activated protein kinase 10	1.0	1.3	2.6	0.7	1.0	2.2	0.6	2.4
17	NM_024273	RIKEN cDNA 4930455C21 gene	1.0	2.2	3.3	1.5	1.0	0.8	0.5	0.5
18	NM_009216	Somatostatin receptor 1	1.0	3.6	5.4	4.0	1.0	0.8	0.6	0.4
19	NM_146309	Olfactory receptor 1337	1.0	1.4	2.6	2.2	1.0	0.5	1.0	0.7
20	NM_145847	Vomeronasal 1 receptor, J3	1.0	1.9	3.2	2.9	1.0	0.7	0.9	0.7
21	BC067397	Reduced expression 2	1.0	1.1	1.4	1.0	1.0	0.5	0.7	0.6
22	NM_145489	Expressed sequence AI661453	1.0	1.0	1.9	0.9	1.0	1.0	1.0	0.8
23	AK147634	RAB GTPase activating protein 1-like	1.0	1.4	2.9	2.5	1.0	1.0	1.0	1.0
24	NM_016874	Deformed epidermal autoregulatory factor 1 (Drosophila)	1.0	1.5	1.7	2.2	1.0	1.0	1.3	1.1
25	NM_011199	Parathyroid hormone receptor 1	1.0	1.4	2.8	3.0	1.0	1.3	2.1	1.4
26	NM_016707	B-cell CLL/lymphoma 11A (zinc finger protein)	1.0	1.3	2.4	3.4	1.0	0.9	1.9	1.3
27	AF072758	Solute carrier family 27 (fatty acid transporter), member 3	1.0	1.3	2.3	3.5	1.0	0.8	1.6	1.1
28	BC052169	Tetraspanin 18	1.0	1.3	3.1	2.0	1.0	0.6	2.2	0.8
29	NM_016749	Myosin binding protein H	1.0	3.7	8.4	8.2	1.0	1.1	2.9	1.4
30	BC026978	IQ motif containing C	1.0	0.9	1.3	0.7	1.0	1.5	1.5	1.3
31	NM_145462	DNA segment, Chr 14, ERATO Doi 500, expressed	1.0	1.0	1.4	1.2	1.0	2.1	2.4	1.9
32	BF464708	RIKEN cDNA 9230110C19 gene	1.0	1.0	1.8	1.0	1.0	1.1	1.8	1.6
33	AK015120	Mus musculus, clone IMAGE:4483401, mRNA	1.0	1.4	1.8	0.7	1.0	0.7	1.0	1.1

34	AK086813	0 day neonate lung cDNA, RIKEN full-length enriched library, clone:E030002K04 product:hypothetical protein, full insert sequence	1.0	1.4	1.8	1.2	1.0	0.8	1.7	1.3
35	NM_080845	Formiminotransferase cyclodeaminase	1.0	1.3	1.1	0.9	1.0	1.5	2.1	1.7
36	NM_172728	CAMP responsive element binding protein 5	1.0	1.6	1.3	1.0	1.0	2.6	2.9	1.9
37	NM_007870	Deoxyribonuclease 1-like 3	1.0	1.1	1.4	1.0	1.0	1.5	1.7	1.5
38	AK021377	Transcribed locus	1.0	1.5	1.7	1.2	1.0	1.2	1.5	1.1
39	M97635	Transcription factor 12	1.0	1.2	1.3	1.0	1.0	1.1	1.5	1.0
40	BC024471	HEAT repeat containing 1	1.0	1.1	1.6	1.0	1.0	1.0	1.1	1.1
41	AK017052	Transcribed locus	1.0	1.0	1.7	1.4	1.0	1.1	1.0	0.6
42	NM_053231	Vomeronasal 1 receptor, C1	1.0	0.9	1.8	0.9	1.0	1.2	1.2	0.8
43	BB479526	Transcribed locus	1.0	1.1	1.4	0.4	1.0	1.0	0.9	0.8
44	AK039104	Ring finger protein 190	1.0	0.8	1.3	0.9	1.0	1.6	1.5	1.2
45	BF456094	Transcribed locus	1.0	0.8	1.2	1.0	1.0	0.9	0.7	1.0
46	NM_134236	Vomeronasal 1 receptor, H11	1.0	1.0	1.4	1.5	1.0	1.5	0.7	1.3
47	NM_026094	ATPase, class I, type 8B, member 3	1.0	1.7	1.5	1.4	1.0	1.8	1.1	0.5
48	NM_011521	Syndecan 4	1.0	1.4	1.3	1.2	1.0	2.0	1.4	0.7
49	NM_080436	Retinol dehydrogenase 9	1.0	1.6	1.2	1.6	1.0	1.5	1.2	1.1
50	BB069382	Transcribed locus	1.0	1.6	1.7	1.6	1.0	1.2	0.4	0.7
51	BB546359	Adenylate kinase 5	1.0	1.6	1.9	2.1	1.0	0.9	0.9	0.5
52	NM_008398	Integrin alpha 7	1.0	1.7	1.7	1.5	1.0	1.0	1.2	0.7
53	NM_013640	Proteasome (prosome, macropain) subunit, beta type 10	1.0	1.2	1.9	1.4	1.0	1.0	2.1	0.9
54	NM_009046	Avian reticuloendotheliosis viral (v-rel) oncogene related B	1.0	1.7	1.9	1.5	1.0	1.3	1.7	1.0
55	NM_146004	CDNA sequence BC024997	1.0	0.9	1.2	1.5	1.0	0.8	2.2	0.9
56	D83147	Sine oculis-related homeobox 2 homolog (Drosophila)	1.0	1.3	1.5	1.3	1.0	1.1	2.9	0.7
57	NM_009921	Cathelicidin antimicrobial peptide	1.0	1.7	2.0	3.3	1.0	1.4	0.8	1.5
58	NM_011904	Tolloid-like 2	1.0	2.0	2.1	3.6	1.0	1.7	1.3	1.1
59	NM_080438	Glycine receptor, alpha 3 subunit	1.0	3.4	1.8	2.6	1.0	1.5	1.1	1.5
60	NM_008260	Forkhead box A3	1.0	1.0	0.7	1.1	1.0	2.0	1.2	0.9
61	NM_008620	Guanylate nucleotide binding protein 4	1.0	1.6	1.6	2.1	1.0	2.2	1.3	1.6
62	AI586049	Glutamate-cysteine ligase, catalytic subunit	1.0	1.8	1.3	1.8	1.0	2.8	1.0	1.7
63	NM_007921	Arginyl aminopeptidase (aminopeptidase B)	1.0	3.0	1.9	1.7	1.0	2.1	1.2	1.3
64	NM_011498	Basic helix-loop-helix domain containing, class B2	1.0	2.0	1.6	1.3	1.0	2.0	1.2	1.2
65	NM_010168	Coagulation factor II	1.0	2.5	2.7	1.6	1.0	1.4	1.1	0.6
66	NM_013521	Formyl peptide receptor 1	1.0	3.1	1.9	1.7	1.0	2.5	1.2	1.1
67	AK004006	Cartilage intermediate layer protein 2	1.0	3.6	1.7	1.3	1.0	1.8	1.4	1.1
68	BE981214	RIKEN cDNA C130039O16 gene	1.0	1.3	1.4	0.8	1.0	2.6	1.6	1.7
69	X82786	Antigen identified by monoclonal antibody Ki 67	1.0	1.3	1.4	0.9	1.0	1.9	1.6	1.4
70	NM_007609	Caspase 4, apoptosis-related cysteine peptidase	1.0	2.1	1.6	1.4	1.0	1.8	1.2	1.4
71	BB091104	Transcribed locus	1.0	4.3	2.2	2.2	1.0	1.4	0.8	0.9
72	NM_011905	Toll-like receptor 2	1.0	5.5	3.3	2.5	1.0	3.2	1.6	1.4
73	NM_033075	DNA segment, Chr 17, human D6S56E 5	1.0	4.9	5.5	2.7	1.0	3.4	2.0	1.6
74	NM_011684	Vomeronasal 1 receptor, A2	1.0	2.4	1.0	1.6	1.0	4.4	2.2	1.4
75	NM_007707	Suppressor of cytokine signaling 3	1.0	3.8	1.5	1.2	1.0	4.6	1.9	0.9
76	X02333	Colony stimulating factor 2 (granulocyte-macrophage)	1.0	3.7	2.5	1.8	1.0	4.0	2.1	1.1
77	NM_013693	Tumor necrosis factor	1.0	6.0	3.2	2.1	1.0	3.4	1.8	1.1
78	NM_009856	CD83 antigen	1.0	7.1	2.4	1.6	1.0	4.6	1.2	0.7
79	NM_008361	Interleukin 1 beta	1.0	15.3	5.9	2.7	1.0	10.1	4.3	3.5
80	NM_009396	Tumor necrosis factor, alpha-induced protein 2	1.0	10.5	2.7	1.7	1.0	10.9	3.3	1.8
81	NM_021274	Chemokine (C-X-C motif) ligand 10	1.0	9.7	7.4	1.6	1.0	10.6	3.3	1.6
82	NM_016960†	Chemokine (C-C motif) ligand 20	1.0	122.1	5.4	3.5	1.0	82.3	5.1	2.6
83	NM_008176†	Chemokine (C-X-C motif) ligand 1	1.0	89.6	12.0	4.2	1.0	94.9	19.4	5.1
84	NM_009140†	Chemokine (C-X-C motif) ligand 2	1.0	211.9	31.9	4.6	1.0	282.8	47.9	4.9
85	NM_011315†	Serum amyloid A 3	1.0	15.4	63.8	36.7	1.0	12.3	62.5	42.6

*Fold-Change calculated relative to control. †Valdation of at least one timepoint, p-value <0.1 (Realtime PCR). C: Control, 1.5: 1.5 hours post LPS, 6: 6 hours post LPS, 12: 12 hours post LPS.

Table 6. CCSP dependent and LPS responsive alterations to gene expression.

Row	Acc Num	Name	Fold-Change*			
			C	1.5	6	12
1	NM_009141	Chemokine (C-X-C motif) ligand 5	2.9	1.1	1.7	1.2
2	NM_011337	Chemokine (C-C motif) ligand 3	1.1	0.8	0.6	0.6
3	NM_009841	CD14 antigen	1.1	1.3	1.4	1.1
4	NM_009890	Cholesterol 25-hydroxylase	1.4	1.2	1.2	1.3
5	NM_031168	Interleukin 6	1.1	1.4	1.3	1.2
6	NM_025416	Thioesterase superfamily member 5	1.3	1.9	2.1	2.0
7	NM_030701	G protein-coupled receptor 109A	1.2	1.1	1.4	0.9
8	X80332	RAB20, member RAS oncogene family	1.3	1.3	1.4	1.2
9	NM_153408	Lung-inducible neuralized-related C3HC4 RING domain protein	1.3	1.3	1.8	1.0
10	NM_019948	C-type lectin domain family 4, member e	1.0	1.5	0.7	1.5
11	NM_007972	Coagulation factor X	1.2	1.1	1.1	1.2
12	NM_145209	2'-5' oligoadenylate synthetase-like 1	0.9	1.6	1.2	1.6
13	NM_011332	Chemokine (C-C motif) ligand 17	0.6	1.2	1.6	1.3
14	NM_011314	Serum amyloid A 2	0.2	1.0	0.5	1.3
15	AK009605	NADPH oxidase organizer 1	1.7	1.3	1.5	1.3
16	NM_010766	Macrophage receptor with collagenous structure	1.5	1.6	0.7	0.9
17	NM_008198	Complement factor B	1.3	0.8	0.6	0.8
18	AK015290	Coiled-coil domain containing 116	1.3	1.5	1.3	1.3
19	NM_145594	Fibrinogen-like protein 1	1.8	1.6	1.2	2.2
20	NM_007705[†]	Cold inducible RNA binding protein	4.0	1.2	2.1	1.6
21	AK007714	Fas apoptotic inhibitory molecule 3	2.6	1.1	1.5	0.5
22	NM_028807	RIKEN cDNA 1200009I06 gene	1.7	1.1	1.4	0.7
23	AK020278	RIKEN cDNA 9130211I03 gene	1.8	1.4	1.5	0.7
24	NM_153074	Leucine rich repeat containing 25	1.3	1.3	1.9	0.8
25	BC018416	Serine (or cysteine) peptidase inhibitor, clade A (alpha-1 antiproteinase, antitrypsin), member 10	1.4	1.3	1.9	2.5
26	NM_016850	Interferon regulatory factor 7	1.3	1.9	1.2	1.6
27	NM_029796	Leucine-rich alpha-2-glycoprotein 1	1.3	1.6	1.9	1.3
28	NM_011593	Tissue inhibitor of metalloproteinase 1	1.2	1.0	1.4	1.5
29	U89889	Hemopexin	1.7	1.1	1.5	1.8
30	NM_054037[‡]	Secretoglobin, family 3A, member 1	3.1	1.7	1.1	0.7
31	AK007956	RIKEN cDNA 1810065E05 gene	1.4	1.6	1.2	1.4
32	AI426026	Developing brain homeobox 1	2.6	1.9	2.0	2.0
33	NM_029733	RIKEN cDNA 2010005H15 gene	1.4	1.1	2.7	2.5
34	NM_013650	S100 calcium binding protein A8 (calgranulin A)	1.0	0.9	1.8	1.2
35	NM_023124	Histocompatibility 2, K1, K region	2.1	3.0	2.0	3.6
36	NM_010391	Histocompatibility 2, Q region locus 10	1.3	1.4	2.6	1.5
37	AK007169	Predicted gene, EG665024	1.4	1.6	2.5	1.7
38	NM_033175	Small proline rich-like 1	1.1	1.5	1.8	1.6
39	NM_021406	Triggering receptor expressed on myeloid cells 1	1.0	1.1	2.1	2.1
40	AK020597	RIKEN cDNA 9530047P18 gene	1.6	1.7	2.3	1.3
41	AK014899	RIKEN cDNA 4921515G04 gene	1.5	1.4	1.7	1.4
42	AK008234	Glucosaminyl (N-acetyl) transferase 3, mucin type	1.6	2.1	1.7	1.6
43	NM_023835	Tripartite motif protein 12	0.9	1.5	1.8	1.6
44	BY598616	Transcribed locus	0.9	1.1	2.1	1.5
45	BB102105	Pogo transposable element with ZNF domain	0.9	1.0	1.5	1.7
46	BB232450	Retinoblastoma 1	0.7	12.9	1.0	1.8
47	AK006226	Cytokine-dependent hematopoietic cell linker	0.3	2.7	0.9	2.4
48	AV271377	RIKEN cDNA 1700008F21 gene	0.6	2.7	0.9	1.3
49	AK010743	Developmental pluripotency associated 2	1.2	3.6	0.8	1.3
50	AV253409	RIKEN cDNA A730032A03 gene	1.9	2.9	3.5	2.0
51	BC024515	Gastrin releasing peptide	1.7	1.7	3.2	2.7
52	BC010324	Immunoglobulin heavy chain (J558 family)	2.6	1.8	3.0	2.9
53	J00544[‡]	Immunoglobulin joining chain	5.3	2.7	1.7	3.3
54	BC010327	Immunoglobulin heavy chain 6 (heavy chain of IgM)	9.2	2.7	2.0	5.2

*Fold-Change calculated relative Wild-type, [†]Validation of at least one timepoint, p-value <0.1 (Realtime).

[‡]Previously validated using S1-nuclease protection. C:control, 1.5: 1.5 hours post LPS, 6: 6 hours post LPS, 12: 12 hours post LPS.

B.2 SUPPLEMENTARY FIGURES

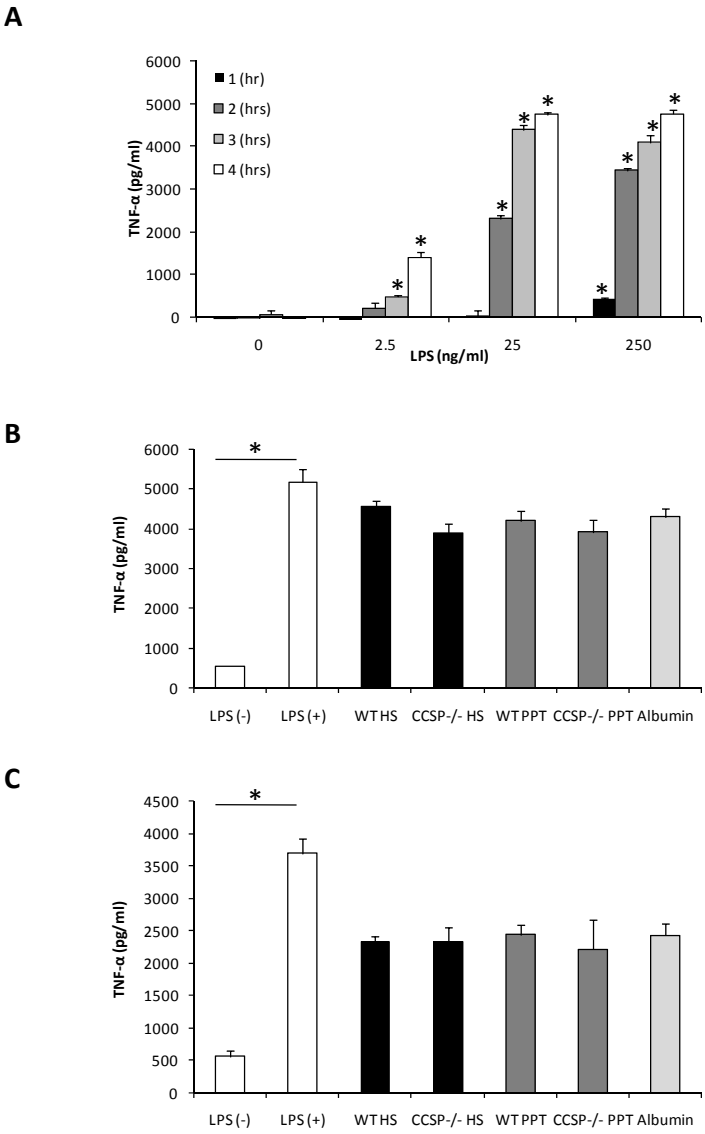

Figure 25. CCSP does not directly regulate the macrophage response to LPS.

(A) Raw264.7 macrophages were exposed to 2.5, 25, and 250ng/ml LPS for 1.0 (black), 2,0 (dark grey), 3.0 (light grey), and 4.0 hours (white). Cell free supernatant was collected by centrifugation at 300g for 5 minutes. TNF-α protein abundance was measured using an ELISA as described in materials and methods. Using this dose

Figure 25 Continued.

response and time-course the 25ng/ml dose of LPS and 2 hour exposure time for subsequent experiments was chosen. (B and C) WT and CCSP-/- lavage were physically and biochemically fractionated to enrich for CCSP according to a previously published protocol by Gupta and colleagues[196]. Briefly, WT and CCSP-/- lavage was centrifuged at 225,000 g (HS = highspeed) to remove surfactant aggregates. Further biochemical enrichment for CCSP was conducted using a perchloric acid precipitation procedure (PPT). CCSP enrichment was quantified by gel electrophoresis, silver staining, and MS identification (Data not shown). CCSP-/- lavage was also fractionated for use as a negative control. Two experiments were conducted to test the direct affects of CCSP on the macrophage response. Experiment one (B) tested whether CCSP interacts with macrophages to alter the response to LPS. Raw264.7 macrophages were incubated overnight with WT and CCSP-/- HS (Black), WT and CCSP-/- PPT (dark grey), or albumin (protein control, light grey) at 12.5ug/ml. The next morning cells were washed once with PBS and stimulated with LPS at 25ng/ml for 2.0hours. Raw264.7 cells that were not incubated with fractionated protein were used as a control (white). Cell free supernatant was collected by centrifugation at 300g for 5 minutes. TNF-α protein abundance was measured using an ELISA as described in materials and methods. WT fractionated protein did not affect macrophage responsiveness when compared to KO protein. Experiment two (C), tested whether the fractionated proteins could attenuate the activity of LPS. WT and CCSP-/- HS (Black), WT and CCSP-/- PPT (dark grey), or albumin (protein control, light grey) at 12.5 ug/ml were incubated with LPS for 30 minutes at room temperature and then added to Raw264.7 cells for 2 hours. As a control LPS not pre-incubated with protein fractionates was used (white). Cell free supernatant was collected by centrifugation at 300g for 5 minutes. TNF-α protein abundance was measured using an ELISA as described in materials and methods. Surprisingly, all extracts reduced the responsiveness of macrophages to LPS. However, albumin attenuated the response to a similar level, arguing that this affects was due to non-specific interaction of protein with LPS. Cumulatively, these results argue that CCSP does not directly regulate macrophage responsiveness to LPS. (*Asterisk* denotes unpaired student's t-test p-value<0.05).

APPENDIX C

PUBLICATION LIST

Peer Reviewed Manuscripts

1. Reynolds SD, Reynolds PR, **Snyder JC**, Whyte F, Paavola KJ, Stripp BR. Ccsp regulates cross talk between secretory cells and both ciliated cells and macrophages of the conducting airway. *Am J Physiol Lung Cell Mol Physiol* 2007;293(1):L114-123.
2. Zemke AC, **Snyder JC**, Brockway BL, Drake J, Reynolds SD, Kaminsk N, Stripp BR. Molecular staging of epithelial maturation using secretory cell-specific genes as markers. *Am J Resp Cell Mol Bio.* 40, 340-348 (2008)[189].
3. **Snyder JC**, Zemke AC, Stripp BR. The reparative capacity of airway epithelium impacts deposition and remodeling of extracellular matrix. *Am J Resp Cell Mol Bio* 2008 (In Press, Accepted for Publication October 2008)[128].
4. **Snyder JC**, Reynolds SD, Hollingsworth JW, Li ZW, Kaminski N, Stripp BR. Clara cells attenuate the inflammatory response through regulation of macrophage function. *Am J Resp Cell Mol Bio* 2009 (In Press, Accepted for Publication April 2009).
5. Giangreco A, Arwert E, Roswell I, **Snyder J**, Watt F, Stripp B. Stem cells are dispensable for lung homeostasis but restore airways after injury. *PNAS* 2009 (In Press, Accepted for Publication April 2009).

Review Articles

1. **Snyder, J.C**., Teisanu, R.M. & Stripp, B.R. Endogenous lung stem cells and contribution to disease. *J Pathol* 217, 254-264 (2009)[128]*.
2. Teisanu RM, **Snyder JC**, Stripp BR. Cell Therapy for Lung Disease. Resident stem cells of the lung. Book chapter (In Press).

*Copyright ©2009 Pathological Society of Great Britain and Ireland, first published by John Wiley & Sons, Ltd.

ABBREVIATIONS

Table 7. List of Abbreviations.

2D-DIGE	Two dimensional-difference gel electrophoresis
AC	Adenocarcinoma
AKP2	Alkaline phosphatase, liver/bone/kidney
ALI	Air liquid interface
ALI*	Acute lung injury
ANXA1	Annexin A1
APC	Adenomatosis polyposis coli
ARDS	Acute respiratory distress syndrome
AREG	Amphiregulin
ASF	Airway surface fluid
AT1I	Alveolar type 1 cell
AT2	Alveolar type 2 cll
BADJ	Bronchoalveolar duct junction
BAL	Bronchoalveolar lavage
BALF	Bronchoalveolar lavage fluid
BASC	Bronchoalveolar stem cell
Bmi1	Bmi1 polycomb ring finger oncogene
BMP	Bone morphogenetic protein
BrdU	5-bromo-2-deoxyuridine
CATNNB1	catenin (cadherin associated protein), beta 1
CCSP	Clara cell secretory protein
CCSP-/-	Homozygous knock-out for CCSP
CD133	Prominin 1
CD14	CD14 antigen
CD31	Platelet/endothelial cell adhesion molecule 1
CD34	CD34 antigen
CD45	Protein tyrosine phosphatase, receptor type, C
CF	Cystic fibrosis
CFTR	Cystic fibrosis transmembrane conductance regulator
CGRP	Calcitonin gene-related peptide
CLD	Chronic Lung Disease

CldU	5-Chlor-2-deoxyuridine
CRE	Cre recombinase
DAPI	4',6-diamidino-2-phenylindole
ECM	Extracellular matrix
EGF	Epidermal growth factor
EGFR	Epidermal growth factor receptor
EMTU	Epithelial mesenchymal trophic unit
ERRFI1	ERBB receptor feedback inhibitor 1
GATA-6	GATA binding protein 6
GCV	Ganciclovir
HSV-tk	Herpes simplex virus-thymidine kinase
IdU	5-Iodo-2-deoxyuridine
IL-6	Interleukin 6
KRAS	v-Ki-ras2 Kirsten rat sarcoma viral oncogene
LCC	Large cell carcinoma
LGALS1	Lectin, galactose binding, soluble 1
LPS	Lipopolysaccharide
MALDI-TOF	Matrix-assisted laser desorption/ionization-Time of flight
MMP-7	Matrix metallopeptidase 7
MS	Mass spectroscopy
MUC5AB	Mucin 5AB
MUC5AC	Mucin 5AC
NEB	Neuroepithelial body
NFATc1	Nuclear factor of activated T-cells, cytoplasmic, calcineurin-dependent 1
Nf-KB	Nuclear factor kappa B
Nkx2.1	Nk2 homeobox 1
NSCLC	Non-small cell lung cancer
P38	Mitogen-activated protein kinase 14
PCL	Pericilliary layer
PI3K	Phosphatidylinositol 3-kinase
PLAT	Plasminogen activator, tissue
PLAUR	plasminogen activator, urokinase receptor
PNEC	Pulmonary neuroendocrine cell
PTEN	phosphatase and tensin homolog
Sca-1	Lymphocyte antigen 6 complex, locus A
SCC	Squamous cell carcinoma
SCID	Severe combined immunodeficiency
SCLC	Small cell lung cancer
SP-C	Surfactant protein C
STAT-3	Signal transducer and activator of transcription 3

TIMP1	Tissue inhibitor of metalloproteinase 1
TLR4	Toll-like receptor 4
TNC	Tenascin C
TNFRSF12A	Tumor necrosis factor receptor superfamily, member 12A
TNF-α	Tumor necrosis factor-alpha
TWEAK	Tumor necrosis factor-like weak inducer of apoptosis
vCCSP	Variant CCSP expressing cell (aka vClara)
vClara	Variant Clara cell (aka vCCSP)
WNT	wingless-related MMTV integration site
WT	Wildtype
α-SMA	actin, alpha 2, smooth muscle, aorta

BIBLIOGRAPHY

1. Snyder, J.C., Teisanu, R.M. & Stripp, B.R. Endogenous lung stem cells and contribution to disease. *J Pathol* **217**, 254-264 (2009).
2. Hansen, J.E., Ampaya, E.P., Bryant, G.H. & Navin, J.J. Branching pattern of airways and air spaces of a single human terminal bronchiole. *J Appl Physiol* **38**, 983-989 (1975).
3. D.J. Beech, P.D.S., C.V. Howard, D. van Velzen,. Lung development: Number of terminal bronchiolar duct endings and gas exchange surface area in victims of sudden infant death syndrome. *Pediatric Pulmonology* **31**, 339-343 (2001).
4. Liu, X., Driskell, R.R. & Engelhardt, J.F. Stem cells in the lung. *Methods Enzymol* **419**, 285-321 (2006).
5. Boers, J.E., Ambergen, A.W. & Thunnissen, F.B. Number and proliferation of basal and parabasal cells in normal human airway epithelium. *Am J Respir Crit Care Med* **157**, 2000-2006 (1998).
6. Boers, J.E., Ambergen, A.W. & Thunnissen, F.B. Number and proliferation of clara cells in normal human airway epithelium. *Am J Respir Crit Care Med* **159**, 1585-1591 (1999).
7. Plopper, C.G., Hill, L.H. & Mariassy, A.T. Ultrastructure of the nonciliated bronchiolar epithelial (Clara) cell of mammalian lung. III. A study of man with comparison of 15 mammalian species. *Experimental lung research* **1**, 171-180 (1980).
8. Castleman, W.L., Dungworth, D.L. & Tyler, W.S. Intrapulmonary airway morphology in three species of monkeys: a correlated scanning and transmission electron microscopic study. *Am J Anat* **142**, 107-121 (1975).
9. ten Have-Opbroek, A.A. The structural composition of the pulmonary acinus in the mouse. A scanning electron microscopical and developmental-biological analysis. *Anat Embryol (Berl)* **174**, 49-57 (1986).
10. Tyler, W.S. Comparative subgross anatomy of lungs. Pleuras, interlobular septa, and distal airways. *The American review of respiratory disease* **128**, S32-36 (1983).
11. Pack, R.J., Al-Ugaily, L.H. & Morris, G. The cells of the tracheobronchial epithelium of the mouse: a quantitative light and electron microscope study. *J Anat* **132**, 71-84 (1981).
12. Low, F.N. The pulmonary alveolar epithelium of laboratory mammals and man. *The anatomical record* **117**, 241-263 (1953).
13. Cardoso, W.V. & Lu, J. Regulation of early lung morphogenesis: questions, facts and controversies. *Development* **133**, 1611-1624 (2006).
14. Metzger, R.J., Klein, O.D., Martin, G.R. & Krasnow, M.A. The branching programme of mouse lung development. *Nature* **453**, 745-750 (2008).

15. Okubo, T. & Hogan, B.L. Hyperactive Wnt signaling changes the developmental potential of embryonic lung endoderm. *J Biol* **3**, 11 (2004).
16. Rawlins, E.L. & Hogan, B.L. Epithelial stem cells of the lung: privileged few or opportunities for many? *Development* (2006).
17. Deterding, R.R. & Shannon, J.M. Proliferation and differentiation of fetal rat pulmonary epithelium in the absence of mesenchyme. *J Clin Invest* **95**, 2963-2972 (1995).
18. Shannon, J.M. Induction of alveolar type II cell differentiation in fetal tracheal epithelium by grafted distal lung mesenchyme. *Dev Biol* **166**, 600-614 (1994).
19. Shannon, J.M., Nielsen, L.D., Gebb, S.A. & Randell, S.H. Mesenchyme specifies epithelial differentiation in reciprocal recombinants of embryonic lung and trachea. *Dev Dyn* **212**, 482-494 (1998).
20. Shu, W., *et al.* Wnt/beta-catenin signaling acts upstream of N-myc, BMP4, and FGF signaling to regulate proximal-distal patterning in the lung. *Dev Biol* **283**, 226-239 (2005).
21. Mucenski, M.L., *et al.* Beta-catenin regulates differentiation of respiratory epithelial cells in vivo. *Am J Physiol Lung Cell Mol Physiol* **289**, L971-979 (2005).
22. Mucenski, M.L., *et al.* beta-Catenin is required for specification of proximal/distal cell fate during lung morphogenesis. *J Biol Chem* **278**, 40231-40238 (2003).
23. Zhang, Y., *et al.* A Gata6-Wnt pathway required for epithelial stem cell development and airway regeneration. *Nat Genet* **40**, 862-870 (2008).
24. Dunsmore, S.E., *et al.* Matrilysin expression and function in airway epithelium. *J Clin Invest* **102**, 1321-1331 (1998).
25. Meban, C. Cytochemistry of the gas-exchange area in vertebrate lungs. *Progress in histochemistry and cytochemistry* **17**, 1-54 (1987).
26. Wright, J.R. Immunoregulatory functions of surfactant proteins. *Nat Rev Immunol* **5**, 58-68 (2005).
27. Elizur, A., *et al.* Clara cells impact the pulmonary innate immune response to LPS. *Am J Physiol Lung Cell Mol Physiol* **293**, L383-392 (2007).
28. Elizur, A., *et al.* Tumor necrosis factor-alpha from macrophages enhances LPS-induced clara cell expression of keratinocyte-derived chemokine. *Am J Respir Cell Mol Biol* **38**, 8-15 (2008).
29. Knowles, M.R. & Boucher, R.C. Mucus clearance as a primary innate defense mechanism for mammalian airways. *J Clin Invest* **109**, 571-577 (2002).
30. Cole, A.M., Dewan, P. & Ganz, T. Innate antimicrobial activity of nasal secretions. *Infect Immun* **67**, 3267-3275 (1999).
31. Kerem, B., *et al.* Identification of the cystic fibrosis gene: genetic analysis. *Science* **245**, 1073-1080 (1989).
32. Davis, P.B. Cystic Fibrosis Since 1938. *Am. J. Respir. Crit. Care Med.* **173**, 475-482 (2006).
33. Koay, M.A., *et al.* Macrophages are necessary for maximal nuclear factor-kappa B activation in response to endotoxin. *American journal of respiratory cell and molecular biology* **26**, 572-578 (2002).
34. Li, Q. & Verma, I.M. NF-kappaB regulation in the immune system. *Nat Rev Immunol* **2**, 725-734 (2002).

35. Skerrett, S.J., *et al.* Respiratory epithelial cells regulate lung inflammation in response to inhaled endotoxin. *Am J Physiol Lung Cell Mol Physiol* **287**, L143-152 (2004).
36. Sadikot, R.T., *et al.* Targeted immunomodulation of the NF-kappaB pathway in airway epithelium impacts host defense against Pseudomonas aeruginosa. *J Immunol* **176**, 4923-4930 (2006).
37. Cheng, D.S., *et al.* Airway Epithelium Controls Lung Inflammation and Injury through the NF-{kappa}B Pathway. *J Immunol* **178**, 6504-6513 (2007).
38. Dodge, D.E., Plopper, C.G. & Rucker, R.B. Regulation of Clara cell 10 kD protein secretion by pilocarpine: quantitative comparison of nonciliated cells in rat bronchi and bronchioles based on laser scanning confocal microscopy. *American journal of respiratory cell and molecular biology* **10**, 259-270 (1994).
39. Dodge, D.E., Rucker, R.B., Singh, G. & Plopper, C.G. Quantitative comparison of intracellular concentration and volume of Clara cell 10 KD protein in rat bronchi and bronchioles based on laser scanning confocal microscopy. *The journal of histochemistry and cytochemistry* **41**, 1171-1183 (1993).
40. Bernard, A., Marchandise, F.X., Depelchin, S., Lauwerys, R. & Sibille, Y. Clara cell protein in serum and bronchoalveolar lavage. *Eur Respir J* **5**, 1231-1238 (1992).
41. Bernard, A.M., Gonzalez-Lorenzo, J.M., Siles, E., Trujillano, G. & Lauwerys, R. Early decrease of serum Clara cell protein in silica-exposed workers. *Eur Respir J* **7**, 1932-1937 (1994).
42. Robin, M., *et al.* Serum levels of CC16, SP-A and SP-B reflect tobacco-smoke exposure in asymptomatic subjects. *Eur Respir J* **20**, 1152-1161 (2002).
43. Mattsson, J., Remberger, M., Andersson, O., Sundberg, B. & Nord, M. Decreased serum levels of clara cell secretory protein (CC16) are associated with bronchiolitis obliterans and may permit early diagnosis in patients after allogeneic stem-cell transplantation. *Transplantation* **79**, 1411-1416 (2005).
44. Pilette, C., *et al.* Reduced epithelial expression of secretory component in small airways correlates with airflow obstruction in chronic obstructive pulmonary disease. *Am J Respir Crit Care Med* **163**, 185-194 (2001).
45. Mukherjee, A.B., Zhang, Z. & Chilton, B.S. Uteroglobin: a steroid-inducible immunomodulatory protein that founded the Secretoglobin superfamily. *Endocrine reviews* **28**, 707-725 (2007).
46. Stripp, B.R., *et al.* Clara cell secretory protein: a determinant of PCB bioaccumulation in mammals. *Am J Physiol* **271**, L656-664 (1996).
47. Andersson, O., Nordlund-Moller, L., Barnes, H.J. & Lund, J. Heterologous expression of human uteroglobin/polychlorinated biphenyl-binding protein. Determination of ligand binding parameters and mechanism of phospholipase A2 inhibition in vitro. *J Biol Chem* **269**, 19081-19087 (1994).
48. Barnes, H.J., *et al.* Structural basis for calcium binding by uteroglobins. *J Mol Biol* **256**, 392-404 (1996).
49. Nord, M., Gustafsson, J.A. & Lund, J. Calcium-dependent binding of uteroglobin (PCB-BP/CCSP) to negatively charged phospholipid liposomes. *FEBS Lett* **374**, 403-406 (1995).
50. Zhang, Z., *et al.* Severe fibronectin-deposit renal glomerular disease in mice lacking uteroglobin. *Science* **276**, 1408-1412 (1997).

51. Reynolds, S.D., *et al.* Normal function and lack of fibronectin accumulation in kidneys of Clara cell secretory protein/uteroglobin deficient mice. *Am J Kidney Dis* **33**, 541-551 (1999).
52. Johnston, C.J., Mango, G.W., Finkelstein, J.N. & Stripp, B.R. Altered pulmonary response to hyperoxia in Clara cell secretory protein deficient mice. *Am J Respir Cell Mol Biol* **17**, 147-155 (1997).
53. Harrod, K.S., Mounday, A.D., Stripp, B.R. & Whitsett, J.A. Clara cell secretory protein decreases lung inflammation after acute virus infection. *Am J Physiol* **275**, L924-930 (1998).
54. Mango, G.W., *et al.* Clara cell secretory protein deficiency increases oxidant stress response in conducting airways. *Am J Physiol* **275**, L348-356 (1998).
55. Johnston, C.J., Finkelstein, J.N., Oberdorster, G., Reynolds, S.D. & Stripp, B.R. Clara cell secretory protein-deficient mice differ from wild-type mice in inflammatory chemokine expression to oxygen and ozone, but not to endotoxin. *Exp Lung Res* **25**, 7-21 (1999).
56. Watson, T.M., *et al.* Altered lung gene expression in CCSP-null mice suggests immunoregulatory roles for Clara cells. *Am J Physiol Lung Cell Mol Physiol* **281**, L1523-1530 (2001).
57. Hayashida, S., Harrod, K.S. & Whitsett, J.A. Regulation and function of CCSP during pulmonary Pseudomonas aeruginosa infection in vivo. *Am J Physiol Lung Cell Mol Physiol* **279**, L452-459 (2000).
58. Wang, S.Z., Rosenberger, C.L., Bao, Y.X., Stark, J.M. & Harrod, K.S. Clara cell secretory protein modulates lung inflammatory and immune responses to respiratory syncytial virus infection. *J Immunol* **171**, 1051-1060 (2003).
59. Wang, S.Z., *et al.* CCSP modulates airway dysfunction and host responses in an Ova-challenged mouse model. *Am J Physiol Lung Cell Mol Physiol* **281**, L1303-1311 (2001).
60. Reynolds, S.D., Reynolds, P.R., Pryhuber, G.S., Finder, J.D. & Stripp, B.R. Secretoglobins SCGB3A1 and SCGB3A2 define secretory cell subsets in mouse and human airways. *Am J Respir Crit Care Med* **166**, 1498-1509 (2002).
61. Unlu, M., Morgan, M.E. & Minden, J.S. Difference gel electrophoresis: a single gel method for detecting changes in protein extracts. *Electrophoresis* **18**, 2071-2077 (1997).
62. Reynolds, S.D., *et al.* CCSP regulates cross talk between secretory cells and both ciliated cells and macrophages of the conducting airway. *Am J Physiol Lung Cell Mol Physiol* **293**, L114-123 (2007).
63. van der Flier, L.G. & Clevers, H. Stem Cells, Self-Renewal, and Differentiation in the Intestinal Epithelium. *Annu Rev Physiol* (2008).
64. Barker, N., van de Wetering, M. & Clevers, H. The intestinal stem cell. *Genes Dev* **22**, 1856-1864 (2008).
65. Sangiorgi, E. & Capecchi, M.R. Bmi1 is expressed in vivo in intestinal stem cells. *Nat Genet* **40**, 915-920 (2008).
66. Barker, N., *et al.* Identification of stem cells in small intestine and colon by marker gene Lgr5. *Nature* **449**, 1003-1007 (2007).
67. Radtke, F. & Clevers, H. Self-renewal and cancer of the gut: two sides of a coin. *Science* **307**, 1904-1909 (2005).

68. Clayton, E.*, et al.* A single type of progenitor cell maintains normal epidermis. *Nature* **446**, 185-189 (2007).
69. Jones, P. & Simons, B.D. Epidermal homeostasis: do committed progenitors work while stem cells sleep? *Nat Rev Mol Cell Biol* **9**, 82-88 (2008).
70. Tumbar, T.*, et al.* Defining the epithelial stem cell niche in skin. *Science* **303**, 359-363 (2004).
71. Horsley, V., Aliprantis, A.O., Polak, L., Glimcher, L.H. & Fuchs, E. NFATc1 balances quiescence and proliferation of skin stem cells. *Cell* **132**, 299-310 (2008).
72. Borthwick, D.W., Shahbazian, M., Krantz, Q.T., Dorin, J.R. & Randell, S.H. Evidence for stem-cell niches in the tracheal epithelium. *Am J Respir Cell Mol Biol* **24**, 662-670 (2001).
73. Reynolds, S.D., Giangreco, A., Power, J.H. & Stripp, B.R. Neuroepithelial bodies of pulmonary airways serve as a reservoir of progenitor cells capable of epithelial regeneration. *Am J Pathol* **156**, 269-278 (2000).
74. Hong, K.U., Reynolds, S.D., Giangreco, A., Hurley, C.M. & Stripp, B.R. Clara cell secretory protein-expressing cells of the airway neuroepithelial body microenvironment include a label-retaining subset and are critical for epithelial renewal after progenitor cell depletion. *Am J Respir Cell Mol Biol* **24**, 671-681 (2001).
75. Rawlins, E.L. & Hogan, B.L. Ciliated epithelial cell lifespan in the mouse trachea and lung. *Am J Physiol Lung Cell Mol Physiol* **295**, L231-234 (2008).
76. Teta, M., Long, S.Y., Wartschow, L.M., Rankin, M.M. & Kushner, J.A. Very slow turnover of beta-cells in aged adult mice. *Diabetes* **54**, 2557-2567 (2005).
77. Stripp, B.R. Hierarchical Organization of Lung Progenitor Cells: Is there An Adult Lung Tissue Stem Cell? *Proc Am Thorac Soc* **5**, 695-698 (2008).
78. Stripp, B.R. & Reynolds, S.D. Maintenance and repair of the bronchiolar epithelium. *Proc Am Thorac Soc* **5**, 328-333 (2008).
79. Dor, Y. & Melton, D.A. How important are adult stem cells for tissue maintenance? *Cell Cycle* **3**, 1104-1106 (2004).
80. Teta, M., Rankin, M.M., Long, S.Y., Stein, G.M. & Kushner, J.A. Growth and regeneration of adult beta cells does not involve specialized progenitors. *Dev Cell* **12**, 817-826 (2007).
81. Xu, X.*, et al.* Beta cells can be generated from endogenous progenitors in injured adult mouse pancreas. *Cell* **132**, 197-207 (2008).
82. Evans, M.J., Johnson, L.V., Stephens, R.J. & Freeman, G. Renewal of the terminal bronchiolar epithelium in the rat following exposure to NO2 or O3. *Lab Invest* **35**, 246-257 (1976).
83. Evans, M.J., Cabral-Anderson, L.J. & Freeman, G. Role of the Clara cell in renewal of the bronchiolar epithelium. *Lab Invest* **38**, 648-653 (1978).
84. Stripp, B.R., Maxson, K., Mera, R. & Singh, G. Plasticity of airway cell proliferation and gene expression after acute naphthalene injury. *Am J Physiol* **269**, L791-799 (1995).
85. Shimizu, T., Nishihara, M., Kawaguchi, S. & Sakakura, Y. Expression of phenotypic markers during regeneration of rat tracheal epithelium following mechanical injury. *Am J Respir Cell Mol Biol* **11**, 85-94 (1994).

86. Engelhardt, J.F., Schlossberg, H., Yankaskas, J.R. & Dudus, L. Progenitor cells of the adult human airway involved in submucosal gland development. *Development* **121**, 2031-2046 (1995).
87. Borthwick, D.W., *et al.* Murine submucosal glands are clonally derived and show a cystic fibrosis gene-dependent distribution pattern. *Am J Respir Cell Mol Biol* **20**, 1181-1189 (1999).
88. Hackett, T.L., *et al.* Characterization of side population cells from human airway epithelium. *Stem Cells* **26**, 2576-2585 (2008).
89. Hong, K.U., Reynolds, S.D., Watkins, S., Fuchs, E. & Stripp, B.R. Basal cells are a multipotent progenitor capable of renewing the bronchial epithelium. *Am J Pathol* **164**, 577-588 (2004).
90. Hong, K.U., Reynolds, S.D., Watkins, S., Fuchs, E. & Stripp, B.R. In vivo differentiation potential of tracheal basal cells: evidence for multipotent and unipotent subpopulations. *Am J Physiol Lung Cell Mol Physiol* **286**, L643-649 (2004).
91. Schoch, K.G., *et al.* A subset of mouse tracheal epithelial basal cells generates large colonies in vitro. *Am J Physiol Lung Cell Mol Physiol* **286**, L631-642 (2004).
92. Mahvi, D., Bank, H. & Harley, R. Morphology of a naphthalene-induced bronchiolar lesion. *Am J Pathol* **86**, 558-572 (1977).
93. Buckpitt, A., *et al.* Relationship of cytochrome P450 activity to Clara cell cytotoxicity. II. Comparison of stereoselectivity of naphthalene epoxidation in lung and nasal mucosa of mouse, hamster, rat and rhesus monkey. *J Pharmacol Exp Ther* **261**, 364-372 (1992).
94. Warren, D.L., Brown, D.L. & Buckpitt, A.R. Evidence for cytochrome P-450 mediated metabolism in the bronchiolar damage by naphthalene. *Chemico-biological interactions* **40**, 287-303 (1982).
95. Buckpitt, A., *et al.* Relationship of cytochrome P450 activity to Clara cell cytotoxicity. IV. Metabolism of naphthalene and naphthalene oxide in microdissected airways from mice, rats, and hamsters. *Mol Pharmacol* **47**, 74-81 (1995).
96. Phimister, A.J., Lee, M.G., Morin, D., Buckpitt, A.R. & Plopper, C.G. Glutathione Depletion Is a Major Determinant of Inhaled Naphthalene Respiratory Toxicity and Naphthalene Metabolism in Mice. *Toxicol. Sci.* **82**, 268-278 (2004).
97. Stevens, T.P., McBride, J.T., Peake, J.L., Pinkerton, K.E. & Stripp, B.R. Cell proliferation contributes to PNEC hyperplasia after acute airway injury. *Am J Physiol* **272**, L486-493 (1997).
98. Reynolds, S.D., *et al.* Conditional clara cell ablation reveals a self-renewing progenitor function of pulmonary neuroendocrine cells. *Am J Physiol Lung Cell Mol Physiol* **278**, L1256-1263 (2000).
99. Giangreco, A., Reynolds, S.D. & Stripp, B.R. Terminal bronchioles harbor a unique airway stem cell population that localizes to the bronchoalveolar duct junction. *Am J Pathol* **161**, 173-182 (2002).
100. Kim, C.F., *et al.* Identification of bronchioalveolar stem cells in normal lung and lung cancer. *Cell* **121**, 823-835 (2005).
101. Teisanu, R.M., Lagasse, E., Whitesides, J.F. & Stripp, B.R. Prospective isolation of bronchiolar stem cells based upon immunophenotypic and autofluorescence characteristics. *Stem Cells* (2008).
102. Sumi, Y. & Hamid, Q. Airway remodeling in asthma. *Allergol Int* **56**, 341-348 (2007).

103. Epler, G.R. Bronchiolitis obliterans organizing pneumonia: definition and clinical features. *Chest* **102**, 2S-6S (1992).
104. Hogg, J.C. Pathophysiology of airflow limitation in chronic obstructive pulmonary disease. *Lancet* **364**, 709-721 (2004).
105. Boxall, C., Holgate, S.T. & Davies, D.E. The contribution of transforming growth factor-beta and epidermal growth factor signalling to airway remodelling in chronic asthma. *Eur Respir J* **27**, 208-229 (2006).
106. Holgate, S.T.*, et al.* Epithelial-mesenchymal communication in the pathogenesis of chronic asthma. *Proc Am Thorac Soc* **1**, 93-98 (2004).
107. Coppens, J.T., Van Winkle, L.S., Pinkerton, K. & Plopper, C.G. Distribution of Clara cell secretory protein expression in the tracheobronchial airways of rhesus monkeys. *American journal of physiology. Lung cellular and molecular physiology* **292**, L1155-1162 (2007).
108. Chung, K.F. & Adcock, I.M. Multifaceted mechanisms in COPD: inflammation, immunity, and tissue repair and destruction. *Eur Respir J* **31**, 1334-1356 (2008).
109. Rennard, S.I., Togo, S. & Holz, O. Cigarette Smoke Inhibits Alveolar Repair: A Mechanism for the Development of Emphysema. *Proc Am Thorac Soc* **3**, 703-708 (2006).
110. Shijubo, N.*, et al.* Serum and BAL Clara cell 10 kDa protein (CC10) levels and CC10-positive bronchiolar cells are decreased in smokers. *Eur Respir J* **10**, 1108-1114 (1997).
111. Wang, H.*, et al.* Cigarette smoke inhibits human bronchial epithelial cell repair processes. *Am J Respir Cell Mol Biol* **25**, 772-779 (2001).
112. Cantral, D.E., Sisson, J.H., Veys, T., Rennard, S.I. & Spurzem, J.R. Effects of cigarette smoke extract on bovine bronchial epithelial cell attachment and migration. *American journal of physiology* **268**, L723-728 (1995).
113. Luppi, F.*, et al.* Effects of cigarette smoke condensate on proliferation and wound closure of bronchial epithelial cells in vitro: role of glutathione. *Respiratory Research* **6**, 140 (2005).
114. Van Winkle, L.S.*, et al.* Prior exposure to aged and diluted sidestream cigarette smoke impairs bronchiolar injury and repair. *Toxicol Sci* **60**, 152-164 (2001).
115. Dovi, J.V., He, L.K. & DiPietro, L.A. Accelerated wound closure in neutrophil-depleted mice. *J Leukoc Biol* **73**, 448-455 (2003).
116. Hogg, J.C.*, et al.* The Nature of Small-Airway Obstruction in Chronic Obstructive Pulmonary Disease. *N Engl J Med* **350**, 2645-2653 (2004).
117. Collins, J.F., Orozco, C.R., McCullough, B., Coalson, J.J. & Johanson, W.G. Pulmonary fibrosis with small-airway disease: a model in nonhuman primates. *Experimental lung research* **3**, 91-108 (1982).
118. Wright, R.R. Elastic tissue of normal and emphysematous lungs. A tridimensional histologic study. *Am J Pathol* **39**, 355-367 (1961).
119. Jiang, D., Liang, J. & Noble, P.W. Hyaluronan in tissue injury and repair. *Annu Rev Cell Dev Biol* **23**, 435-461 (2007).
120. Teder, P.*, et al.* Resolution of lung inflammation by CD44. *Science* **296**, 155-158 (2002).
121. Jiang, D.*, et al.* Regulation of lung injury and repair by Toll-like receptors and hyaluronan. *Nature medicine* **11**, 1173-1179 (2005).

122. Reynolds, S.D., *et al.* Conditional stabilization of beta-catenin expands the pool of lung stem cells. *Stem Cells* **26**, 1337-1346 (2008).
123. Ventura, J.J., *et al.* p38alpha MAP kinase is essential in lung stem and progenitor cell proliferation and differentiation. *Nat Genet* **39**, 750-758 (2007).
124. Jackson, E.L., *et al.* Analysis of lung tumor initiation and progression using conditional expression of oncogenic K-ras. *Genes Dev* **15**, 3243-3248 (2001).
125. Yanagi, S., *et al.* Pten controls lung morphogenesis, bronchioalveolar stem cells, and onset of lung adenocarcinomas in mice. *J Clin Invest* **117**, 2929-2940 (2007).
126. Dovey, J.S., Zacharek, S.J., Kim, C.F. & Lees, J.A. Bmi1 is critical for lung tumorigenesis and bronchioalveolar stem cell expansion. *Proc Natl Acad Sci U S A* **105**, 11857-11862 (2008).
127. Yang, Y., *et al.* Phosphatidylinositol 3-kinase mediates bronchioalveolar stem cell expansion in mouse models of oncogenic K-ras-induced lung cancer. *PLoS ONE* **3**, e2220 (2008).
128. Snyder, J.C., Zemke, A.C. & Stripp, B.R. Reparative Capacity of Airway Epithelium Impacts Deposition and Remodeling of Extracellular Matrix. *Am J Respir Cell Mol Biol* (2008).
129. Atkinson, J.J., Adair-Kirk, T.L., Kelley, D.G., Demello, D. & Senior, R.M. Clara cell adhesion and migration to extracellular matrix. *Respir Res* **9**, 1 (2008).
130. Randell, S.H. Airway epithelial stem cells and the pathophysiology of chronic obstructive pulmonary disease. *Proc Am Thorac Soc* **3**, 718-725 (2006).
131. Van Winkle, L.S., Johnson, Z.A., Nishio, S.J., Brown, C.D. & Plopper, C.G. Early events in naphthalene-induced acute Clara cell toxicity: comparison of membrane permeability and ultrastructure. *Am J Respir Cell Mol Biol* **21**, 44-53 (1999).
132. Plopper, C.G., *et al.* Early events in naphthalene-induced acute Clara cell toxicity. II. Comparison of glutathione depletion and histopathology by airway location. *Am J Respir Cell Mol Biol* **24**, 272-281 (2001).
133. Gill, S.E. & Parks, W.C. Metalloproteinases and their inhibitors: regulators of wound healing. *Int J Biochem Cell Biol* **40**, 1334-1347 (2008).
134. Atkinson, J.J., Toennies, H.M., Holmbeck, K. & Senior, R.M. Membrane type 1 matrix metalloproteinase is necessary for distal airway epithelial repair and keratinocyte growth factor receptor expression after acute injury. *Am J Physiol Lung Cell Mol Physiol* **293**, L600-610 (2007).
135. Chen, P., *et al.* Tissue inhibitor of metalloproteinase-1 moderates airway re-epithelialization by regulating matrilysin activity. *Am J Pathol* **172**, 1256-1270 (2008).
136. Puddicombe, S.M., *et al.* Involvement of the epidermal growth factor receptor in epithelial repair in asthma. *FASEB J* **14**, 1362-1374 (2000).
137. Reynolds, S.D., *et al.* Airway injury in lung disease pathophysiology: selective depletion of airway stem and progenitor cell pools potentiates lung inflammation and alveolar dysfunction. *Am J Physiol Lung Cell Mol Physiol* **287**, L1256-1265 (2004).
138. Chomczynski, P. & Sacchi, N. Single-step method of RNA isolation by acid guanidinium thiocyanate-phenol-chloroform extraction. *Anal Biochem* **162**, 156-159 (1987).
139. Zemke, A.C., *et al.* Molecular Staging of Epithlieial Maturation Using Secretory Cell-Specific Genes as Markers. *Am J Respir Cell Mol Biol* (2008).

140. Heid, C.A., Stevens, J., Livak, K.J. & Williams, P.M. Real time quantitative PCR. *Genome Res* **6**, 986-994 (1996).
141. Paivaniemi, O.E., Maasilta, P.K., Alho, H.S., Vainikka, T.L. & Salminen, U.S. Epithelial tenascin predicts obliterative airway disease. *J Heart Lung Transplant* **27**, 400-407 (2008).
142. Langer, D., Ikehara, Y., Takebayashi, H., Hawkes, R. & Zimmermann, H. The ectonucleotidases alkaline phosphatase and nucleoside triphosphate diphosphohydrolase 2 are associated with subsets of progenitor cell populations in the mouse embryonic, postnatal and adult neurogenic zones. *Neuroscience* **150**, 863-879 (2007).
143. Ferby, I., *et al.* Mig6 is a negative regulator of EGF receptor-mediated skin morphogenesis and tumor formation. *Nat Med* **12**, 568-573 (2006).
144. Holgate, S.T., *et al.* Epithelial-mesenchymal interactions in the pathogenesis of asthma. *J Allergy Clin Immunol* **105**, 193-204 (2000).
145. Wang, I.M., *et al.* Gene expression profiling in patients with chronic obstructive pulmonary disease and lung cancer. *Am J Respir Crit Care Med* **177**, 402-411 (2008).
146. Kaarteenaho-Wiik, R., *et al.* Distribution and mRNA expression of tenascin-C in developing human lung. *Am J Respir Cell Mol Biol* **25**, 341-346 (2001).
147. Kaarteenaho-Wiik, R., *et al.* Tenascin-C is highly expressed in respiratory distress syndrome and bronchopulmonary dysplasia. *J Histochem Cytochem* **50**, 423-431 (2002).
148. Matsuda, A., *et al.* Coding SNP in tenascin-C Fn-III-D domain associates with adult asthma. *Hum Mol Genet* **14**, 2779-2786 (2005).
149. Puchelle, E., Zahm, J.M., Tournier, J.M. & Coraux, C. Airway epithelial repair, regeneration, and remodeling after injury in chronic obstructive pulmonary disease. *Proc Am Thorac Soc* **3**, 726-733 (2006).
150. Watt, F.M. & Hogan, B.L. Out of Eden: stem cells and their niches. *Science* **287**, 1427-1430 (2000).
151. Garcion, E., Faissner, A. & ffrench-Constant, C. Knockout mice reveal a contribution of the extracellular matrix molecule tenascin-C to neural precursor proliferation and migration. *Development* **128**, 2485-2496 (2001).
152. Garcion, E., Halilagic, A., Faissner, A. & ffrench-Constant, C. Generation of an environmental niche for neural stem cell development by the extracellular matrix molecule tenascin C. *Development* **131**, 3423-3432 (2004).
153. Ohta, M., Sakai, T., Saga, Y., Aizawa, S. & Saito, M. Suppression of hematopoietic activity in tenascin-C-deficient mice. *Blood* **91**, 4074-4083 (1998).
154. Nishio, T., *et al.* Tenascin-C regulates proliferation and migration of cultured astrocytes in a scratch wound assay. *Neuroscience* **132**, 87-102 (2005).
155. Iyer, A.K., *et al.* Tenascin cytotactin epidermal growth factor-like repeat binds epidermal growth factor receptor with low affinity. *J Cell Physiol* **211**, 748-758 (2007).
156. Iyer, A.K., Tran, K.T., Griffith, L. & Wells, A. Cell surface restriction of EGFR by a tenascin cytotactin-encoded EGF-like repeat is preferential for motility-related signaling. *J Cell Physiol* **214**, 504-512 (2008).
157. Berasain, C., *et al.* Novel role for amphiregulin in protection from liver injury. *J Biol Chem* **280**, 19012-19020 (2005).
158. Berasain, C., *et al.* Amphiregulin: an early trigger of liver regeneration in mice. *Gastroenterology* **128**, 424-432 (2005).

159. Jakubowski, A., *et al.* TWEAK induces liver progenitor cell proliferation. *J Clin Invest* **115**, 2330-2340 (2005).
160. Snyder, J.C., *et al.* Clara Cells Attenuate the Inflammatory Response through Regulation of Macrophage Behavior. *Am J Respir Cell Mol Biol* (2009).
161. Calverley, P.M. & Walker, P. Chronic obstructive pulmonary disease. *Lancet* **362**, 1053-1061 (2003).
162. Braman, S.S. The global burden of asthma. *Chest* **130**, 4S-12S (2006).
163. Aaron, S.D., *et al.* Granulocyte inflammatory markers and airway infection during acute exacerbation of chronic obstructive pulmonary disease. *Am J Respir Crit Care Med* **163**, 349-355 (2001).
164. Broeckaert, F., Clippe, A., Knoops, B., Hermans, C. & Bernard, A. Clara cell secretory protein (CC16): features as a peripheral lung biomarker. *Ann N Y Acad Sci* **923**, 68-77 (2000).
165. Wattiez, R., Hermans, C., Cruyt, C., Bernard, A. & Falmagne, P. Human bronchoalveolar lavage fluid protein two-dimensional database: study of interstitial lung diseases. *Electrophoresis* **21**, 2703-2712 (2000).
166. Hermans, C., *et al.* Serum Clara cell protein (CC16), a marker of the integrity of the air-blood barrier in sarcoidosis. *Eur Respir J* **18**, 507-514 (2001).
167. Sarafidis, K., *et al.* Clara cell secretory protein (CC16) as a peripheral blood biomarker of lung injury in ventilated preterm neonates. *European journal of pediatrics* **167**, 1297-1303 (2008).
168. Schrama, A.J.J., *et al.* Cord blood Clara cell protein CC16 predicts the development of bronchopulmonary dysplasia. *European journal of pediatrics* **167**, 1305-1312 (2008).
169. Kropski, J.A., Fremont, R.D., Calfee, C.S. & Ware, L.B. Clara Cell Protein (CC16), a Marker of Lung Epithelial Injury, Is Decreased in Plasma and Pulmonary Edema Fluid From Patients With Acute Lung Injury. *Chest*, - (2009).
170. Lesur, O., *et al.* Outcome value of Clara cell protein in serum of patients with acute respiratory distress syndrome. *Intensive care medicine* **32**, 1167-1174 (2006).
171. Madsen, C., *et al.* Associations between environmental exposures and serum concentrations of Clara cell protein among elderly men in Oslo, Norway. *Environmental Research* **108**, 354-360 (2008).
172. Laing, I.A., *et al.* A polymorphism of the CC16 gene is associated with an increased risk of asthma. *J Med Genet* **35**, 463-467 (1998).
173. Laing, I.A., *et al.* Association between plasma CC16 levels, the A38G polymorphism, and asthma. *Am J Respir Crit Care Med* **161**, 124-127 (2000).
174. Ohchi, T., *et al.* Polymorphism of Clara cell 10-kD protein gene of sarcoidosis. *Am J Respir Crit Care Med* **169**, 180-186 (2004).
175. I. A. Laing, N.H.d.K., S. W. Turner, P. K. Judge, C. M. Hayden, L. I. Landau, J. Goldblatt, P. N. Le Souëf,. Cross-sectional and longitudinal association of the secretoglobin 1A1 gene A38G polymorphism with asthma phenotype in the Perth Infant Asthma Follow-up cohort. *Clinical & Experimental Allergy* **39**, 62-71 (2009).
176. Singh, G. & Katyal, S.L. Clara cells and Clara cell 10 kD protein (CC10). *Am J Respir Cell Mol Biol* **17**, 141-143 (1997).
177. Umland, T.C., *et al.* Structure of a human Clara cell phospholipid-binding protein-ligand complex at 1.9 A resolution. *Nat Struct Biol* **1**, 538-545 (1994).

178. Beato, M. Binding of steroids to uteroglobin. *The Journal of steroid biochemistry* **7**, 327-334 (1976).
179. Miyazaki, S., Ishikawa, F., Fujikawa, T., Nagata, S. & Yamaguchi, K. Intraperitoneal injection of lipopolysaccharide induces dynamic migration of Gr-1high polymorphonuclear neutrophils in the murine abdominal cavity. *Clin Diagn Lab Immunol* **11**, 452-457 (2004).
180. Dolinay, T.*, et al.* Gene expression profiling of target genes in ventilator-induced lung injury. *Physiol Genomics* **26**, 68-75 (2006).
181. Selman, M.*, et al.* Gene expression profiles distinguish idiopathic pulmonary fibrosis from hypersensitivity pneumonitis. *Am J Respir Crit Care Med* **173**, 188-198 (2006).
182. Dave, N.B. & Kaminski, N. Analysis of microarray experiments for pulmonary fibrosis. *Methods Mol Med* **117**, 333-358 (2005).
183. Ben-Dor, A.*, et al.* Tissue classification with gene expression profiles. *J Comput Biol* **7**, 559-583 (2000).
184. Novershtern, N., Itzhaki, Z., Manor, O., Friedman, N. & Kaminski, N. A Functional and Regulatory Map of Asthma. *Am J Respir Cell Mol Biol* (2007).
185. You, Y., Richer, E.J., Huang, T. & Brody, S.L. Growth and differentiation of mouse tracheal epithelial cells: selection of a proliferative population. *Am J Physiol Lung Cell Mol Physiol* **283**, L1315-1321 (2002).
186. Becker, M.N., Diamond, G., Verghese, M.W. & Randell, S.H. CD14-dependent lipopolysaccharide-induced beta-defensin-2 expression in human tracheobronchial epithelium. *J Biol Chem* **275**, 29731-29736 (2000).
187. Schurr, J.R.*, et al.* Central role of toll-like receptor 4 signaling and host defense in experimental pneumonia caused by Gram-negative bacteria. *Infect Immun* **73**, 532-545 (2005).
188. Hollingsworth, J.W.*, et al.* Ambient ozone primes pulmonary innate immunity in mice. *J Immunol* **179**, 4367-4375 (2007).
189. Zemke, A.C.*, et al.* Molecular staging of epithelial maturation using secretory cell-specific genes as markers. *Am J Respir Cell Mol Biol* **40**, 340-348 (2009).
190. Visintin, A., Latz, E., Monks, B.G., Espevik, T. & Golenbock, D.T. Lysines 128 and 132 enable lipopolysaccharide binding to MD-2, leading to Toll-like receptor-4 aggregation and signal transduction. *J Biol Chem* **278**, 48313-48320 (2003).
191. Castaneda, F., Rosin-Steiner, S. & Jung, K. Functional genomics analysis of low concentration of ethanol in human hepatocellular carcinoma (HepG2) cells. Role of genes involved in transcriptional and translational processes. *Int J Med Sci* **4**, 28-35 (2006).
192. Perroud, B.*, et al.* Pathway analysis of kidney cancer using proteomics and metabolic profiling. *Mol Cancer* **5**, 64 (2006).
193. Yuan, W.*, et al.* Commonly dysregulated genes in murine APL cells. *Blood* **109**, 961-970 (2007).
194. Smookler, D.S.*, et al.* Tissue inhibitor of metalloproteinase 3 regulates TNF-dependent systemic inflammation. *J Immunol* **176**, 721-725 (2006).
195. Harrod, K.S. & Jaramillo, R.J. Pseudomonas aeruginosa and tumor necrosis factor-alpha attenuate Clara cell secretory protein promoter function. *Am J Respir Cell Mol Biol* **26**, 216-223 (2002).

196. Gupta, R.P., Patton, S.E., Jetten, A.M. & Hook, G.E. Purification, characterization and proteinase-inhibitory activity of a Clara-cell secretory protein from the pulmonary extracellular lining of rabbits. *Biochem J* **248**, 337-344 (1987).
197. Burmeister, R.*, et al.* A two-receptor pathway for catabolism of Clara cell secretory protein in the kidney. *J Biol Chem* **276**, 13295-13301 (2001).
198. Mukherjee, A.B.*, et al.* Uteroglobin: a novel cytokine? *Cell Mol Life Sci* **55**, 771-787 (1999).
199. Diaz Gonzalez, K. & Nieto, A. Binding of uteroglobin to microsomes and plasmatic membranes. *FEBS Lett* **361**, 255-258 (1995).
200. Bin, L.H., Nielson, L.D., Liu, X., Mason, R.J. & Shu, H.B. Identification of uteroglobin-related protein 1 and macrophage scavenger receptor with collagenous structure as a lung-specific ligand-receptor pair. *J Immunol* **171**, 924-930 (2003).
201. Diakonova, M.*, et al.* Localization of five annexins in J774 macrophages and on isolated phagosomes. *J Cell Sci* **110 (Pt 10)**, 1199-1213 (1997).
202. Kusumawati, A., Liautard, J.P. & Sri Widada, J. Implication of annexin 1 in phagocytosis: effects of n-terminal domain deletions and point mutations of the phosphorylation site Ser-27. *Cell Biol Int* **25**, 809-813 (2001).
203. Murray, R.Z., Kay, J.G., Sangermani, D.G. & Stow, J.L. A role for the phagosome in cytokine secretion. *Science* **310**, 1492-1495 (2005).
204. Srivastava, M.*, et al.* The inflammatory versus constitutive trafficking of mononuclear phagocytes into the alveolar space of mice is associated with drastic changes in their gene expression profiles. *The journal of immunology* **175**, 1884-1893 (2005).
205. Maus, U.*, et al.* The role of CC chemokine receptor 2 in alveolar monocyte and neutrophil immigration in intact mice. *American journal of respiratory and critical care medicine* **166**, 268-273 (2002).
206. Kim, E.Y.*, et al.* Persistent activation of an innate immune response translates respiratory viral infection into chronic lung disease. *Nature medicine* **14**, 633-640 (2008).
207. Singh, J. & Schwartz, D.A. Endotoxin and the lung: Insight into the host-environment interaction. *J Allergy Clin Immunol* **115**, 330-333 (2005).
208. Chen, P.*, et al.* Tissue inhibitor of metalloproteinase-1 moderates airway re-epithelialization by regulating matrilysin activity. *The American journal of pathology* **172**, 1256-1270 (2008).
209. McGuire, J.K., Li, Q. & Parks, W.C. Matrilysin (matrix metalloproteinase-7) mediates E-cadherin ectodomain shedding in injured lung epithelium. *The American journal of pathology* **162**, 1831-1843 (2003).
210. Kida, H.*, et al.* GP130-STAT3 Regulates Epithelial Cell Migration and Is Required for Repair of the Bronchiolar Epithelium. *Am J Pathol* **172**, 1542-1554 (2008).
211. Berasain, C.*, et al.* Amphiregulin: an early trigger of liver regeneration in mice. *Gastroenterology* **128**, 424-432 (2005).
212. Berasain, C.*, et al.* Novel role for amphiregulin in protection from liver injury. *The Journal of biological chemistry* **280**, 19012-19020 (2005).
213. Lin, K.L., Suzuki, Y., Nakano, H., Ramsburg, E. & Gunn, M.D. CCR2+ Monocyte-Derived Dendritic Cells and Exudate Macrophages Produce Influenza-Induced Pulmonary Immune Pathology and Mortality. *J Immunol* **180**, 2562-2572 (2008).